

Disease modelling of a human
neurodevelopmental disorder using
mouse embryonic stem cells

Inauguraldissertation

zur

Erlangung der Würde eines Doktors der Philosophie

vorgelegt der

Philosophisch-Naturwissenschaftlichen Fakultät

der Universität Basel

von

Morteza Yazdani Shektaei

aus Sari, Iran

Basel, August 2011

Genehmigt von der Philosophisch
Naturwissenschaftlichen Fakultät

Auf Antrag von:

Prof. Markus Rüegg
Prof. Yves-Alain Barde

Basel den 19 Oktober, 2010

Prof. Dr. Martin Spiess
Dekan

Summary

As cultured embryonic stem (ES) cells can be differentiated in neurons under well-defined conditions, they provide a unique opportunity to model and study diseases of the nervous system such as Rett syndrome. Most cases of this tragic neurodevelopmental disorder affecting about 1 young girl in 10'000 are caused by mutations in *MECP2*, a gene encoding the methyl-CpG-binding protein 2. Despite the generation of very useful mouse models recapitulating some important features of Rett syndrome, like the lack of normal brain growth, breathing arrhythmia and movement deficits, the function of MeCP2 in the brain remains unclear at this point. A few years ago, our laboratory established a differentiation procedure allowing the generation of virtually pure progenitors defined as Pax6-positive radial glial cells. As they do *in vivo*, these cells go on to generate glutamatergic neurons. One key characteristic of this system is that essentially all cells differentiate synchronously and I used it during the course of my PhD thesis to compare wild-type ES cells with ES cells lacking MeCP2. During the transition from progenitors to neurons, the size of nuclei increases by about 40% within a period of about 10 days, while nuclei of neurons lacking MeCP2 fail to grow at the same rate. Both the acute re-expression of MeCP2 in MeCP2 Stop-Floxed neurons following the excision of a stop cassette using Cre, as well as the viral delivery of MeCP2 to *null* neurons were found to rescue the small nuclear size phenotype. In an effort to correlate the size of the nuclei with their transcriptional activity, I compared the rate of total *in vitro* RNA transcription in pure nuclei isolated from wild-type vs. *Mecp2* ^{-/-} (*null*) and *Mecp2* Stop-Floxed ES cell-derived neurons. Regardless of the type of MeCP2 mutation, the neuronal nuclei lacking MeCP2 were found to be significantly less transcriptionally active compared to the wild-type nuclei. These results suggest that MeCP2 may have a general, genome-wide role in regulating the rate of RNA transcription, including ribosomal RNA that represents the major species investigated in such experiments. As BDNF levels have been reported to be reduced in the brain of *Mecp2* ^{-/-} mice, I also examined if ES cell-derived neuron lacking MeCP2 would reflect this potentially important aspect of the disease, since decreased levels of BDNF could be hoped to be corrected and to improve

the patients' condition. At about 15 days *in vitro*, the levels of BDNF were found to be reduced by about 30% and the acute expression of MeCP2 was found to restore the expression of BDNF to levels similar to those seen in wild-type neurons.

In the second part of my work, I found that the sphingosine-1 phosphate analogue fingolimod (FTY720), recently introduced as the first oral treatment of multiple sclerosis, increases BDNF levels both in wild-type and *Mecp2*^{-/-} ES cell-derived neurons by mechanisms involving MAPK signaling and neuronal activity. In MeCP2 mutant mice, FTY720 increases BDNF levels in the striatum as well its volume, ameliorates locomotor activity and extends the lifespan by 50%.

As microcephaly is one of major symptoms of Rett syndrome, I also investigated in the third part of my PhD work the effects of the lack of MeCP2 on cell proliferation. While MeCP2-deficient ES cells do not have a proliferation defect, neuronal progenitors lacking MeCP2 generate fewer neurons compared with wild-type cells. This difference between ES cells and neuronal progenitors may result from the fact that the levels of MeCP2 expression are much higher in neurons and neuronal progenitors compared to ES cells.

Taken together, my results show that an ES cell based system represent a useful tool to understand molecular mechanisms underlying human neurological disorders.

Table of Contents

1. Introduction	7
1.1. Rett syndrome	8
1.2. MeCP2 function	10
1.3. RTT animal models.....	11
1.4. ES cell-derived neurons	13
1.5. Aim of this thesis	14
2. Materials and Methods	15
2.1. Cell cultures	15
2.1.1. Mouse embryonic fibroblast cultures.....	15
2.1.2. Mouse embryonic stem cells cultures	16
2.1.3. Primary cortical neurons cultures	18
2.1.4. Primary cortical glial cultures	18
2.1.5. HEK-293 cells cultures	18
2.2. Western blot.....	19
2.3. Quantitative real-time RT-PCR	20
2.4. Cloning and lentivirus generation.....	21
2.5. Assessment of the cell proliferation.....	24
2.6. Immunostaining and nuclear size measurement	24
2.7. Nuclei purification and in vitro transcription assay	25
2.7.1. Nuclear purification from cultured cells	25
2.7.2. Nuclear purification from tissue	26
2.7.3. In vitro transcription	27
2.8. Animal work	28
2.8.1. <i>MECP2</i> mutant mice.....	28
2.8.2. BDNF ELISA measurements.....	28
2.8.3. Running wheel assay.....	29
3. Results	30
3.1. Neuronal differentiation of <i>MECP2</i> mutant ES cell lines	30
3.1.1. <i>MECP2</i> mutant ES cell lines.....	30
3.1.2. Neuronal differentiation of various <i>MECP2</i> mutant ES cells.....	32
3.2. Progenitors lacking MeCP2 produce fewer neurons	34
3.2.1. Loss of <i>MECP2</i> does not affect the growth of ES cells.....	34
3.2.2. Progenitors lacking MeCP2 generate fewer neurons compared with wild-type cells	37
3.2.3. Neuronal progenitors lacking MeCP2 proliferate less than wild-type progenitors	39
3.3. MeCP2 regulates the size of neuronal nuclei.....	40
3.3.1. Nuclei lacking MeCP2 fail to grow during neuronal maturation	40
3.3.2. Nuclear size of ES cell-derived neurons correlates with their levels of MeCP2	42
3.3.3. Primary neurons of <i>MECP2</i> -deficient mice have smaller nuclei.....	43
3.3.4. Re-expression of MeCP2 rescues the small nuclei phenotype	45
3.3.5. Regulation of nuclear size by MeCP2 is cell autonomous	47

3.3.6.	MeCP2-deficient glia do not have small nuclei.....	48
3.3.7.	In vivo measurements of neuronal nuclei size.....	52
3.3.8.	Reduced rate of global transcription in MeCP2-deficient neurons.....	54
3.4.	FTY720 increases BDNF levels and improves the symptoms in mice lacking MeCP2	57
3.4.1.	Reduced levels of BDNF in <i>MECP2</i> <i>-/y</i> neurons	57
3.4.2.	Reduced levels of BDNF in various brain regions of <i>MECP2</i> <i>-/y</i> mice ...	58
3.4.3.	FTY720 increases BDNF expression in wild-type cortical neurons	59
3.4.4.	FTY720 increases CREB phosphorylation by activating NMDA receptors and MAPK pathway.....	61
3.4.5.	FTY720 increases BDNF expression in <i>MECP2</i> deficient neurons and brains	63
3.4.6.	FTY720 improves the motor performance of <i>MECP2</i> <i>-/y</i> mice	64
3.4.7.	FTY720 increases the lifespan of <i>MECP2</i> <i>-/y</i> mice	66
4.	Discussion	68
4.1.	Lack of <i>MECP2</i> affects the proliferation of neuronal progenitors but not the ES cells	68
4.2.	MeCP2 regulates the size of neuronal nuclei.....	71
4.3.	FTY720 increases BDNF expression and improves the symptoms of mouse models of Rett syndrome	80
5.	References.....	87
6.	Acknowledgements.....	95
7.	Curriculum vitae	96

1. Introduction

“Men ought to know that from the brain, and from the brain only, arise our pleasures, joys, laughter and jests, as well as our sorrows, pains, grief and tears. It is the same thing which makes us mad or delirious, inspires us with dread or fear, whether by night or by day, brings sleeplessness, inopportune mistakes, aimless anxieties, absent-mindedness, and acts that are contrary to habit”. Hippocrates 460-377 BC

The brain is the most complex and fascinating organ in the human body. Together with the spinal cord and the peripheral nervous system, it directs the function of all other organs. Not only can it process and interpret sensory signals, but it also can store information for long periods of time. Defects in neural development can lead to severe problems, including for example a relatively frequent condition designated autism. While autism is a complex disease likely to have more than just one genetic explanation, one condition, Rett syndrome, appears to be experimentally approachable. It is a devastating neurodevelopmental disorder mainly affecting young girls, all of them having autistic traits. Essentially all cases of Rett syndrome are caused by mutations in the X-linked gene *MECP2*. The affected girls have a short period of apparently normal development but after 6 to 18 months they go through a period of developmental stagnation accompanied by neurological symptoms ranging from seizure to breathing arrhythmia, mental retardation, microcephaly and autism. Unlike many other neurological disorders, very useful mouse models exist for the Rett syndrome, mainly due to the monogenic nature of the disease and the fact that *MECP2* is located on the X chromosome in both mouse and human. In spite of this, the role of MeCP2 in brain function is still very unclear at this point. The aim of my work was to try and improve our understanding of the role of MeCP2 in developing neurons using a novel cell culture system.

1.1. Rett syndrome

In 1954, Dr. Andreas Rett, a pediatrician and neurologist in Vienna, Austria, and his nurse first noticed two girls as they sat in his waiting room with their mothers. They observed these children making the same repetitive hand-washing motions. Dr. Rett then compared their clinical and developmental histories and discovered they were very similar. This coincidental occurrence prompted Dr. Rett to search for more patients with the same unusual behavior. In 1966, Dr. Rett described similar findings in 22 patients, reporting for the first time a unique clinical entity that now bears his name (Rett, 1966). But it would not be until 17 years later that Rett syndrome (RTT) became recognized in the medical community when Dr. Bengt Hagberg, a Swedish neurologist, and his colleagues reported 35 cases of RTT in the English language (Hagberg *et al.*, 1983), and recognized this clinical entity as a condition “similar to a virtually overlooked syndrome described by Rett in the German literature.”

Rett syndrome is a postnatal progressive neurodevelopmental disorder affecting ~1 in 10’000 females (Rett, 1966). The affected girls develop normally until 6-18 months, achieving the appropriate milestone, such as ability to walk and some times even speaking a few words. However, there is considerable variability in the severity of the symptoms (see below). The brief period of developmental progress is followed by stagnation distinguished by growth arrest and microcephaly. After this, patients go through a rapid regression phase. The previously acquired skills are lost and a variety of symptoms develop including mental retardation, autistic features, breathing arrhythmia, loss of motor coordination, seizure, loss of purposeful hand use and development of stereotypic hand movements instead (Figure 1.1) (Chahrour and Zoghbi, 2007). Kerr and colleagues found an annual mortality rate in Rett syndrome of 1.2% (Kerr *et al.*, 1997). Autopsy studies show a 12%–34% reduction in brain weight and volume in patients with RTT (Jellinger *et al.*, 1988) with a reduction in the neuronal size in the cortex, thalamus, basal ganglia, amygdala, and hippocampus. In addition, an increase in neuronal cell packing in the hippocampus is reported (Kaufmann and Moser, 2000).

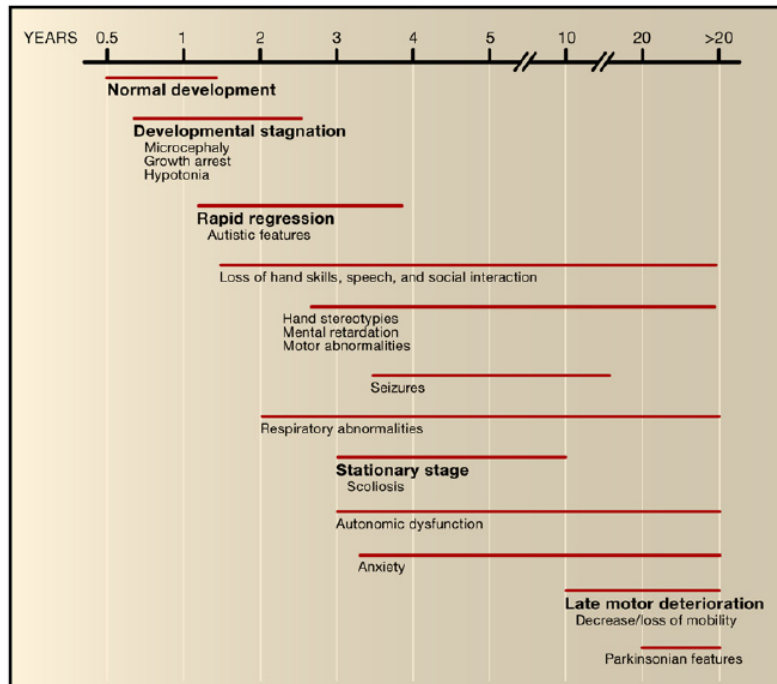


Figure 1-1 Onset and progression of RTT clinical phenotypes (adapted from Chahrour and Zoghbi, 2007)

Given that the vast majority of patients with RTT are females, early studies postulated an X-linked dominant mode of inheritance. In 1999, the group of Dr. Huda Zoghbi found that the gene methyl-CpG-binding protein 2 (*MECP2*), located in Xq28, was mutated in more than 95% cases of classical Rett syndrome (Amir *et al.*, 1999).

More than 99% of RTT cases are sporadic. Most of the mutations in *MECP2* arise *de novo* in paternal germline, thus explaining the sporadic nature of RTT and its occurrence predominantly in girls (Chahrour and Zoghbi, 2007, Trappe *et al.*, 2001).

Mutations affecting the nuclear localization (NLS) of MeCP2 or early truncating mutations tend to cause more severe phenotypes than missense mutations, whereas C-terminal deletions are associated with milder phenotypes (Naidu *et al.*, 2003, Smeets *et al.*, 2005).

A major source of the phenotypic variability associated with different *MECP2* mutations in females is the pattern of X chromosome inactivation (XCI) (Chahrour and Zoghbi,

2007). In females, only one of the two X chromosomes is active in each cell. The inactive X chromosome is silenced by packaging into transcriptionally inactive heterochromatin (Chow *et al.*, 2005). X-inactivation occurs so that the female, with two X chromosomes, does not have twice as many X chromosome gene products as the male, which only possess a single copy of the X chromosome. The XCI is thought to be a random process occurring during gastrulation (Okamoto *et al.*, 2004), such that roughly half of the cells have the maternal X chromosome active and the other half have the paternal X chromosome active. In male mutants, with only one X chromosome, all the cells express the mutant allele which may often be lethal. However, a female with a *MECP2* mutation is typically mosaic, whereby part of her cells express the mutant *MECP2* allele while the others express the wild-type *MECP2* allele. In some extreme cases, most of the cells inactivate the mutant X chromosome, so that some patients may be only mildly affected or are even asymptomatic carriers of *MECP2* mutations. The latter cases are usually identified because of the occurrence of RTT in their offspring (Dayer *et al.*, 2007) and some have probably been misdiagnosed as being autistic patients.

1.2. *MeCP2* function

MeCP2 is a protein that binds to the methylated DNA, *in vitro* and *in vivo* (Skene *et al.*, 2010). It has been known for many years that cytosine in the sequence CpG is frequently methylated in the vertebrate genome by DNA methyltransferase (Bestor *et al.*, 1988). Some areas of genome are methylated more heavily than others and the highly methylated areas tend to be less transcriptionally active through mechanisms not fully understood. DNA methylation is then generally thought to act as a landmark for transcriptional suppression. However, DNA methylation *per se* can not convey any message and it is believed that methylation of DNA attracts binding of proteins that interpret the methylation (Bird and Wolffe, 1999).

MeCP2 was identified in a screen to find proteins that bind specifically to methylated and not non-methylated DNA probes (Lewis *et al.*, 1992). MeCP2 binds to one symmetric methyl-CpG pair through its methyl-binding domain (MBD) (Meehan *et al.*, 1992). MeCP2 was then initially thought to function as a global transcriptional repressor (Nan *et al.*, 1997). However, transcriptional profiling of *MECP2* knock-out mice revealed rather subtle, but consistent, down-regulation in the expression of many genes in the brain (Chahrour *et al.*, 2008). If MeCP2 were a general transcriptional repressor, one would expect instead increased expression of many genes in its absence. How MeCP2 affects the transcription of genes relevant to brain development remains unclear at this point.

1.3. RTT animal models

Like in humans, the mouse *MECP2* gene is located on the X chromosome. Shortly after the discovery of the genetic basis of Rett syndrome, mouse lines were generated, by targeting of the *MECP2* gene, in the hope of mimicking relevant aspects of human RTT (Chen *et al.*, 2001, Guy *et al.*, 2001).

Heterozygous female mutants (*MECP2* +/-) seem normal for the first three to four months, but begin to show symptoms such as weight gain, reduced activity and ataxic gait (Chen *et al.*, 2001, Guy *et al.*, 2001). At a later age, they frequently displayed tremor, heavy breathing and cold extremities indicating autonomic abnormalities that are also characteristics of human patients.

In male animals, removal of *MECP2* leads to generation of a *null* mutant (*MECP2* -/y). While the animals are viable at birth, they show symptoms around weaning. They develop a stiff, uncoordinated gait and reduced spontaneous movement between three and eight weeks of age. Most animals develop hind-limb clasping and irregular breathing and subsequently die at around postnatal day 54 (Guy *et al.*, 2001). Brains of *MECP2*-null

mice are significantly smaller than wild-types, with an increase in cell packing density and reduction in neuronal and neuronal nuclei size (Chen *et al.*, 2001). The smaller brain and the general reduction of neuronal cell size in the *MECP2*-deficient mice are consistent with what has been described in human RTT patients.

Strikingly, the group of Adrian Bird showed that re-expression of MeCP2 from its endogenous promoter, even in severely symptomatic mice, leads to a robust reversal of the phenotypes (Guy *et al.*, 2007). While this experiment does not suggest an immediate therapeutic approach to RTT, it establishes the principle of reversibility in this mouse model. This observation is almost unique in the field of disease modeling and raises hopes that the lack of MeCP2 does not lead to irreversible changes in the developing brain, such as death of large number of neurons for example. This striking observation is somewhat reminiscent of previous results obtained by the group of René Hen and colleagues indicating that huntingtin aggregates disappear, as do the behavioral anomalies, when the production of the mutant protein is discontinued in transgenic mice (Yamamoto *et al.*, 2000)

Currently, the search for therapeutic approaches relies mostly on the lessons learned from the mouse model. One of the genes whose expression appears to be affected in the brains of *MECP2* mutant mice is increasingly regarded as an “endogenous neuroprotectant”, brain-derived neurotrophic factor (*BDNF*) (Chang *et al.*, 2006, Tremblay *et al.*, 1999). Chang and colleagues also showed that BDNF expression levels can greatly affect the disease progression in the MeCP2 mutant mice. Over-expression and down-regulation of BDNF in forebrain of *MECP2* null mice were shown to improve and worsen the symptoms, respectively (Chang *et al.*, 2006). These results suggest that BDNF and the up-regulation of its expression may be a useful avenue to follow to develop new approaches to treat Rett syndrome.

1.4. **ES cell-derived neurons**

MeCP2 is highly expressed not only in brain but also in lung, heart and kidney (Shahbazian *et al.*, 2002a). Work with mouse models of RTT suggests that the main cell type affected in the Rett syndrome are neurons, as specific removal of MeCP2 in neurons of forebrain results in Rett-like phenotype in mice (Chen *et al.*, 2001). In addition, re-expression of MeCP2 only in post-mitotic neuron rescued the Rett syndrome in mice (Luikenhuis *et al.*, 2004). Recently, it was shown that in adult mice brains, the levels of MeCP2 are about six times higher in neuronal nuclei, compared with glial nuclei (Skene *et al.*, 2010). These data suggest an important role for MeCP2 in neurons compared to glia. Therefore, it would be useful to learn more about the function of MeCP2 in neurons. However, this remains a challenging objective with traditional systems such as brain or tissues culture lysates given their cellular heterogeneity and the difficulties in following defined cell population over time. To circumvent these difficulties, I used mouse embryonic stem (ES) cells. Under suitable tissue culture conditions, ES cell can usefully recapitulate early events in neurogenesis (Bibel *et al.*, 2004, Nikolettou *et al.*, 2007). As wild-type or genetically modified ES cells can be grown in unlimited quantities, their differentiation into neurons represents an attractive model for studying the function of genes involved in neurological disorders, such as Rett syndrome. A few years ago, our laboratory established a robust differentiation protocol (Bibel *et al.*, 2007, Bibel *et al.*, 2004) leading to the generation of well-defined and virtually pure populations of Pax6-positive radial glial (RG) cells with a profile and developmental potential characteristic of Pax6-positive RG cells of the cortex. Like their *in vivo* counterparts, these progenitors generate homogeneous populations of glutamatergic neurons (>95%).

1.5. *Aim of this thesis*

The aim of this thesis was to increase our understanding of the Rett syndrome at the cellular and molecular levels using a novel cellular assay. I also attempted to use the knowledge derived from these experiments to begin to address the disease and possible treatments at the organism level.

2. Materials and Methods

2.1. Cell cultures

2.1.1. Mouse embryonic fibroblast cultures

EB medium

	Concentration	Supplier
FCS	10%	Gibco, heat inactivated 30 min at 55°C
Non-Essential Amino Acids	1x	Gibco # 11140-035
Glutamine 100x (200 mM)	1x (2 mM)	Gibco # 25030-024
β -mercaptoethanol	0.001%	Sigma # M7522
DMEM	To final volume	Gibco # 21969-035

ES medium

	Concentration	Supplier
FCS	15%	Gibco, heat inactivated 30 min at 55°C
LIF	10^3 unit/ml (approx. 10 ng/ml)	Chemicon, # ESG1107, 10^7 units/ml leukemia inhibitory factor
Non-Essential Amino Acids	1x	Gibco # 11140-035
Glutamine 100x (200 mM)	1x (2 mM)	Gibco # 25030-024
β -mercaptoethanol	0.001%	Sigma # M7522
DMEM	To final volume	Gibco # 21969-035

Immortalized mouse embryonic feeders (MEFs) were grown in EB medium on 0.2% gelatin (Sigma # G-1890) coated tissue culture dishes (Nunc # 150288) for 2-4 days at 37°C (7% CO₂). As soon as they reached confluence, they were inactivated with 10 µg/ml Mitomycin C (Sigma # M0503) for 2 hours at 37°C, washed with PBS (Gibco # 14190) and let recover, for at least 2 hours, in ES medium until ES cells were plated on them.

2.1.2. Mouse embryonic stem cells cultures

N2 medium

	Final concentration	Supplier
Human Apo-Transferrin	50 µg/ml	Sigma # T-1147
Insulin	25 µg/ml	Sigma # I-6634
BSA	50 µg/ml	Sigma # A-9418
Progesterone	6 ng/ml	Sigma # P-8783
Putrescine	16 ng/ml	Sigma # P-7505
L-Glutamine	0.146 mg/ml	Gibco # 25030-024
Sodium Selenite	5.19 ng/ml	Sigma # S-5261
DMEM & F12	Mixed 1:1 to final volume of 250 ml	Gibco # 21969-035 Gibco # 21765-029

Complete medium

Aqueous solutions	Stock sol.	Final conc.	Supplier
L-Alanine	2 mg/ml	2 µg/ml	Sigma # A-7627
Biotine	0.1 mg/ml	0.1 µg/ml	Sigma # B-4501
L-Carnitine	2 mg/ml	2 µg/ml	Sigma # C-0283
Ethanolamine	1 mg/ml	1 µg/ml	Sigma # E-9508
D+ Galactose	15 mg/ml	15 µg/ml	Sigma # G-0625
L-Proline	7.76 mg/ml	7.76 µg/ml	Sigma # P-0380
Putrescine	16.1 mg/ml	16.1 µg/ml	Sigma # P-7505
Na-Selenite	0.016 mg/ml	0.016 µg/ml	Sigma # S-1382
Vit. B12	0.34 mg/ml	0.34 µg/ml	Sigma # V-2876
Zinc Sulfate	0.194 mg/ml	0.194 µg/ml	Sigma # Z-4750
Gluthation	1 mg/ml	1 µg/ml	Sigma # G-6013

SOD	2.5 mg/ml	2.5 µg/ml	Sigma # S-2515
Ethanol solutions	Stock solution.	Final conc.	Supplier
Linoleic acid	100 mg/ml	1 µg/ml	Sigma # L-1376
Linolen acid	100 mg/ml	1 µg/ml	Sigma # -2376
Progesterone	0.63 mg/ml	6.3 ng/ml	Sigma # P-8783
all trans Retinol	10 mg/ml	100 ng/ml	Sigma # R-7632
Retinylacetat	10 mg/ml	100 ng/ml	Sigma # R-7882
Tocopherol	100 mg/ml	1 µg/ml	Sigma # T-3251
Tocopherolacetat	100 mg/ml	1 µg/ml	Sigma # T-3001

For 400 ml complete medium, 1 gr BSA (Sigma # A-9418), 2 mg transferrin (Sigma # T-1147) and 1.6 mg Insulin (Sigma # I-6643) are dissolved in 30 ml DMEM and the remaining components are added. DMEM is added to final volume and medium is filtered and stored at 4°C for several weeks. Glutamine is added freshly before using the medium.

The *MECP2* mutant ES cell lines were a gift from Adrian Bird and Jacky Guy (Edinburgh, UK). ES cells were cultured and differentiated into neurons as described previously (Bibel *et al.*, 2007, Bibel *et al.*, 2004). Briefly, murine embryonic stem cells were grown on inactivated MEFs for 3-6 passages at 37°C (7% CO₂) in the ES medium containing Leukemia Inhibitory Factor (Bilguvar *et al.*), at 10³ unit/ml, to avoid the differentiation. Cells were splitted 1/10 every second day, the medium was changed every other day. ES cells were then passed on gelatin-coated dishes until no MEF were present. As soon as a homogeneous monolayer of ES cells was obtained, 4 million cells were plated on bacterial dishes (Greiner, Bio-one 94/16 with vents, # 633102) in EB medium where ES cells form cellular aggregates. Every second day the medium was changed, from day 4, after plating, retinoic acid (Sigma, # R-2625; final conc. 5 µM) was added to the medium. On day 8 the aggregates were dissociated with freshly prepared trypsin (Sigma, # T-8802; 0.05% trypsin in 0.04% EDTA/PBS) and the neuronal precursors plated on poly-D-ornitine (Sigma # P-8638) and laminin (Mencarelli *et al.*, 11234217001) coated 6-well plates (5 millions precursors in each well) in N2 medium. After 2 days the medium was replaced by complete medium.

2.1.3. Primary cortical neurons cultures

Cerebral cortex of E16 mouse embryos were dissected in PBS containing glucose (0.2%) and BSA (0.1%), and treated with 0.5% trypsin for 10 min at 37°C followed by mechanical dissociation. After centrifugation (5 min at 1'000 rpm), cells were plated in Neurobasal medium (Gibco # 21103), supplemented with B27 (Invitrogen # 080085-SA) 2%, glutamine 0.2 mM, and Pen/Strep (Invitrogen # 15140122) at a density of 125'000 cell/cm² in cell culture plates, with or without glass cover-slips, treated overnight with 100 µg/ml poly-L-lysine (Sigma # 25988-63-0).

2.1.4. Primary cortical glial cultures

Cerebral cortex of P2 mice were dissected in PBS containing glucose (0.2%) and BSA (0.1%), and treated with 0.5% trypsin for 10 min at 37°C followed by mechanical dissociation. After centrifugation (5 min at 1'000 rpm), cells from each brain were plated onto one 10-cm cell culture dish in the medium containing 20% FCS, 1% non-essential amino acids, 0.2 mM glutamine, DMEM and Pen/Strep. Lack of appropriate coating for neurons and usage of serum containing medium eliminate the chance of neuronal survival while it provides the condition for growth of glia. At the time of plating, the genotype of the pups was not known and tail samples were used for subsequent genotyping.

2.1.5. HEK-293 cells cultures

HEK-293 cells were cultured in EB medium containing 10% FCS, 1% non-essential amino acids, 0.2 mM glutamine, DMEM and Pen/Strep at 37°C (5% CO₂).

2.2. Western blot

Cells were collected ice cold PBS and lysed on ice for 30min using RIPA buffer (Tris-HCl 25 mM pH 8.0, NaCl 150 mM, Triton X-100 1%, Sodium Deoxycholate 1%, SDS 0.1%), containing protease inhibitors (Complete Protease Inhibitor Cocktail Tablets; Roche # 11697498001) and phosphatases inhibitors (Phosphatases inhibitors Cocktails 1 and 2, Sigma # P2850 & P5726). Supernatants were collected after 30 min centrifugation at 12'000g and protein concentration was determined by BCA assay (BCA Protein Assay, Pierce # 23225). Equal amounts of total protein were loaded and separated by electrophoresis using NOVEX 4-12% gradient SDS-polyacrylamide gels (Invitrogen # EC60352BOX), and transferred to nitrocellulose membranes (GE Biosciences # RPN3032D). For quantitative Western blotting, equal numbers of nuclei were loaded in the gel instead of equal amount of proteins. Primary antibodies and concentrations used are as follows:

Antibody	Dilution	Supplier
rabbit polyclonal anti-MeCP2	1:1'000	Millipore # 07-013
rabbit polyclonal anti-Histone H3	1:3'000	Abcam # ab7766
rabbit polyclonal anti-phospho- CREB	1:1'000	Upstate # 06-519
mouse monoclonal anti-phospho-ERK1/2	1:2'000	Cell Signal # 9102
mouse monoclonal anti-Synaptophysin	1:1'000	Sigma # S5768
mouse monoclonal anti-Actin	1:10'000	Sigma # A2228
mouse monoclonal anti- β -III-Tubulin	1:10'000	Covance # MMS-435P

Secondary antibodies coupled to horseradish peroxidase were used at a final concentration of 1:10'000. Membranes were developed using ECL (GE Biosciences # RPN2106), or ECL-Plus reagents (GE Biosciences # RPN2132). Densitometric quantification was performed with the free software ImageJ.

2.3. Quantitative real-time RT-PCR

Total RNA (0.5 µg) was extracted using RNeasy Plus Mini Kit (QIAGEN # 74134), reverse-transcribed using SuperScript-III Reverse Transcriptase (Invitrogen # 11754-050) and random primers (Invitrogen # AM5722G) according to manufacturer's instructions, and re-suspended in a final volume of 400 µl. qRT-PCR reactions were performed in a final volume of 25 µl containing TaqMan Universal Master Mix (Mencarelli *et al.*, 4304437), 5 µl cDNA, specific primer sets for the mouse *BDNF* gene (exon VIII) or mouse *GAPDH* gene at 0.9 µM, and specific TaqMan probes (5' modification: FAM and 3' modification: TAMRA) for each gene at 0.25 µM. The PCR was performed using an ABI Prism 7'000 Sequence Detection System (Applied Biosystems) in 96-Multiwell plates. The TaqMan primer/probes sets used are as follows:

Primer/Probe	Sequence
BDNF forward primer	5'-GGG AGC TGA GCG TGT GTG A-3'
BDNF reverse primer	5'-CGT CCC GCC AGA CAT GTC-3'
BDNF TaqMan Probe	5'-CGA GTG GGT CAC AGC GGC AGA-3'
GAPDH forward primer	5'- TGT GTC CGT CGT GGA TCT GA-3'
GAPDH reverse primer	5'-CCT GCT TCA CCA CCT TCT TGA-3'
GAPDH TaqMan Probe	5'- CCG CCT GGA GAA ACC TGC CAA GTA TG-3'

The specific levels of the BDNF transcript were normalized to the levels for GAPDH according to the C_t method, and statistical significance was determined by the Student's *t*-test method.

2.4. Cloning and lentivirus generation

To express the genes of interest with high efficiency in neuronal cultures a lentiviral system was used (Gascon *et al.*, 2008). For the biosafety reasons, the lentiviral system used is composed of 3 vectors. Two of these vectors (pMD2.G psPax2, kindly provided by Prof. Didier Trono, Ecole Polytechnique Fédérale de Lausanne, Switzerland) encode for the viral backbone and the third one, pLL-Syn-DsRed-Syn-EGFP (Figure 2-1), is the vector introducing the desired gene into the viral genome to be delivered and expressed in the neurons. The human synapsin promoter, a neuron specific promoter, was used to ensure the expression of the desired genes in neurons. The dual promoter nature of the virus makes it possible that at the same time the gene of interest i.e. *MECP2* and a reporter gene *EGFP* would be expressed. This way, efficiency of infection is monitored by assessing number of the cells expressing the EGFP protein under the fluorescence microscope.

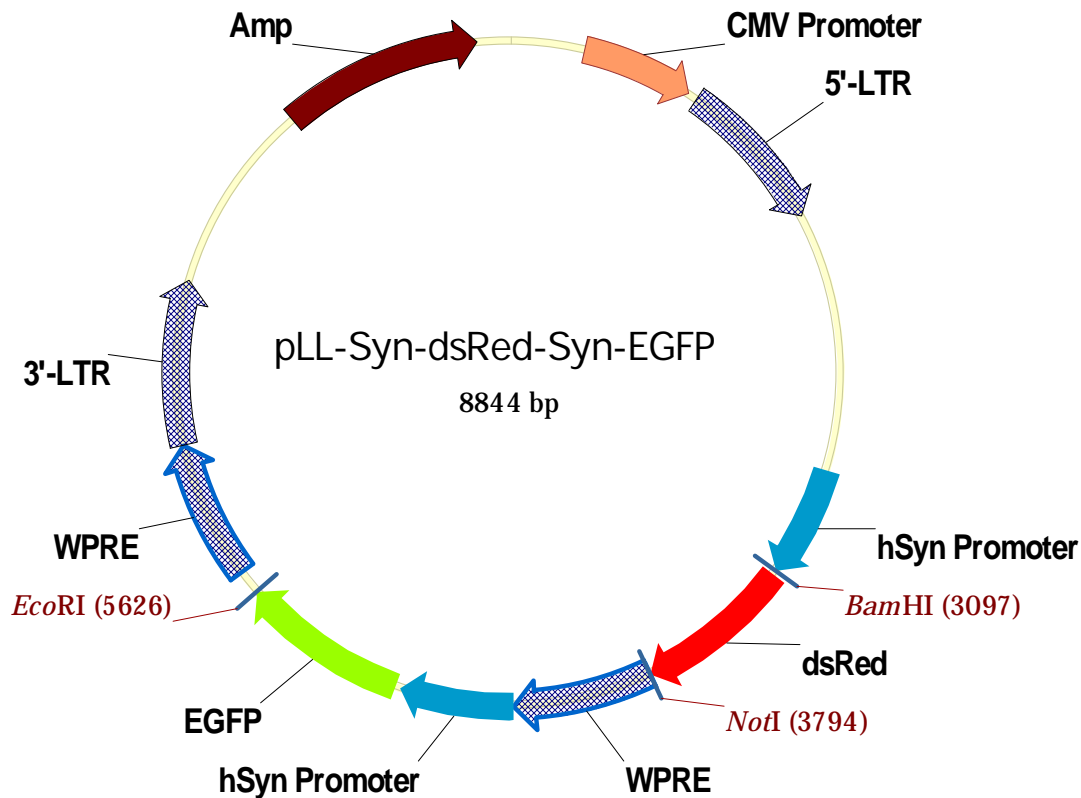


Figure 2-1 Schematic representation of the pLL-Syn-DsRed-Syn-EGFP lentiviral vector

In order to introduce our genes of interests into viral vector, the pLL-Syn-DsRed-Syn-EGFP was digested with BamHI & NotI which resulted in removal of DsRed.

To generate the pLL-Syn-CRE-Syn-EGFP, the CRE was amplified from the pcDNA-CRE. To make sure that the CRE enters into the nucleus of the neurons, Nuclear Localization Signal (NLS) of the SV40 T Antigen (PKKKRKV) was inserted into the N-terminal of the CRE right after the start codon. CRE contains a BamHI restriction site which would cause problem during the cloning procedure as the pLL-Syn-DsRed-Syn-EGFP was digested with the BamHI. Therefore, a BglIII restriction site was inserted into the amplifying primer of the CRE, as BglIII is compatible with BamHI. The CRE amplifying primers are as follows:

Primer	Sequence	Features
CRE forward Primer	5'-CG AGA TCT ATG <i>CCT AAG</i> <i>AAG AAG AGA AAG GTG</i> TCC AAT TTA CTG ACC GTA CAC CAA-3'	Bold letters: BglIII restriction site Italic letters encode for the SV40 Tag NLS
CRE reverse primer	5'-AA GCG GCC GCC TAA TCG CCA TCT TCC AGC AG-3'	Bold letters: NotI restriction site

After amplification with PCR, the PCR product was digested with BglIII and NotI and ligated with the digested vector.

To amplify the wild-type *MECP2*, the total RNA from the wild-type ES cell-derived neurons was extracted and reverse-transcribed into cDNA which was subsequently used in the PCR reaction as the template. To make the MeCP2 detection easier, both in the Western blot and in the immunostaining, I inserted a *c-myc* tag in the N terminal of the MeCP2. The following primer sets were used to amplify *MECP2*:

Primer	Sequence	Features
MeCP2 forward Primer	5'-CG AGA TCT ATG <i>GAA CAA AAA</i> <i>CTC ATC TCA GAA GAG GAT CTG</i> GTA GCT GGG ATG TTA GGG CTC AGG -3'	Bold letters: BglII restriction site Italic letters encode for the <i>c-myc</i>
MeCP2 reverse primer	5'- AA GCG GCC GCT CAG CTA ACT CTC TCG GTC ACG GG -3'	Bold letters: NotI restriction site

The MeCP2 S421A was generated using the site directed mutagenesis kit (Stratagene # 200518) according to the manufacturer's instructions. The primers used for mutagenesis are as follows:

Primer	Sequence
MeCP2 S421A forward	5'-CCC CGA GGA GGC GCA CTG GAA AGC GAT GGC TG-3'
MeCP2 S421A reverse	5'-CAG CCA TCG CTT TCC AGT GCG CCT CCT CGG GG-3'

Similar to the CRE, the PCR product was digested with BglII & NotI and ligated into the digested pLL-Syn-Syn-EGFP vector.

To produce the lentivirus, the 3 vectors were transfected in roughly 50% confluent HEK-293 cells using Fugene-6 reagent (Mencarelli *et al.*, 11814443001). Three days post transfection, lentiviruses were concentrated from the medium of HEK-293 cells using Lenti-X concentrator (Clontech # 631232), resuspended in the complete medium and kept at -80°C until used.

2.5. Assessment of the cell proliferation

For the ES cells, progenitors and neurons, the cells were washed with warm PBS and trypsinized and counted using a cell counter (NucleoCounter, Chemometec). For ES cells that had formed aggregate, they were trypsinized with freshly prepared trypsin (0.05% trypsin in 0.04% EDTA/PBS). EB medium was used to inactivate the trypsin and aggregates were further dissociated by pipetting up and down. The cells were then filtered using 40 μ m Nylon cell strainer (BD Falcon # 352340) and counted using the cell counter.

To assess the cell proliferation, 10 μ M BrdU (Sigma # B5002) was added to the cultures of progenitors, on glass coverslips, for a period of 30 minutes after which cells were washed once with warm PBS and fixed with 4% Paraformaldehyde (PFA) for 15 minutes at 37°C. The staining was done with the BrdU Detection Kit II (Mencarelli *et al.*, 11299964001) according to the manufacturer's instructions. The number of the cells with dark nuclei (stained for the BrdU incorporated in the nucleus) was divided to total numbers of the cells in each picture to calculate the percentage of the cells dividing within the BrdU pulse. Student *t*-test was used to perform the statistical analysis.

2.6. Immunostaining and nuclear size measurement

For immunocytochemistry (Ariani *et al.*), cells were grown on glass coverslips, washed twice with warm PBS, fixed for 15 minutes with 4% PFA at 37°C. Unspecific antibody binding was prevented with blocking solution (10% horse serum, 0.1% Tween 20 in PBS) for 1 hour at room temperature. The primary antibodies were added in the blocking solution and kept over night in the humid chambers at 4°C. Primary antibodies and dilutions used are as follows:

Antibody	Dilution	Supplier
rabbit polyclonal anti-MeCP2	1:200	Millipore # 07-013
mouse monoclonal anti-GFAP	1:500	Sigma # G3893
rat monoclonal anti-CD11b	1:1'000	Abcam # ab6332
mouse monoclonal anti- β -III-Tubulin	1:1'000	Covance # MMS-435P

Secondary antibodies coupled to the fluorophore were all used at a final concentration of 1:1'000.

For immunohistochemistry, animals were heavily sedated by intraperitoneal injection of Ketalar (Parke Davies, 5 mg/kg) / Rompun (Bayer Health Care, 100 mg/kg) and perfused transcardially with 4% PFA in 1x PBS. The brains were removed and kept in fixative over night. Serial coronal 15-20 μ m thick sections were obtained with a cryostat (Leica). The immunostaining of the brain sections has been performed similarly to that of cells in culture, starting with blocking.

The free software ImageJ was used for nuclear size measurement. All the pictures were taken with 40X objective in our fluorescence microscope. In the software setting, 1 pixel was set equal to 0.115 μ m. By putting a line around the hoechst nuclear staining the software calculates the surface of the nuclei automatically and student *t*-test was used for statistical analysis.

2.7. Nuclei purification and in vitro transcription assay

2.7.1. Nuclear purification from cultured cells

Cell were washes twice with ice cold PBS and then collected with 1 ml of PBS containing the complete protease inhibitor (Mencarelli *et al.*) using a cell scraper. Cells

were transferred to an eppendorf tube and collected with centrifugation at 800 g for 5 minutes. To lyse the cell membrane, the cellular pellets were resuspended in 10X volume of 250-STM, 0.1% NP40 (250 mM sucrose, 50 mM Tris-HCl (pH 8.0), 5 mM MgCl₂ and complete protease inhibitor) and kept on ice for 10 minutes then centrifuged at 800g for 10 minutes. The pellet contains the nuclei and some cellular organelles. To get rid of these organelles and obtain highly pure nuclei, the nuclear pellets were resuspended in 1 ml of 2M-STM (2 M sucrose, 50 mM Tris-HCl (pH 8.0), 5 mM MgCl₂, and complete protease inhibitor) and centrifuged at 65'000g for 30 minutes. The pellet consists of highly purified nuclei.

2.7.2. Nuclear purification from tissue

Animals were scarified using CO₂, the brain was taken out and the cerebral cortex isolated on ice cold metal block. The cerebral cortex then was sliced using a razor on the ice cold metal block until it lost its structure and became very soft and immediately transferred to a 2 ml glass douncer (Wheaton, USA) and homogenized in the presence of 1 ml of 250-STM, 0.5% NP40 (250 mM sucrose, 50 mM Tris-HCl (pH 8.0), 5 mM MgCl₂ and complete protease inhibitor) by 10 time up and down of the pistol. This mixed was transferred to an eppendorf tube and kept on ice for 10 minutes. After 10 minutes of centrifugation at 800 g, the pellet was resuspended in 1 ml of 2 M-STM (2 M sucrose, 50 mM Tris-HCl (pH 8.0), 5 mM MgCl₂, and complete protease inhibitor) and centrifuged at 65'000 g for 30 minutes. The pellet consists of highly purified nuclei (Figure 2.2).

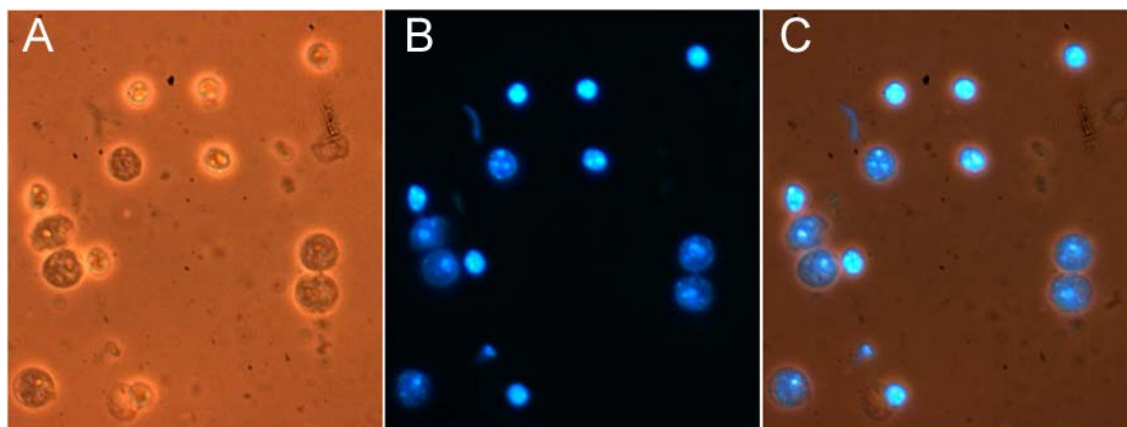


Figure 2-2 Purified nuclei from cerebral cortex. Cerebral cortical nuclei were purified as described above and nuclei purity was assessed. (A) Phase contrast image of the purified nuclei (B) Hoechst staining of the nuclei (C) The Hoechst staining overlaps with the phase contrast boundaries of nuclei proving absence of cellular debris and high purity of the nuclei preparation

2.7.3. In vitro transcription

The nuclear pellets were resuspended in 600 μL 2X elongation buffer (100 mM Tris-HCl (pH 8.0), 5 mM MgCl_2 , 5 mM MnCl_2 , β -mercaptoethanol 10 mM and complete protease inhibitor). A dilution series of the nuclei was made for counting from 100 μL of the purified nuclei. The nuclei were counted using the cell counter (NucleoCounter, Chemometec). The number of the nuclei was adjusted, with 2X elongation buffer, to have desired numbers in 100 μL e.g. 250'000 nuclei in 100 μL . The *in vitro* transcription started by addition of 100 μL of the nuclei to 100 μL of the reaction mixture (ATP, CTP and GTP ribonucleotides each at a final concentration of 0.6 mM, 1 μCi of [^{32}P]-UTP, 40 units of RNase Inhibitor (Roche) in water). The reaction was performed at 37°C for 0, 30 or 45 minutes. The reaction was stopped by addition of 800 μL of TRIzol (Invitrogen) to each tube. The RNA purification was performed according to the manufacturer's instructions (TRIzol, Invitrogen). The radioactivity incorporated into total RNA was measured using tri-carb liquid scintillation counter (Packard) and student *t*-test used for the statistical analysis.

2.8. Animal work

2.8.1. MECP2 mutant mice

I used the *MECP2* mutant mice generated by Adrian Bird (Guy *et al.*, 2001). The mice were obtained from the Jackson Laboratory (stock number 003890; B6.129P2(C)-*Mecp2*^{tm1.1Bird/J}) and registered in the Biozentrum central animal facility as the code 20250. As the male hemizygote mutants (*MECP2* -/y) are sterile, the mating scheme is to breed wild-type B6 males with heterozygote (*MECP2* +/-) females. As the *MECP2* gene is located on the X chromosome in mice, like in humans, the offspring have one of the following genotypes: ♂ *MECP2* +/y, ♂ *MECP2* -/y, ♀ *MECP2* +/+ or ♀ *MECP2* +/- . The male knock-outs were used for the experimental purposes and their wild-type littermates as control. The heterozygote females were used for mating. The genotyping was done according to the protocol provided by the Jackson Laboratory for this line. All the experiment involving usage of wild-type and mutant mice were done under the official permission from the Basel Cantonal Veterinary (the code of approved permission: 2299).

2.8.2. BDNF ELISA measurements

After sacrifice (see above), brains were removed and dissected to various parts on an ice cold metal block. Various parts were immediately shock frozen in the liquid nitrogen and stored at -80°C until used.

The ELISA assays were performed using an optimized version of the protocol established in our laboratory (Kolbeck *et al.*, 1999).

2.8.3. Running wheel assay

To assess the locomotor performance of the mice, we used the running wheel assay. In this assay, mice are kept in the cages that contain a running wheel. This wheel is connected to a computer recording the distance ran by the mice. 3 days prior to start of experiment mice were moved to these cages to learn how to use the wheel and also get used to the environment of the new cage. Data on the running distances were automatically calculated and saved by the computer and student *t*-test used for the statistical analysis.

3. Results

3.1. Neuronal differentiation of *MECP2* mutant ES cell lines

All *MECP2* mutant ES cell lines were kindly provided by the group of Dr. Adrian Bird, University of Edinburgh, UK (Guy *et al.*, 2007, Guy *et al.*, 2001). All the mutations were generated in male (XY) E14 ES cells background used as wild-type control in all the experiments.

3.1.1. *MECP2* mutant ES cell lines

The *MECP2* gene contains 4 exons. Exon 1 codes for 24 amino acids, exon 2 encodes for 9 amino acids, exon 3 encodes for 117 amino acids and the exon 4 encodes for the rest of the 357 amino acids as well as for the 3'UTR (Figure 3.1).

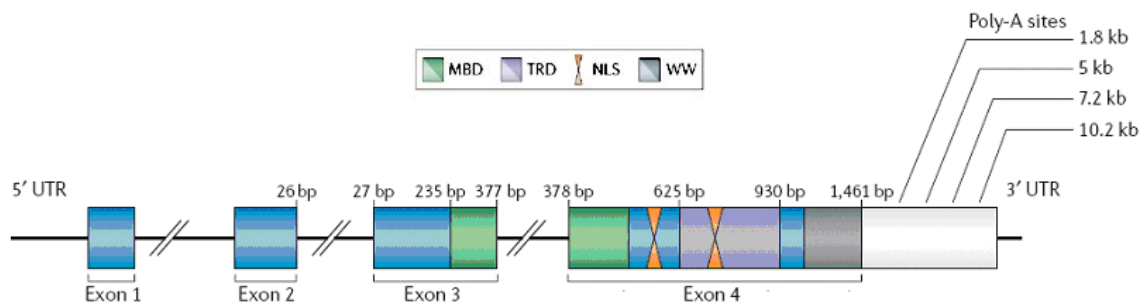


Figure 3-1 *MECP2* gene structure. Part of methyl-binding domain (MBD) is coded by the exon 3 and the rest by the exon 4. The transcriptional repressor domain (TRD) is entirely coded by the exon 4 as well as both of the nuclear localization signals (NLS)

Part of the methyl-binding domain (MBD) (Nan *et al.*, 1997, Nan *et al.*, 1993) is coded by exon 3 and the rest by exon 4. The transcriptional repressor domain (TRD) (Nan *et al.*, 1997) is entirely coded by the exon 4. In addition, both of the known nuclear localization signals of MeCP2 are encoded by exon 4. Considering the very small size of the first two exons of *MECP2* and the fact that most of the protein, as well as all the well known functional domains are located in the exons 3 & 4, Guy and colleagues decided to flank the exon 3 and the entire protein coding part of the exon 4 by 2 loxP sites (Guy *et al.*, 2001). This led to the generation of a floxed allele of the *MECP2* (*MECP2* loxP/y). Upon Cre treatment of the loxP allele, a null allele of *MECP2* was generated (*MECP2* -/y) (Figure 3.2).

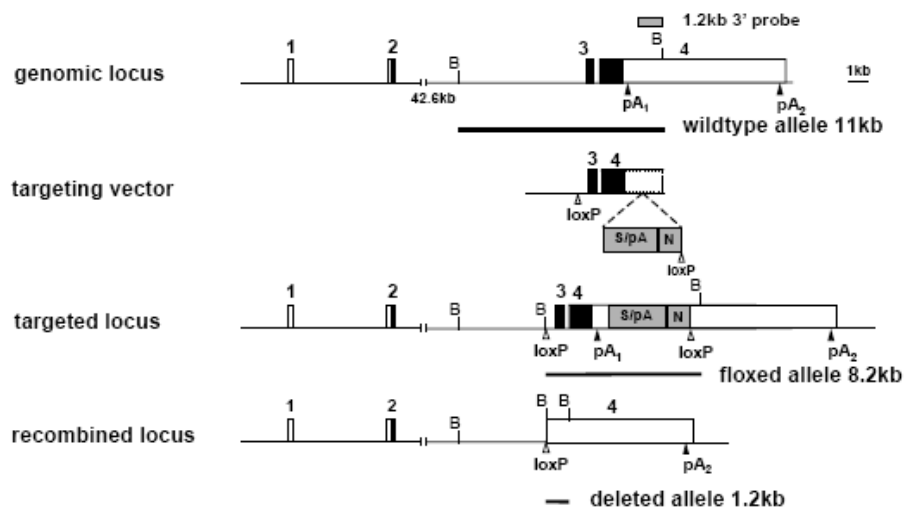


Figure 3-2 Targeting strategy of the *MECP2* gene to generate the flox and the null alleles (Adapted from Guy *et al.*, 2001)

For the reversal experiment (see introduction), Guy and colleagues inserted a stop cassette (both transcriptional and translational) flanked by 2 loxP sites between exon 2 and 3 (Guy *et al.*, 2007). This led to generation of *MECP2* Stop/y allele in which the stop cassette prevents the expression/translation of the MeCP2 transcript. Upon Cre treatment of the *MECP2* Stop/y allele, the stop cassette is removed leading to a re-expression from the endogenous promoter (Figure 3.3).

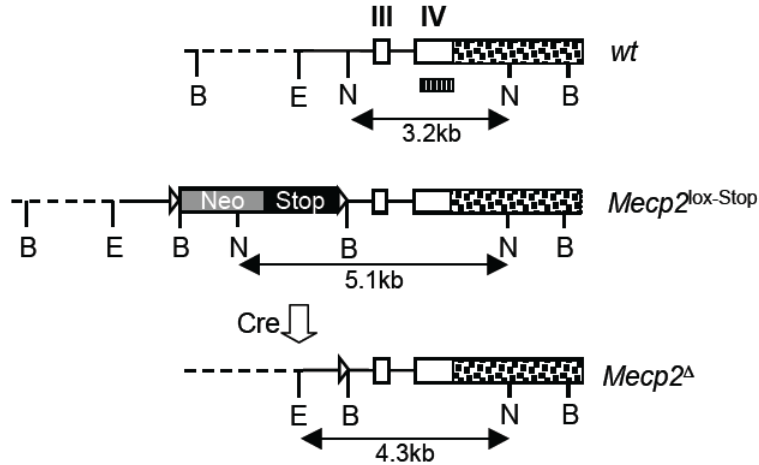


Figure 3-3 Targeting strategy of the *MECP2* gene to generate the lox-Stop allele (Adapted from Guy *et al.*, 2007)

3.1.2. Neuronal differentiation of various *MECP2* mutant ES cells

The four ES cell lines (wild-type, *MECP2* loxP/y, *MECP2* -/y and *MECP2* Stop/y) were differentiated into neurons according to the protocol of Bibel *et al.*, 2004 and Bibel *et al.*, 2007.

Regardless of the type of mutation, differentiation of all the four ES cell lines resulted in highly pure neuronal cultures which could be maintained easily for as long as one month without any obvious degeneration. The levels of synaptophysin, a synaptic vesicular protein widely used as a marker of synapse formation and neuronal maturation (Calhoun *et al.*, 1996), were assessed in the neuronal cultures obtained from *MECP2* loxP/y and *MECP2* -/y ES cells. Western blots were performed with cells lysed at day 4, 7, 14 and 21 after dissociation of the cellular aggregates, by loading equal quantities of protein lysates from each sample. In both cultures, regardless of presence or absence of MeCP2, there is significant increase in the expression of synaptophysin between the first and the second week, indicating both wild-type and mutant neurons mature following a similar time course (Figure 3.4).

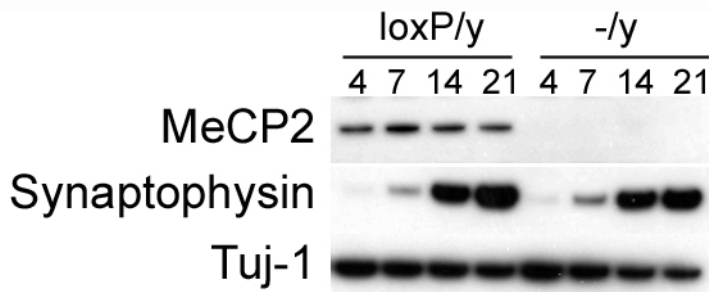


Figure 3-4 Both *MECP2* loxP/y and *MECP2* -/y neurons mature similarly in culture. Equal amounts of protein lysates from *MECP2* loxP/y and *MECP2* -/y ES cell-derived neurons at different ages (4, 7, 14 and 21 DIV) were loaded in the SDS-gel and the expression of MeCP2 and Synaptophysin were assessed by immunoblotting. Tubulin β -III (Tuj-1) is used as the loading control

To assess the expression levels of MeCP2 in neurons generated from various ES cell lines, Western blot analysis were performed with equal amounts of protein lysates obtained from the 2-weeks-old neuronal cultures (Figure 3.5).

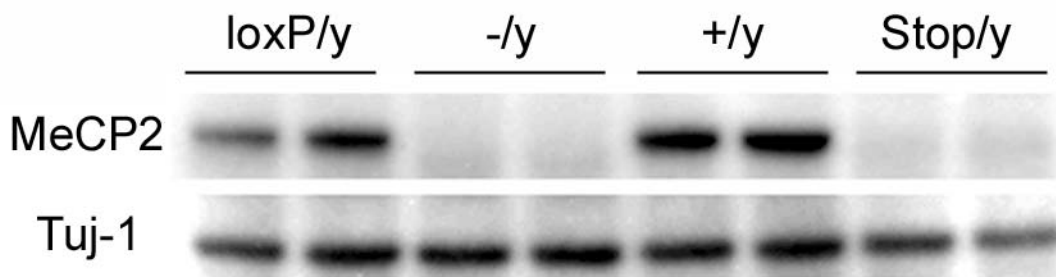


Figure 3-5 Expression of MeCP2 at protein levels in neurons generated from 4 ES cell lines with various mutations in the *MECP2* gene. Equal amounts of protein lysates from wild type (*MECP2* +/y), *MECP2* -/y, *MECP2* loxP/y and *MECP2* Stop/y ES cell-derived neurons were loaded in the Western blot gel and the levels of MeCP2 were assessed by immunoblotting. Tubulin β -III (Tuj-1) is used as the loading control

As expected, the wild-type (*MECP2* +/y) ES cell-derived neurons have the highest expression of the MeCP2 while the *MECP2* -/y neurons do not express any detectable

MeCP2. The *MECP2* Stop/y neurons express very little, if any, MeCP2 which shows that the floxed-stop cassette inserted into the gene functions efficiently in preventing the expression of MeCP2. Interestingly, the *MECP2* loxP/y neurons express MeCP2 at lower levels compared with wild-type neurons. This could be explained by the fact that to generate the floxed allele of *MECP2*, a neomycin selection cassette (Figure 3.2) was inserted into the 3'UTR of the gene in the exon 4 which led to the disruption of the 3'UTR (Guy *et al.*, 2001). This in turn could affect the translation efficiency/stability of the MeCP2 mRNA. In line with this, mice harboring this allele display abnormalities such as learning and motor deficits, decreased anxiety, altered social behavior and disrupted breathing patterns (Samaco *et al.*, 2008).

3.2. Progenitors lacking MeCP2 produce fewer neurons

Despite the normal appearance of neuronal cultures generated from the *MECP2* mutant ES cells, the *MECP2* -/y neuronal cultures always ended up at a lower density than wild-type cultures, in spite of identical plating densities. As it has been reported that *MECP2* mutant lymphocytes obtained from the human RTT patients proliferate slower than wild-type lymphocytes (Balmer *et al.*, 2002), I checked the effect of the lack of MeCP2 on cell proliferation.

3.2.1. Loss of *MECP2* does not affect the growth of ES cells

Two wild-type ES cell lines (R1 and E14) and 2 different clones of *MECP2* -/y ES cells were used to make sure that the data obtained on proliferation are solely due to presence or absence of MeCP2 rather than any line or ES cell clone-specific behavior. Proliferation of ES cells were measured at two stages of differentiation: ES cells in monolayer and the cellular aggregate stage (Bibel *et al.*, 2007, Bibel *et al.*, 2004)

After the third passage on gelatin coated plates (see materials and methods), equal numbers of ES cell (7.5 millions), from each genotype (wild-type and *MECP2* *-/y*) were plated in 10-cm dishes in quadruplicate. Forty eighth ours later, the numbers of ES cells produced were counted using a cell counter. Interestingly, proliferation of ES cells lacking MeCP2 was not significantly different from the wild-type ES cells (wild-type: 62.44 million \pm 2.871 millions, N = 8, *MECP2* *-/y*: 66.81 millions \pm 1.562 millions, N = 8, *P* = 0.0654, Student *t*-test).

Similarly, cellular aggregates were generated from equal numbers of both wild-type and *MECP2* *-/y* ES cells and the number of the cells counted after 2, 4 and 8 days (Table 3.1).

Table 3-1 Proliferation of wild-type and *MECP2* *-/y* mutant ES cells assessed at aggregate stage. Number of the cells (shown in millions) generated from 4 millions ES cells after 2, 4 and 8 days were counted and the data shown as mean \pm S.E.M

	Day 2 (N=3)	Day 4 (N=3)	Day 8 (N=4)
Wild-type	29.27 \pm 1.67	23.00 \pm 0.577	24.13 \pm 1.375
<i>MECP2</i> <i>-/y</i>	29.00 \pm 0.577	24.33 \pm 1.856	20.10 \pm 2.050

These experiments revealed that the lack of MeCP2 does not affect the proliferation of ES cells at the stage of cellular aggregates (Figure 3.6). However, the number of cells obtained from the *MECP2* *-/y* ES cells at 8 days i.e. 4 days post-treatment with retinoic acid, was slightly less than number of cells generated from wild-type ES cells, although the differences do not reach statistical significance (Figure 3.6).

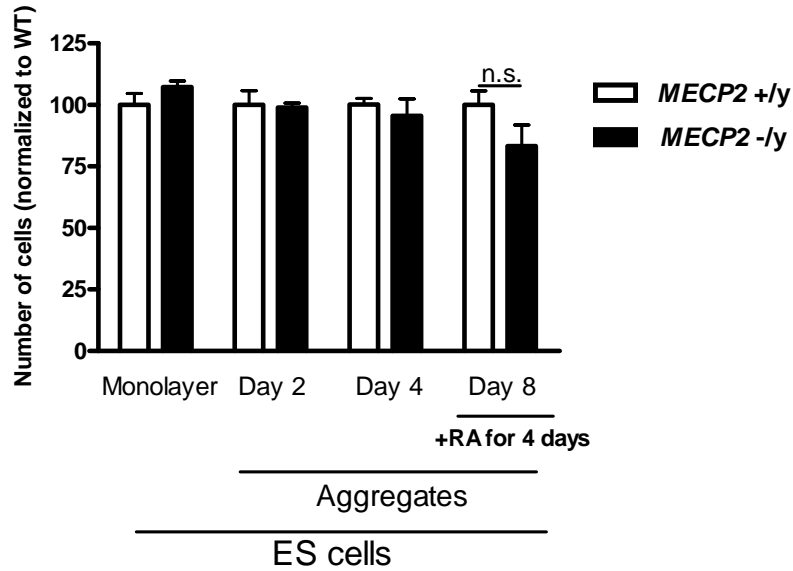


Figure 3-6 Proliferation of ES cells, both in monolayer and in cellular aggregate stage, is not affected by presence or lack of MeCP2. Cell numbers at each stage were normalized to the values obtained from wild-type ES cells and shown as mean \pm S.E.M

ES cells were found to express very low levels of MeCP2 compared to neurons (Figure 3.7.A) and retinoic acid treatment to significantly induce the expression of MeCP2 (Figure 3.7.B).

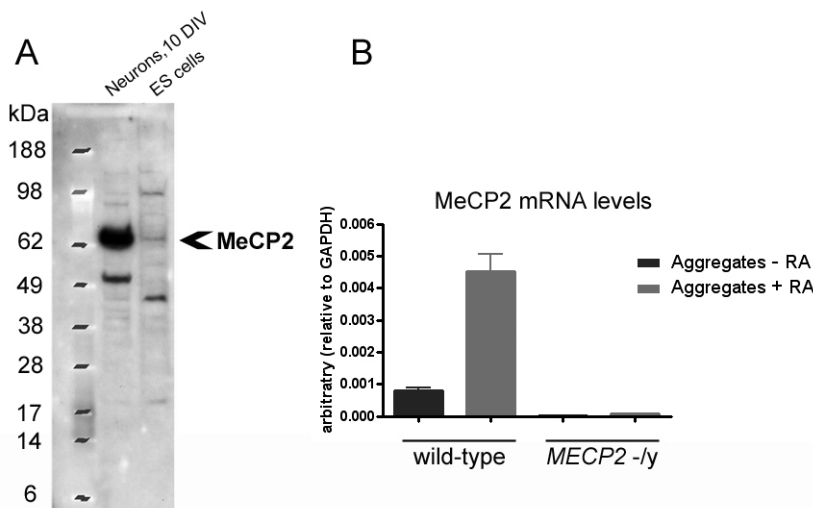


Figure 3-7 MeCP2 expression in ES cells in monolayer and cellular aggregate stages and in ES cell-derived neurons (A) Western blot analysis with one million purified nuclei from 10 DIV ES cell-derived

neurons and ES cells in monolayer (before aggregation) show significantly lower levels of MeCP2 expression in ES cells compared to the neurons. The arrow head points to the band corresponding to the MeCP2 protein (B) MeCP2 mRNA levels measured by quantitative real-time RT-PCR in cellular aggregates before and 4 days after treatment with retinoic acid shows a significant induction of MeCP2 expression by retinoic acid treatment (values shown as mean \pm S.E.M, N=3)

3.2.2. Progenitors lacking MeCP2 generate fewer neurons compared with wild-type cells

As the absence of MeCP2 had no effect on proliferation of ES cells, the question arose if the proliferation of neuronal progenitors would be affected compared with wild-type cells. Indeed, before neuronal differentiation, the ES cell-derived progenitors go through one or even 2 rounds of cell division. Wild-type and *MECP2* *-/-* aggregates were dissociated at day 8 and 5 millions progenitors were plated onto poly-ornitin/laminin coated plates. Subsequently, the cultures were trypsinised at different time points and the number of cells was counted using a cell counter. While after 6 days the number of neurons generated from wild-type ES progenitors was significantly higher than the starting cell number plated (Table 3.2), the number of neurons generated from *MECP2* *-/-* progenitors was not.

Table 3-2 Effect of lack of MeCP2 on proliferation of the neuronal progenitors. Number of cells (millions) generated from the initial 5 millions of progenitors plated at DIV 0 from both genotypes; wild-type and *MECP2* *-/-*. In all case the values are shown as mean \pm S.E.M, N= 6

	Day 0	Day 1	Day 2	Day 3	Day 6
Wild-type	5	4.70 \pm 0.11	6.63 \pm 0.41	8.52 \pm 0.22	8.80 \pm 0.39
<i>MECP2</i> <i>-/-</i>	5	3.31 \pm 0.37	4.00 \pm 0.64	4.62 \pm 0.79	4.44 \pm 0.72

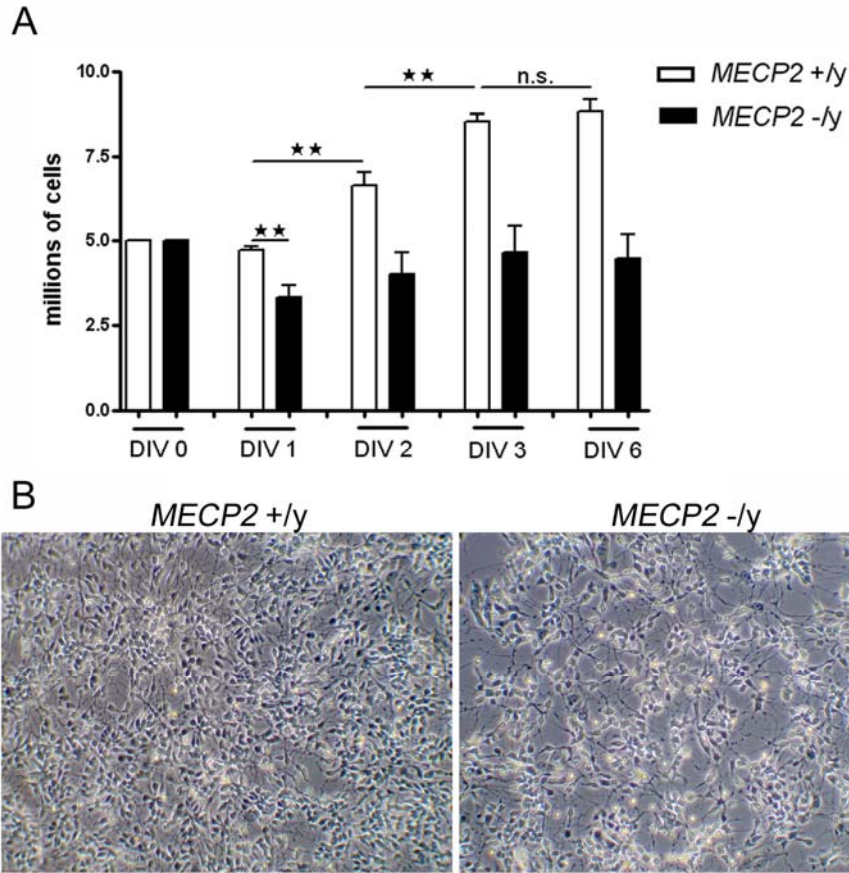


Figure 3-8 MeCP2-deficient neuronal progenitors produce fewer neurons than wild-type progenitors.

(A) The number of cells almost double after plating wild-type progenitors while this increase is absent in cells lacking MeCP2 (mean \pm S.E.M, $**P < 0.01$, Student *t*-test) (B) Phase contrast picture of wild-type and MeCP2-deficient progenitors at DIV 1

The increase in the cell number of the wild-type progenitors coincides with a marked increase in the expression of MeCP2 at the protein levels (Figure 3.9).

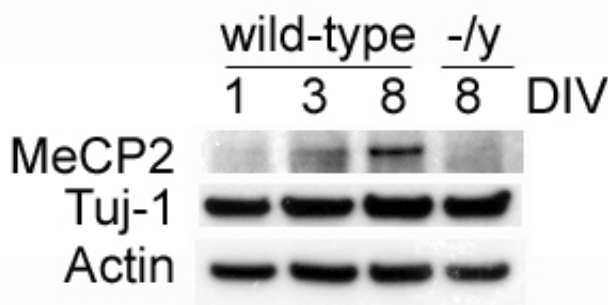


Figure 3-9 MeCP2 expression increases with neuronal maturation. Equal amounts of wild-type ES cell-derived neuron lysates (1, 3 and 8 DIV) were loaded on SDS-gel and MeCP2 expression was assessed by immunoblotting. A significant increase in the expression of MeCP2 during the first week post-dissociation of aggregates is evident. The Actin and Tuj-1 were used as loading controls

3.2.3. Neuronal progenitors lacking MeCP2 proliferate less than wild-type progenitors

In addition to reduced proliferation of progenitors, the smaller number of neurons generated from the *MECP2* $-/y$ ES cells could also be explained by increased cell death. However, as RTT brains show no obvious degeneration or atrophy (Chahrour and Zoghbi, 2007), I then decided to assess the effect of lack of MeCP2 on proliferation. Two hours after dissociation, cultures of wild-type and *MECP2* $-/y$ progenitors were exposed to 30 minutes of BrdU pulse, a modified analogue of cytosine that is only incorporated in the nuclei of dividing cells. Cells were then fixed and stained with an antibody against BrdU. Quantification of the BrdU labeling shows that while more than half of the cells in wild-type cultures incorporate BrdU within 30 minutes pulse, much fewer (almost 27%) of the *MECP2* $-/y$ progenitors incorporate the BrdU (Figure 3.10).

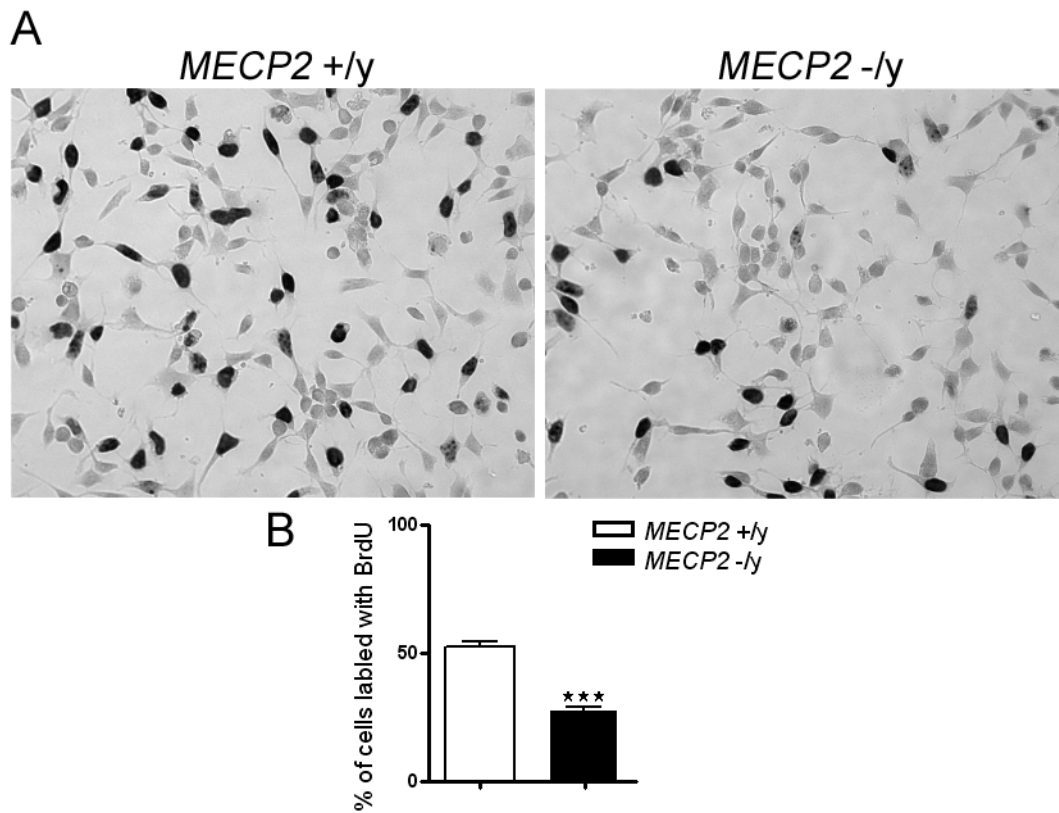


Figure 3-10 Proliferation defect of the MeCP2-deficient neuronal progenitors. (A) Phase contrast image of wild-type (*MECP2* $+/y$) and *MECP2* $-/y$ progenitors pulsed with BrdU for 30 minutes, 2 hours

post-dissociation. The dark labelled nuclei are those that have incorporated BrdU (B) To quantify the percentage of the cells incorporating BrdU, the number of cells with dark nuclei was divided by the total number of cells (mean \pm S.E.M, *** $P < 0.0001$, Student *t*-test)

3.3. *MeCP2 regulates the size of neuronal nuclei*

Beside their lower density, the neurons obtained from the *MECP2* $-/-$ ES cells looked very similar to wild-type neurons. However, closer examination revealed that they have smaller nuclei compared with the wild-type neurons. As MeCP2 is a nuclear protein and the size and shape of nuclei is thought to have a direct correlation with chromosome localization and gene expression (Trinkle-Mulcahy and Lamond, 2008), I decided to assess the regulation of neuronal nuclear size by MeCP2 in more detail. While, this phenotype has already been reported in some brain areas of mice lacking MeCP2 (Chen *et al.*, 2001), this aspect of MeCP2 research has not been followed up. In particular, it is unknown if it affects only neurons or other cell types, if it is cell autonomous or not, or even if it appears during development or it is part of a regressive event occurring only after the disease begins to be established.

3.3.1. Nuclei lacking MeCP2 fail to grow during neuronal maturation

The size of nuclei was determined at day 3, as by this time most progenitors have already dropped out of the cell cycle so I would avoid any variation in the nuclear size as a result of the mitosis. 8 days was chosen as the time point representing young neurons (Figure 3.4) and 26 days mature neurons. During the transition from progenitors to young neurons a significant increase in the size of neuronal nuclei was found in wild-type neurons (Table 3.3). The nuclei of the wild-type neurons continue growing with maturation as the nuclei of the 26 days *in vitro* (DIV) old wild-type neurons were again significantly bigger than the nuclei of the 8 DIV neurons.

When measured at 3 days *in vitro* culture, the nuclei of the *MECP2* *-/y* neurons were of the same size of aged matched wild-types but at 8 days *in vitro* culture while the nuclei of the wild-types had enlarged significantly, the nuclei of the *MECP2* *-/y* neurons failed to grow (Figure 3.11) and remained at the same size as the nuclei of the 3 days *in vitro* neurons.

Table 3-3 Quantification of nuclear size of wild-type and *MECP2* *-/y* neurons (mean \pm S.E.M)

	DIV 3	DIV 8	DIV 26
<i>MECP2</i> <i>+/y</i>	19.67 $\mu\text{m}^2 \pm 0.4072 \mu\text{m}^2$	27.78 $\mu\text{m}^2 \pm 0.3033 \mu\text{m}^2$	31.68 $\mu\text{m}^2 \pm 1.186 \mu\text{m}^2$
<i>MECP2</i> <i>-/y</i>	19.97 $\mu\text{m}^2 \pm 0.3869 \mu\text{m}^2$	19.32 $\mu\text{m}^2 \pm 0.1902 \mu\text{m}^2$	23.40 $\mu\text{m}^2 \pm 0.677 \mu\text{m}^2$

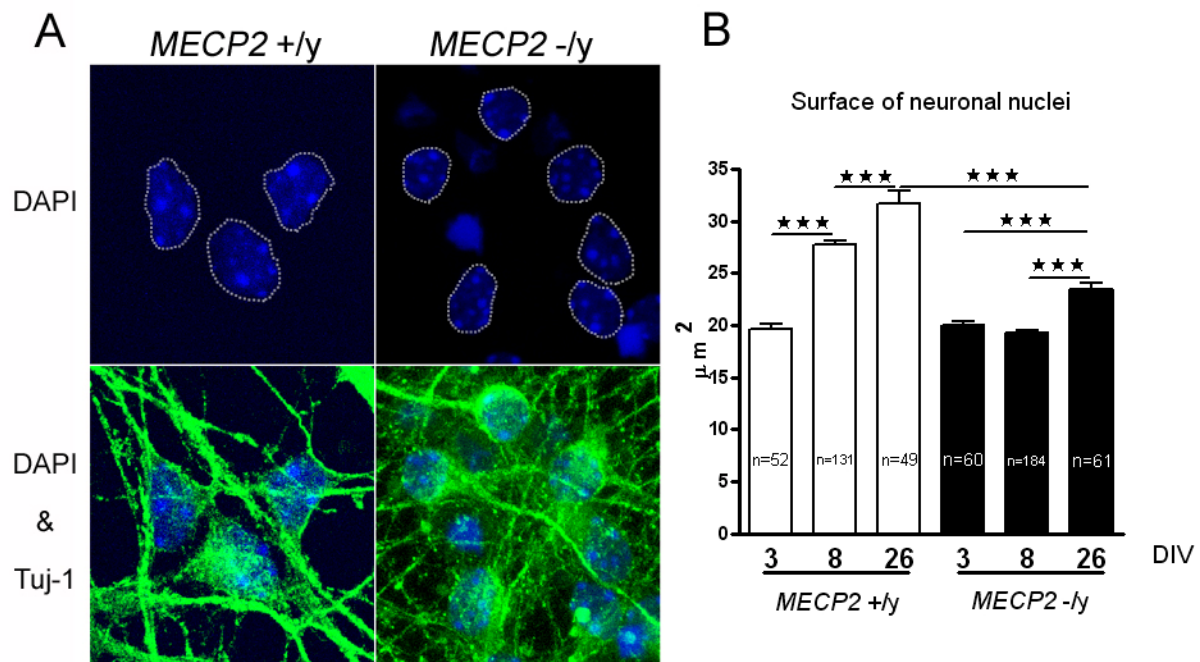


Figure 3-11 Nuclei of the *MECP2* *-/y* neurons fail to grow. (A) ES cell-derived neurons were stained at DIV 8 with antibodies against the neuron specific marker Tuj-1 and the 4',6-diamidino-2-phenylindole (DAPI), a fluorescent dye that binds to DNA. DAPI staining shows that the nuclei of the *MECP2* *-/y* neurons are smaller than wild-types (B) Quantification of nuclear surface of neurons during the course of neuronal maturation (mean \pm S.E.M, *** $P < 0.0001$, Student *t*-test)

The increase in the nuclear size of wild-type neurons from day 3 to 8 is accompanied with a significant increase in the expression of MeCP2 (Figure 3.9). During this time period, the size of mutant nuclei remains constant.

3.3.2. Nuclear size of ES cell-derived neurons correlates with their levels of MeCP2

At 3 days *in vitro*, the nuclei of neurons generated from either wild-type or the 3 mutant ES lines were essentially of the same size (Table 3.4). But, at 8 days *in vitro*, the *MECP2* *-/y* and *MECP2* Stop/*y* both had smaller nuclei compared to the wild-type neurons. The size of the nuclei of *MECP2* loxP/*y* neurons was between that of wild-type and *MECP2* *-/y* (Figure 3.12).

Table 3-4 Quantification of nuclear sizes of ES cell-derived neurons with various mutations in *MECP2* at DIV 3 and 8 (mean \pm S.E.M)

	DIV 3	DIV 8
<i>MECP2</i> <i>+/y</i>	19.50 $\mu\text{m}^2 \pm 0.3326 \mu\text{m}^2$	27.64 $\mu\text{m}^2 \pm 0.2648 \mu\text{m}^2$
<i>MECP2</i> <i>-/y</i>	19.96 $\mu\text{m}^2 \pm 0.4292 \mu\text{m}^2$	19.18 $\mu\text{m}^2 \pm 0.159 \mu\text{m}^2$
<i>MECP2</i> loxP/ <i>y</i>	20.46 $\mu\text{m}^2 \pm 0.373 \mu\text{m}^2$	24.51 $\mu\text{m}^2 \pm 0.4331 \mu\text{m}^2$
<i>MECP2</i> Stop/ <i>y</i>	20.56 $\mu\text{m}^2 \pm 0.3829 \mu\text{m}^2$	20.15 $\mu\text{m}^2 \pm 0.3970 \mu\text{m}^2$

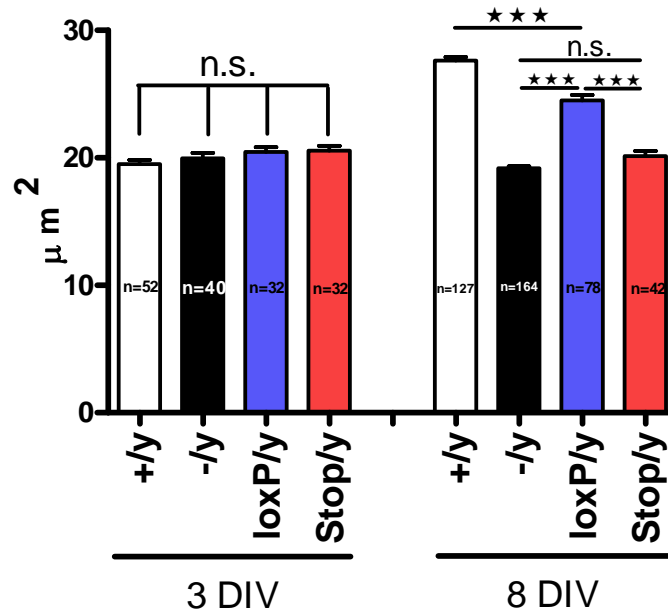


Figure 3-12 The size of nuclei in ES cell-derived neurons correlates with their levels of MeCP2. Quantification of nuclear size of wild-type and *MECP2* mutant neurons during the course of neuronal maturation (mean \pm S.E.M, *** $P < 0.0001$, Student *t*-test)

3.3.3. Primary neurons of *MECP2*-deficient mice have smaller nuclei

To check whether the small nuclei phenotype related to the absence of MeCP2 can also be observed in primary cultures, neurons were dissociated from the cerebral cortex of wild-type and *MECP2* *-/y* embryos (see Materials and Methods) and nuclear size determined.

Cortex of E16 embryos were dissected one by one and genotyping performed on tails of embryos after plating. After 16 days *in vitro*, the nuclei of *MECP2* *-/y* cortical neurons ($30.19 \mu\text{m}^2 \pm 0.7291 \mu\text{m}^2$; N = 49) were significantly smaller than that of wild-type ($38.61 \mu\text{m}^2 \pm 1.159 \mu\text{m}^2$; N = 26) cortical neurons (Figure 3.13).

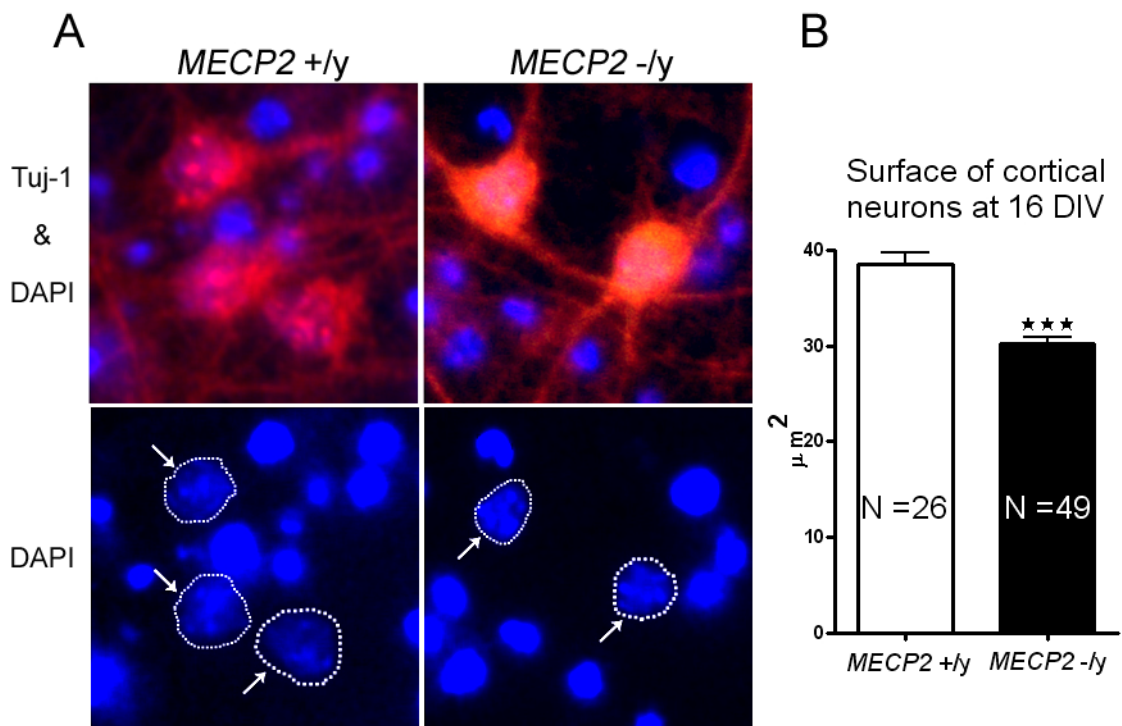


Figure 3-13 MeCP2-deficient cortical neurons have small nuclei. (A) Cortical neurons dissociated from brains of wild-type and *MECP2* *-/y* embryos were stained with antibodies against the neuron specific marker Tuj-1. The nuclei were stained with DAPI. Smaller nuclei of the *MECP2* *-/y* cortical neurons in 16 DIV cultures is evident compared to the wild-types (B) Quantification of nuclear size of wild-type and *MECP2* *-/y* neurons at 16 DIV (mean \pm S.E.M, *** $P < 0.0001$, Student *t*-test)

MeCP2 levels were also assessed by Western blot analysis in 8 DIV wild-type ES cell-derived neurons compared with 16 DIV cortical neurons (Figure 3.14). They were found to be comparable.

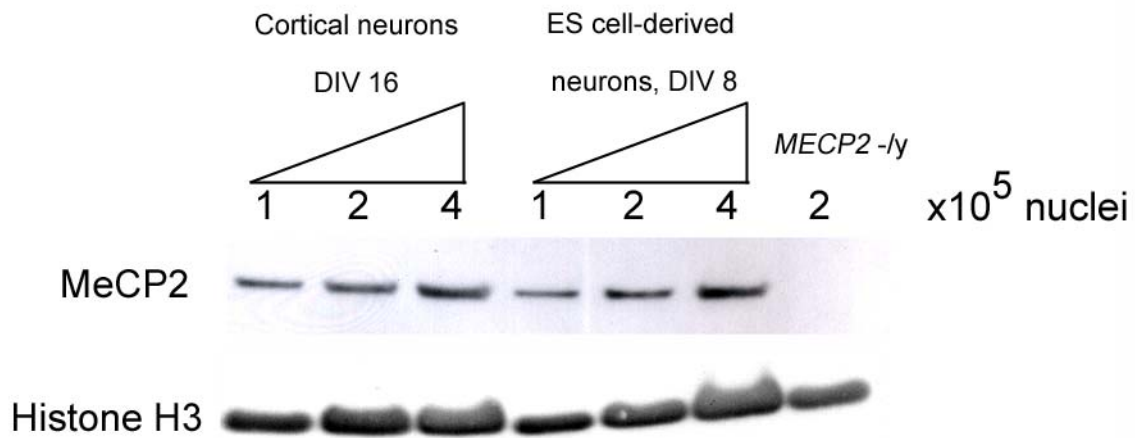


Figure 3-14 Similar levels of MeCP2 in wild-type cortical and ES cell-derived neurons. Western blot analysis on 0.1, 0.2 and 0.4 million purified nuclei comparing the levels of MeCP2 amongst wild-type ES cell-derived neurons at 8 DIV and cortical neurons at 16 DIV. *MECP2* ^{-/y} neuronal lysates were used as negative control for MeCP2 detection. The histone H3 was used as a loading control.

3.3.4. Re-expression of MeCP2 rescues the small nuclei phenotype

As the lack of MeCP2 both in ES cell-derived neurons and cortical neurons was found to be associated with small nuclei phenotype, re-expression of MeCP2 was then attempted. Infection of *MECP2* ^{Stop/y} neurons by Cre-encoding lentiviruses was used for this purpose. MeCP2 re-expression was then assessed by Western blot analysis (Figure 3.15). *MECP2* ^{Stop/y} neurons that were infected with the Cre lentivirus at DIV 2 had significantly bigger nuclei than the neurons that were infected with GFP-encoding lentivirus at DIV 8 (GFP virus infected: $22.01 \mu\text{m}^2 \pm 0.4949 \mu\text{m}^2$; N = 49, Cre virus infected: $31.87 \mu\text{m}^2 \pm 0.8158 \mu\text{m}^2$; N = 51).

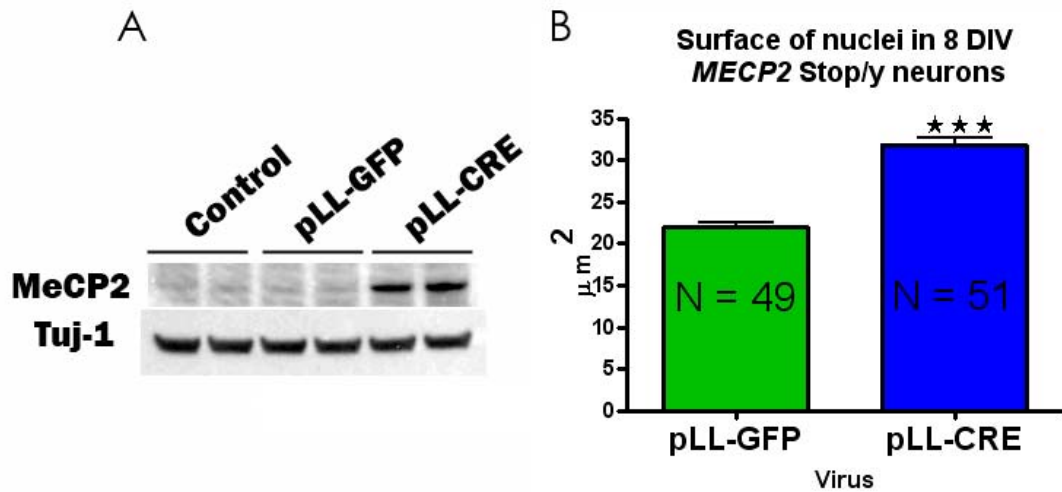


Figure 3-15 Re-expression of MeCP2 rescues the small nuclei phenotype. (A) Infection of *MECP2* Stop/y neuronal culture at DIV 2 with Cre-encoding lentivirused led to a re-expression of MeCP2 from the endogenous promoter, as assessed by Western blot at DIV 8, while control (GFP) virus did not affect the MeCP2 expression (B) Quantification of nuclear surface at DIV 8 in *MECP2* Stop/y neurons infected with either GFP or Cre encoding lentiviruses (mean \pm S.E.M, *** $P < 0.0001$, Student *t*-test)

In a complementary approach, MeCP2 was expressed in *MECP2* $-/y$ ES cell-derived neurons using the same viral delivery system. Knock-out neurons were infected with either a control virus (GFP) or a virus coding for MeCP2 at 2 days *in vitro* and nuclear size was measured 6 days later at 8 DIV. Over-expression of MeCP2 in the knock-out neurons led to a significant enlargement of the nuclei and rescued the small nuclei phenotype (control infected nuclei: $20.95 \mu\text{m}^2 \pm 0.4362 \mu\text{m}^2$; N = 51, MeCP2 infected nuclei: $30.01 \mu\text{m}^2 \pm 0.8065 \mu\text{m}^2$; N = 53).

To test the possibility that phosphorylation of serine 421 is critical (see Zhou *et al.*, 2006), the *MECP2* $-/y$ neurons were also infected at 2 DIV with either control (GFP) virus or a virus coding for MeCP2 mutant with a substitution of serine 421 for alanine (S421A) and the nuclear size was measured at 8 DIV. MeCP2 S421A could also rescue the small nuclei phenotype, to the same extend, as the wild type MeCP2 (MeCP2 S421A infected nuclei: $28.85 \mu\text{m}^2 \pm 0.8017 \mu\text{m}^2$; N = 42). The size of the nuclei of the neurons over-

expressing either wild-type MeCP2 or MeCP2 S421A was indistinguishable (Figure 3.16).

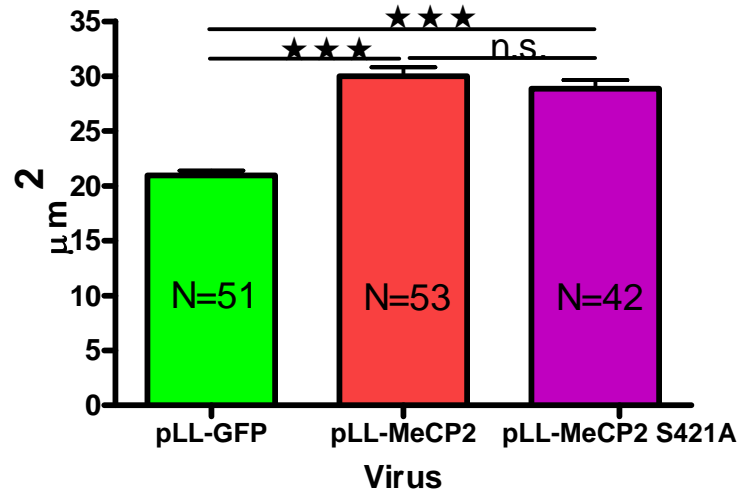


Figure 3-16 Over-expression of both wild-type and non-phosphorylatable forms of MeCP2 (S421A) rescue the small nuclei phenotype in the *MECP2* ^{-/-} neurons. *MECP2* ^{-/-} neurons were infected at DIV 2 with control (GFP), wild-type MeCP2 or MeCP2 S421A encoding lentiviruses. The nuclear sizes of the infected neurons were measured at DIV 8 and shown in this plot (mean ± S.E.M, *** *P*<0.0001, Student *t*-test)

3.3.5. Regulation of nuclear size by MeCP2 is cell autonomous

Recently, a role for MeCP2 in non-neuronal cells has been proposed (see Discussion) raising the possibility that the lack of MeCP2 may affect neuronal function indirectly. To test whether or not the small nucleus phenotype observed in the absence of MeCP2 is cell autonomous or not, *MECP2* ^{-/-} neurons were infected with the viruses coding for MeCP2 at 2 DIV. 18 days later, the nuclear size of the MeCP2 over-expressing and the non-infected neurons in this culture were compared to that of neurons of non-infected sister cultures. While the nuclear size of the *MECP2* ^{-/-} neurons over-expressing MeCP2 had enlarged ($31.16 \mu\text{m}^2 \pm 0.6361 \mu\text{m}^2$; *N* = 132) and the small nuclei phenotype was rescued, the nuclei of the neighboring non-infected neurons ($22.02 \mu\text{m}^2 \pm 0.4081 \mu\text{m}^2$; *N* = 89)

remained as small as nuclei of the control neurons from the non-infected sister cultures ($22.67 \mu\text{m}^2 \pm 0.4320 \mu\text{m}^2$; N = 108) (Figure 3.17).

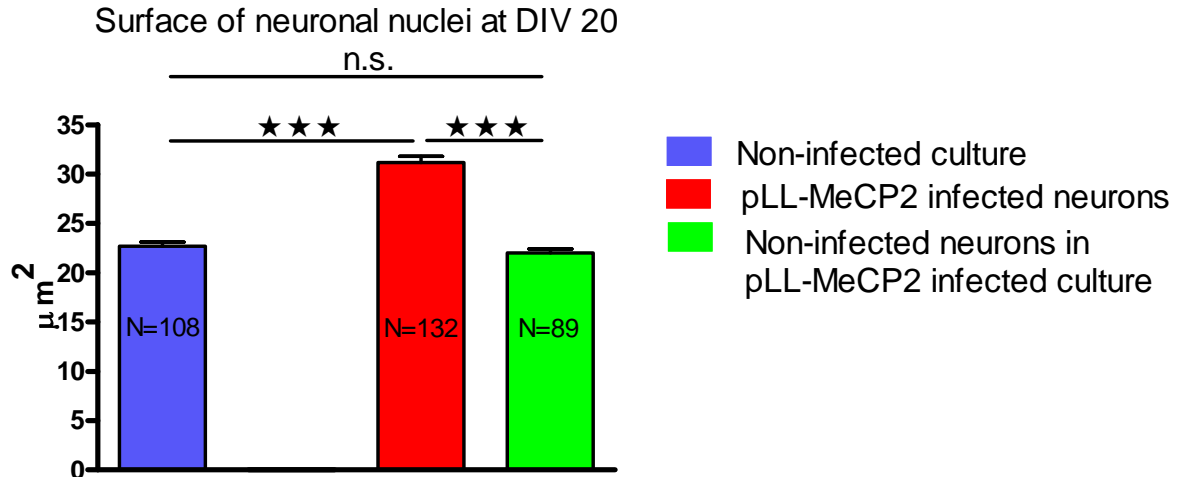


Figure 3-17 Regulation of the neuronal nuclei size by MeCP2 is cell autonomous. The nuclear size of *MECP2* $-/-$ neurons at DIV 20 in non-infected culture was compared to that of the *MECP2* $-/-$ neurons infected with MeCP2 encoding lentiviruses at DIV 2 and the nuclear size of non-infected *MECP2* $-/-$ neurons in the culture where the MeCP2 encoding was added. While over-expression of the MeCP2 in *MECP2* $-/-$ neurons (rate of infection > 50%) rescues the small nuclei phenotype, the non-infected neighbouring neurons remain as small as knock-out neurons in non-infected sister culture (mean \pm S.E.M, *** $P < 0.0001$, Student *t*-test)

3.3.6. MeCP2-deficient glia do not have small nuclei

Given a possible role of MeCP2 in astrocytes (see Discussion), the nuclear size of non-neuronal cells was also assessed with a focus on primary astrocytes and microglia from the brains of wild-type and *MECP2* $-/-$ young mice. Glial cultures were prepared from the brain of P2 pups (see Materials and Methods) and nuclear size was measured 2 weeks later.

The expression of MeCP2 was also assessed in astrocytes and microglial cells. Antibodies against GFAP (Glial fibrillary acidic protein) were used to detect the astrocytes and microglia were detected using antibodies against CD11b (cluster of differentiation molecule 11b or Integrin alpha M).

Immunostaining using antibodies against MeCP2 revealed a clear staining of MeCP2 in the nuclei of astrocytes, but not above the background in the wild-type microglia using *MECP2* ^{-/-} glial cultures as antibody specificity control.

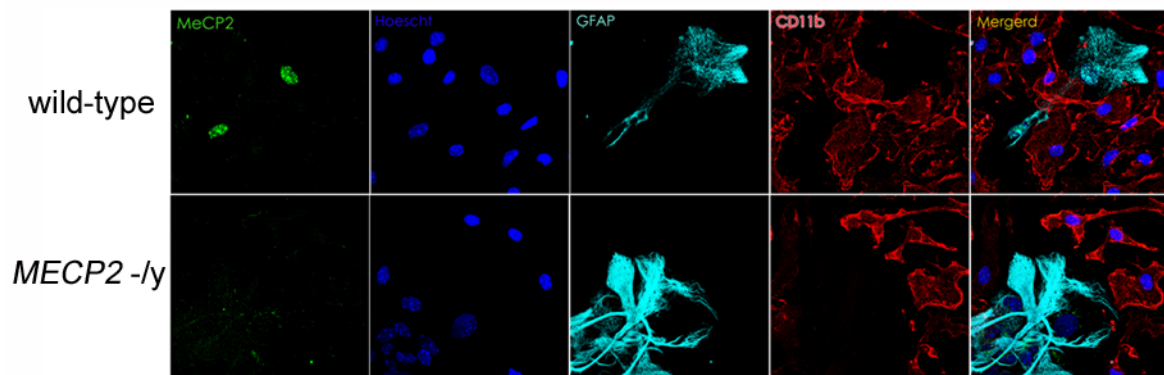


Figure 3-18 Astrocytes, but not microglial cells, express detectable levels of MeCP2. Immunostaining of glial culture obtained from brain of wild-type mice shows a clear staining of MeCP2 in the nuclei of astrocytes (GFAP stained) but not in the nuclei of microglia (CD11b stained). *MECP2* ^{-/-} glia were used to verify the MeCP2 staining

To compare the levels of MeCP2 in astrocytes with neuron, I performed semi-quantitative Western blot analysis. A dilution series of pure nuclei of astrocytes, DIV 3 and 8 wild-type ES cell-derived neurons and nuclei of *MECP2* ^{-/-} neurons as negative control were loaded in the SDS-gel for immunoblotting against MeCP2 (Figure 3.19).

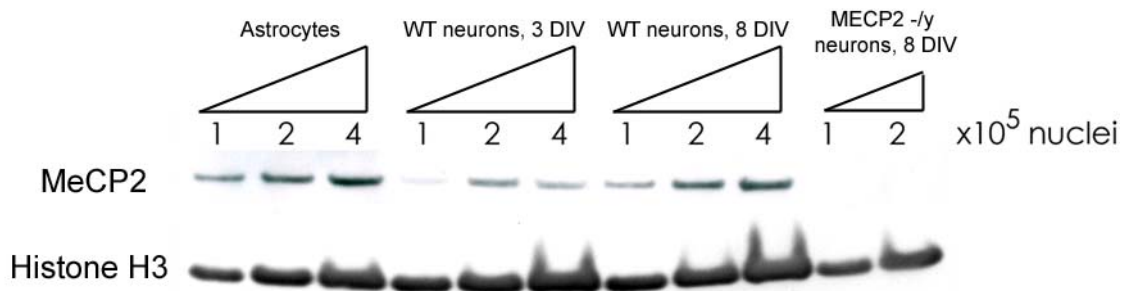


Figure 3-19 Astrocytes express similar levels of MeCP2 compared to the 8 DIV ES cell-derived neurons. Semi-quantitative Western blot on 0.1, 0.2 and 0.4 millions of nuclei of astrocytes, DIV 3 & DIV 8 ES cell-derived neurons. Nuclei of *MECP2* ^{-/-} neurons were used as the negative control for the MeCP2 detection. Histone H3 was used as the loading control

These results indicate that the levels of MeCP2 in primary astrocytes are comparable to those found in 8 days old ES cell-derived neurons. As I have shown that 8 DIV ES cell-derived neurons have similar levels of MeCP2 compared to the 16 DIV primary cortical neurons (Figure 3.14), it seems then that astrocytes, at least *in vitro*, express levels of MeCP2 similar to those found in mature neurons. However, the size of the nuclei of wild-type astrocytes was found not to differ from nuclei of *MECP2* ^{-/-} astrocytes (wild-type: $79.50 \mu\text{m}^2 \pm 1.126 \mu\text{m}^2$; N = 85, *MECP2* ^{-/-}: $77.32 \mu\text{m}^2 \pm 1.140 \mu\text{m}^2$; N = 82)

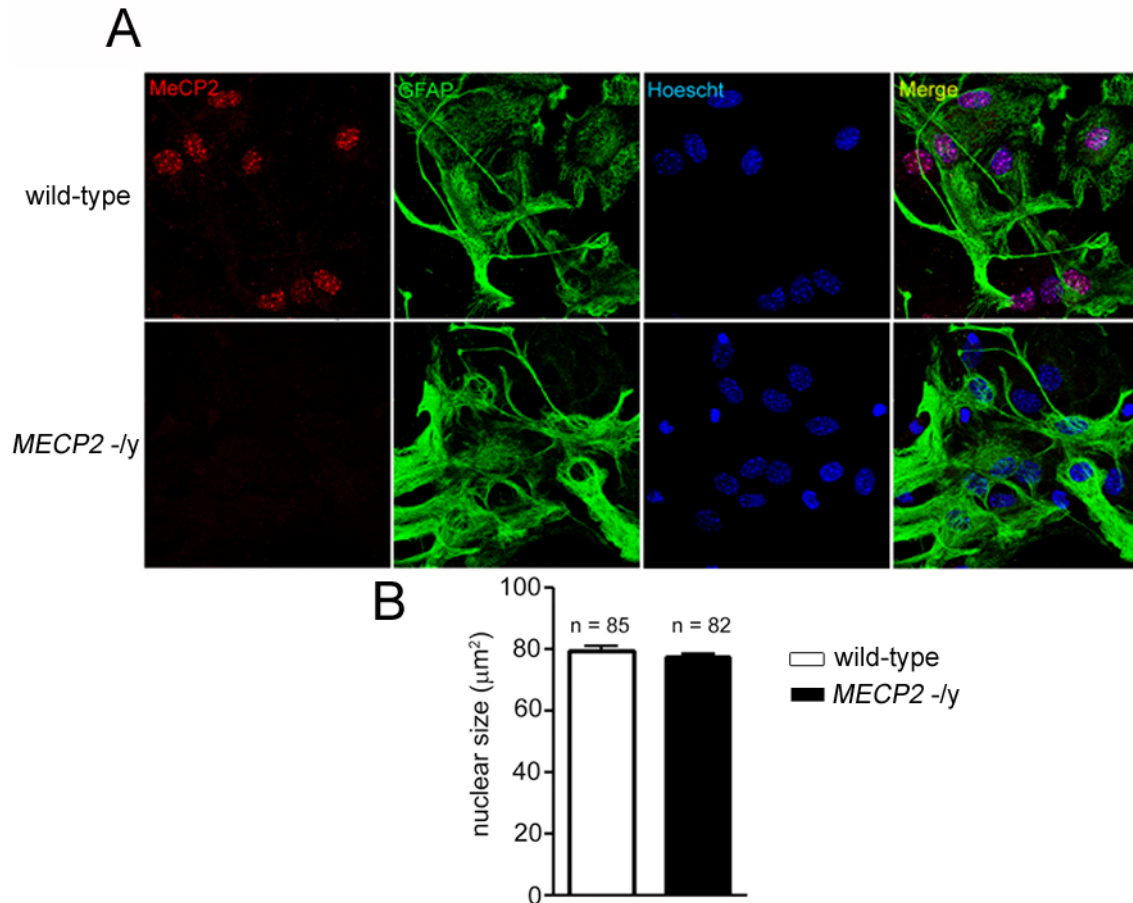


Figure 3-20 MeCP2 does not regulate the nuclear size of astrocytes. (A) Immunostaining of primary astrocytes (GFAP stained) obtained from brain of wild-type and *MECP2* ^{-/y} mice. A clear staining of MeCP2 in wild-type astrocytes, which is absent in nuclei of *MECP2* ^{-/y} astrocytes, colocalizes with the hoechst staining of the nuclei (B) Quantification of the nuclear size reveals no difference between wild-type and *MECP2* ^{-/y} astrocytes (mean ± S.E.M)

Although MeCP2 is not detectable in microglial cells, nuclear size was also compared between wild-types and *MECP2* ^{-/y} microglia. Nuclear size measurement revealed that, much like in case of astrocytes, the wild-type ($29.76 \mu\text{m}^2 \pm 0.518 \mu\text{m}^2$; N = 62) and *MECP2* ^{-/y} ($29.81 \mu\text{m}^2 \pm 0.614 \mu\text{m}^2$; N = 69) microglia also have similar sizes of nuclei (Figure 3.21) which shows the nuclear size of these 2 types of glial cells is not regulated by MeCP2.

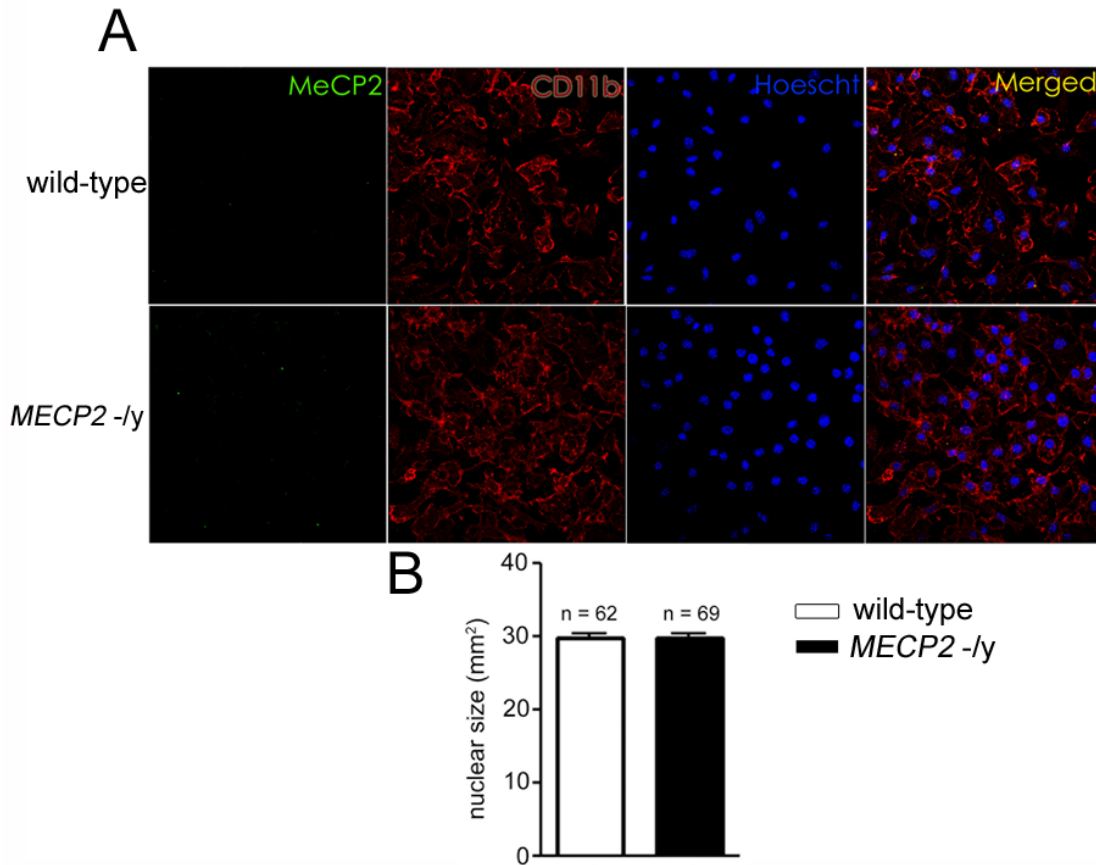


Figure 3-21 Wild-type and *MECP2* -/y microglia have similar nuclear sizes. (A) Immunostaining of primary microglia (CD11b stained) obtained from brain of wild-type and *MECP2* -/y mice. No staining of MeCP2, above background, is detected in the wild-type microglia (B) Quantification of the nuclear size (mean \pm S.E.M) reveals no significant difference in the nuclear size between the wild-type and *MECP2* -/y microglia

3.3.7. In vivo measurements of neuronal nuclei size

The size of neuronal nuclei was then measured in the CA3 area of the hippocampus in 1-week and of 7 months-old mice (Figure 3.22). Much like the *in vitro* situation, there is a significant increase in neuronal nuclear size during the development between 1 week after birth ($46.88 \mu\text{m}^2 \pm 0.5229 \mu\text{m}^2$; N = 304) and 7 months ($82.76 \mu\text{m}^2 \pm 1.388 \mu\text{m}^2$; N = 258).

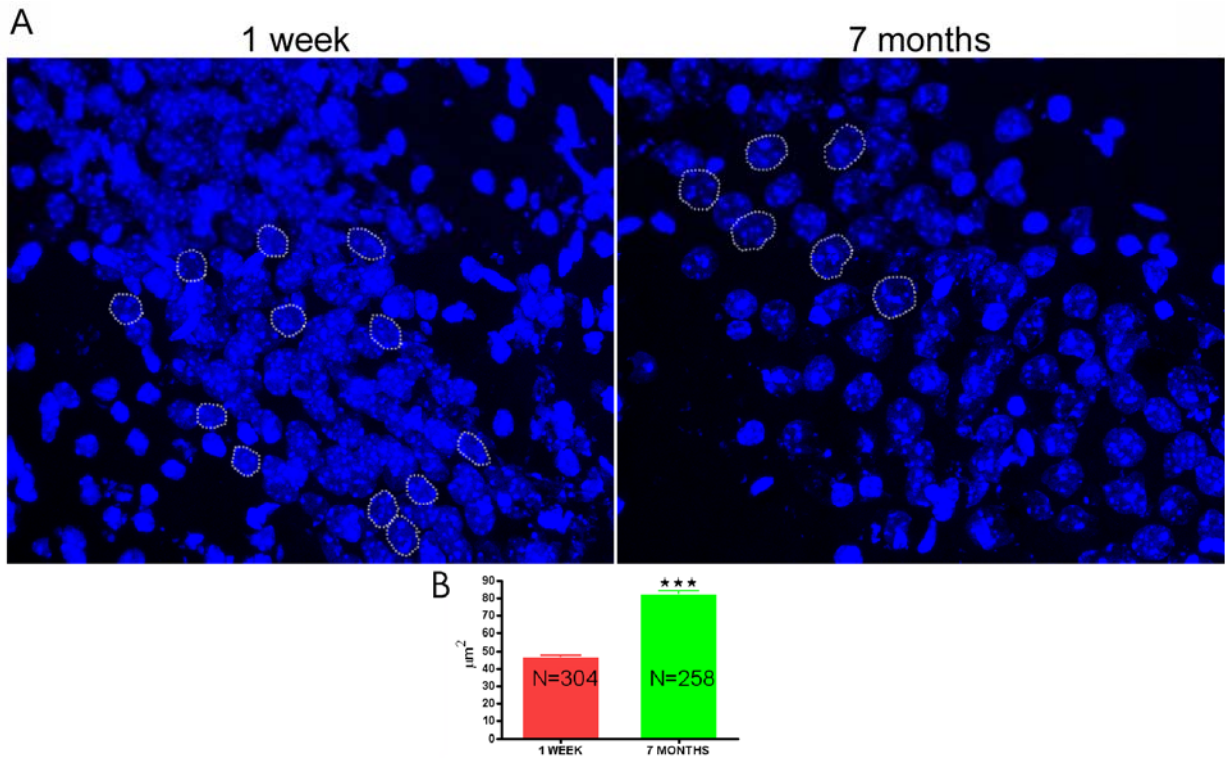


Figure 3-22 Enlargement of the neuronal nuclei in the CA3 area of the hippocampus. (A) DAPI staining of the nuclei in CA3 area of the hippocampus in 1 week and 7 months old wild type mice (B) Quantification of nuclear size in CA3 area shows a significant increase (mean \pm S.E.M, *** $P < 0.0001$, Student t -test) in the nuclear size with age

In the CA3 area of hippocampus of 2 months old mice lacking MeCP2, the neuronal nuclei were significantly smaller (Figure 3.23) than wild-type nuclei (wild-type: $50.52 \mu\text{m}^2 \pm 0.609 \mu\text{m}^2$; $N = 185$, *MECP2* $-/-$: $38.35 \mu\text{m}^2 \pm 0.270 \mu\text{m}^2$; $N = 322$)



Figure 3-23 Neurons in CA3 area of hippocampus of *MECP2* -/y mice have small nuclei. Quantification of neuronal nuclear size in CA3 area (mean \pm S.E.M, *** $P < 0.0001$, Student *t*-test)

3.3.8. Reduced rate of global transcription in MeCP2-deficient neurons

To begin to test for possible functional impact correlating with the small nuclei phenotype, I then measured the global rates of transcription using a modified form of nuclear run-on assay. After incubation of purified nuclei with unlabeled ATP, CTP, GTP and radio-labelled [32P]-UTP, total RNA was extracted and then amount of radioactivity incorporated in the total RNA was measured (Thompson, 1973) in the nuclei of wild-type and *MECP2* -/y neurons at 3, 8 and 13 DIV.

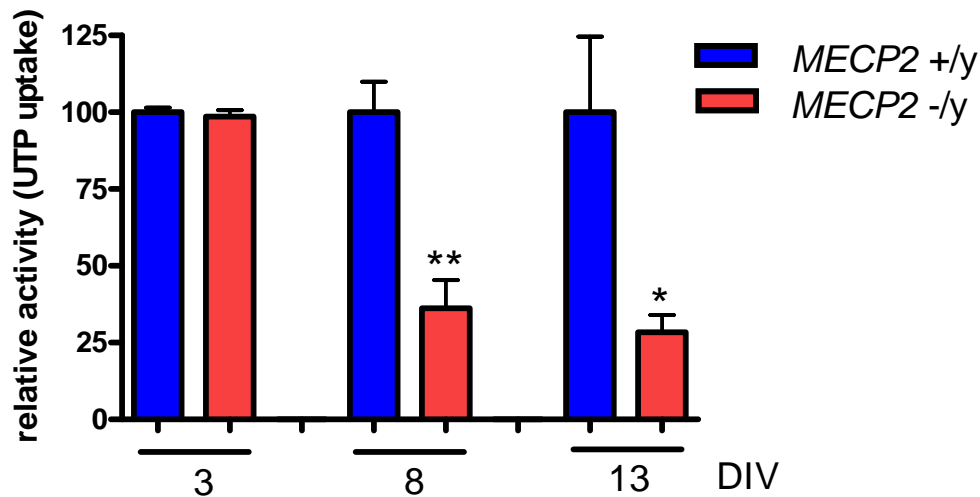


Figure 3-24 Reduced rate of *in vitro* transcription in isolated nuclei of *MECP2* *-/y* ES cell-derived neurons at 8 and 13 DIV but not at 3 DIV compared to wild-types. Equal numbers of nuclei at each age were incubated with unlabeled ATP, CTP, GTP and 1 μ Ci of $[^{32}\text{P}]\text{-UTP}$ for 0 and 30 minutes. The reaction was stopped by addition of TRIzol and total RNA was extracted. The amount of radioactivity incorporated in the total RNA was measured and standardized to the values obtained from wild-types (mean \pm S.E.M, N=3, * $P < 0.05$, ** $P < 0.01$ Student *t*-test)

While at 3 days *in vitro*, *MECP2*-deficient neuronal nuclei are transcriptionally as active as the wild-type neuronal nuclei, at 8 and 13 DIV they are significantly less transcriptionally active compared to the wild-type nuclei (Figure 3.24).

To assess if the reduced rate of *in vitro* transcription is solely due to the lack of MeCP2 and not an ES cell line-specific behavior, I compared the rate of *in vitro* transcription in *MECP2* Stop/*y* neurons, which have small nuclei as well, with the wild-type neurons. I found that the *MECP2* Stop/*y* neuronal nuclei are also significantly less transcriptionally active compared to their aged match wild-type nuclei (Figure 3.25).

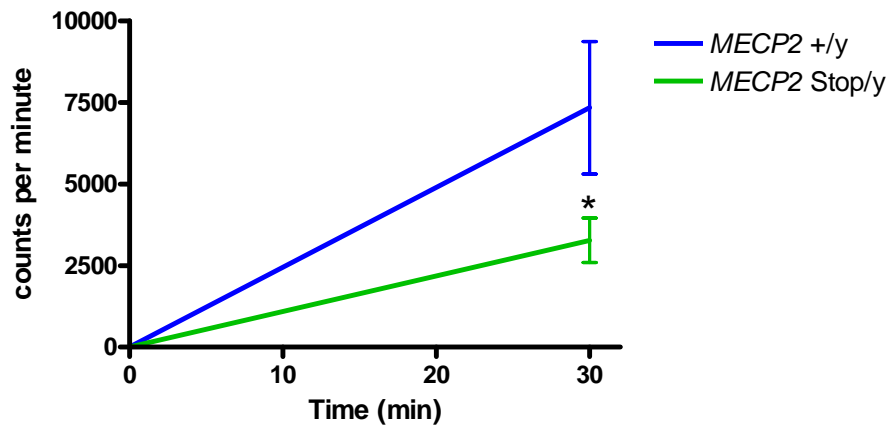


Figure 3-25 Reduced rate of *in vitro* transcription in isolated nuclei of *MECP2* Stop/y ES cell-derived neurons compared with the wild-type nuclei. 0.168 million nuclei of wild-type and *MECP2* Stop/y neurons at 8 DIV were incubated with 5 μ Ci [32 P]-UTP for 0 and 30 minutes. The amount of radioactivity incorporated in the total RNA was then measured (mean \pm S.E.M, N=3, * P <0.05, Student *t*-test)

The possibility that MeCP2 may affect transcriptional activity of glial nuclei was also tested as I had found that the levels of MeCP2 in neurons and astrocytes are comparable (see Figure 3.19). Wild-type and *MECP2* -/y astrocytic nuclei were similarly isolated and used for transcriptional analysis: nuclei of MeCP2-deficient astrocytes were transcriptionally as active as the nuclei of wild-type astrocytes (Figure 3.26)

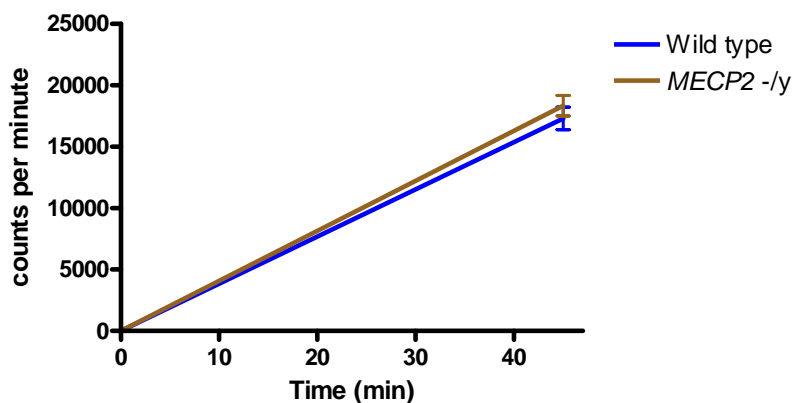


Figure 3-26 The lack of MeCP2 does not affect the global rate of transcription in astrocytes. 0.29 million nuclei of wild-type and *MECP2* -/y astrocytes were incubated with 5 μ Ci [32 P]-UTP for 0 and 45 minutes. Radioactivity incorporated in the total RNA was then measured (mean \pm S.E.M, N=3)

3.4. *FTY720 increases BDNF levels and improves the symptoms in mice lacking MeCP2*

In view of what appears to be a global reduction of transcription rate of neuronal nuclei lacking MeCP2, the possibility was then tested that *BDNF* might be amongst the genes with affected transcription (see also Introduction). Regulation of BDNF expression was also attempted using an orally available compound currently in clinical trial.

3.4.1. Reduced levels of BDNF in *MECP2* *-/y* neurons

Both mRNA and protein measurements showed a significant reduction in the expression of BDNF in 2-weeks-old cultures of *MECP2* *-/y* ES cell-derived neurons as compared to the aged matched wild-type neurons (Figure 3.27).

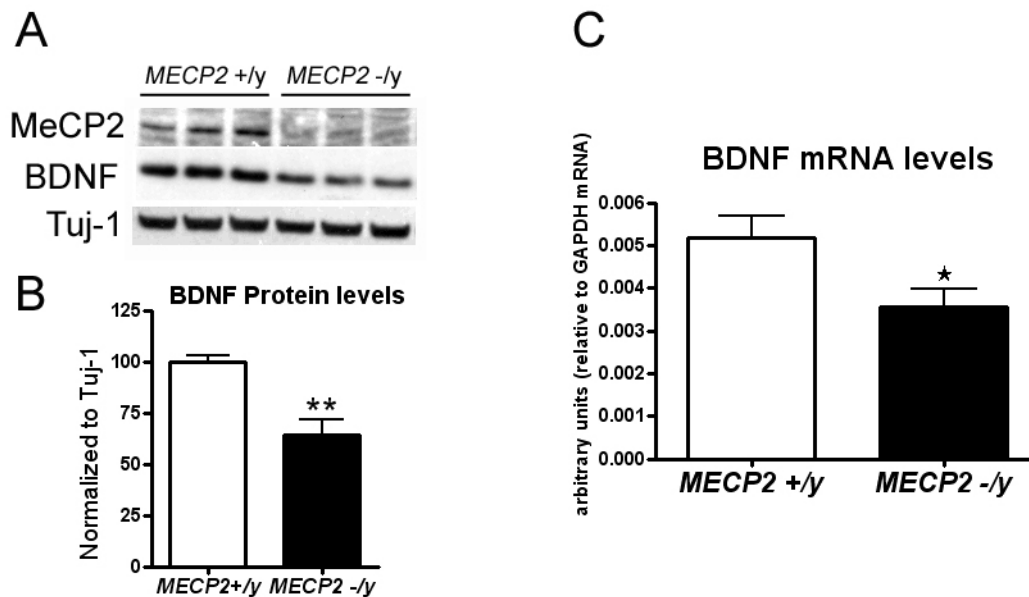


Figure 3-27 Reduced levels of BDNF expression in MeCP2-deficient neurons (A) Equal amount of protein lysates from 2-weeks-old cultures of wild-type and *MECP2* *-/y* ES cell-derived neurons were

loaded in the SDS-gel and expression of BDNF and MeCP2 were assessed using immunoblotting. Tuj-1 was used as loading control (B) Quantification of the Western blot in panel A shows a significant reduction in the BDNF expression (mean \pm S.E.M, $**P<0.01$, Student *t*-test) (C) Reduced levels of BDNF expression in 2-weeks-old cultures of *MECP2* $-/-$ neurons compared to the wild-type neurons assessed by quantitative real-time RT-PCR (mean \pm S.E.M, N=3, $*P<0.05$, Student *t*-test)

3.4.2. Reduced levels of BDNF in various brain regions of *MECP2* $-/-$ mice

Brains of wild-type and *MECP2* $-/-$ mice were dissected at 2 month of age and BDNF measurements performed using an ELISA protocol established in our laboratory (Kolbeck *et al.*, 1999).

In addition to the reported reduction of BDNF in the brain stem (Wang *et al.*, 2006) and cerebellum (Chang *et al.*, 2006), we found that the BDNF levels were also significantly reduced in hippocampus, striatum and the midbrain of the *MECP2* knock-out mice but not in the olfactory bulbs, compared with those determined in wild-type littermates (Figure 3.28)

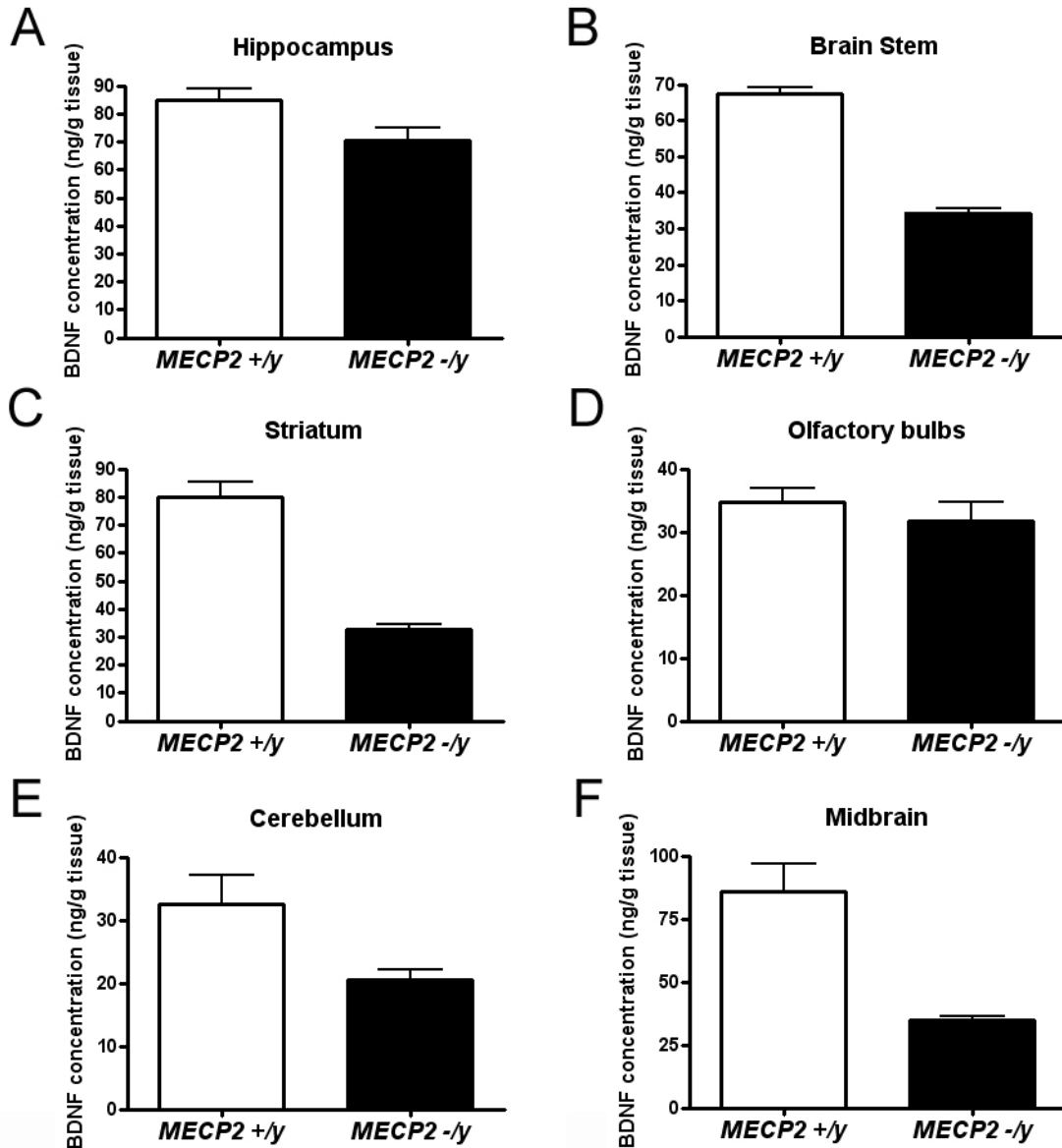


Figure 3-28 Reduced levels of BDNF in (A) hippocampus, (B) brain stem, (C) striatum, (E) cerebellum and (F) midbrain but not in the (D) olfactory bulbs of the MeCP2-deficient mouse brains. All the measurements have been done by ELISA on the brains of 2 months old mice (mean \pm S.E.M, N=3)

3.4.3. FTY720 increases BDNF expression in wild-type cortical neurons

As it would be desirable to increase BDNF levels using small chemical compounds that could be administered orally in patients, the drug FTY720 was next tested. This drug is an analogue of sphingosine-1 phosphate (S1P) that diffuses through the blood-brain barrier

and is phosphorylated to its active moiety FTY720-P. While it is thought to primarily target cells of the immune system, FTY720 receptors are also expressed in microglia, oligodendrocytes, astrocytes and neurons. This drug may be used soon in the context of Multiple Sclerosis (MS) treatment and is advanced in clinical trials for this indication.

Cortical neurons (14-18 DIV) were treated with FTY720-P (10 nM) for different periods of time (4 h, 8 h and 24 h) and BDNF levels analysed. A 2-fold increase of BDNF transcripts was observed after 4 h of FTY720-P stimulation. This increase was persistent after 8 h and 24 h of treatment (Fig. 3.29 A). Protein levels were also found to be increased by Western blot analysis (Fig. 3.29 B). FTY720-P was active only at a concentration range of 10 nM to 100 nM but not at 1 to 10 μ M (Fig. 3.29 C-D), indicating a limited range of efficacies concentration.

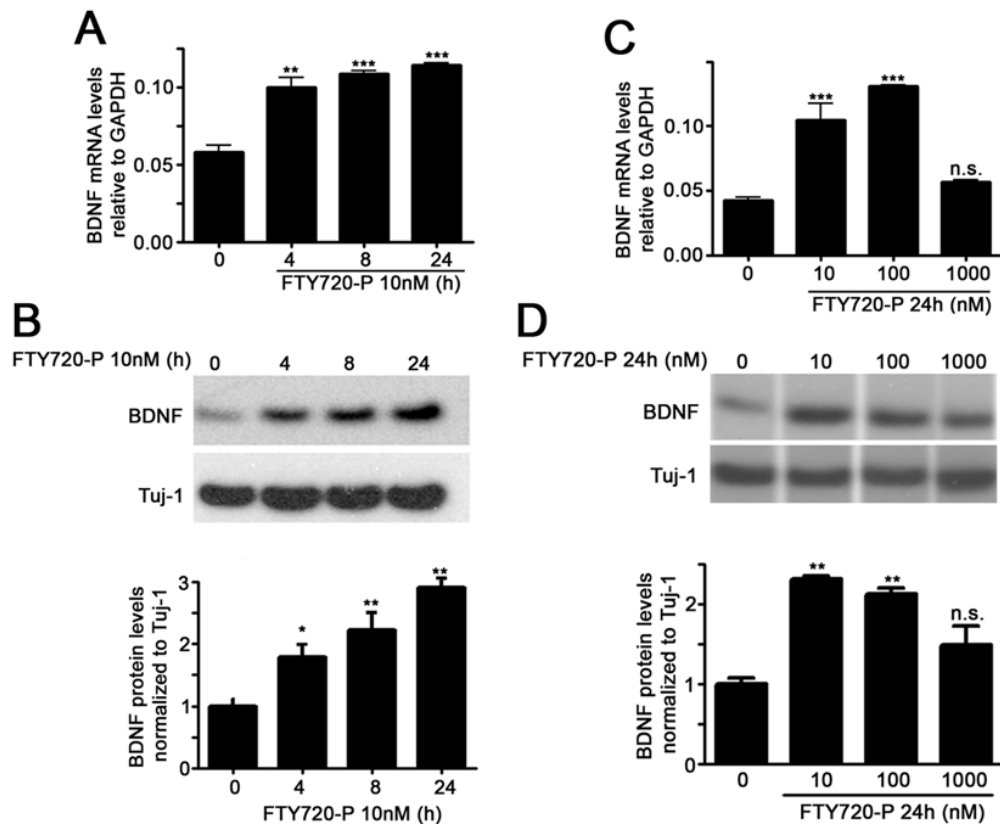


Figure 3-29 FTY720-P increases BDNF expression in wild-type neurons. (A) Quantitative real-time RT-PCR shows a significant increase in BDNF mRNA levels as early as 4 hours after treatment of the neuronal cultures with 10 nM FTY720-P (B) Western blot analysis on neuronal lysates treated with

FTY720-P also show a significant increase in BDNF at the protein levels (C) FTY720-P can stimulate BDNF expression in a concentration range of 10-100 nM as measured by quantitative real-time RT-PCR (D) At the protein levels also FTY720-P dependent increase of BDNF occurs in a range of 10-100 nM concentration (mean \pm S.E.M, N=3, * P <0.05, ** P <0.01, *** P <0.0001 Student t -test)

3.4.4. FTY720 increases CREB phosphorylation by activating NMDA receptors and MAPK pathway

As CREB phosphorylation is known to activate BDNF transcription (Greer and Greenberg, 2008), we next tested if FTY720-P treatment of neurons would cause the CREB phosphorylation. After 30min treatment with FTY720-P (50 nM), the levels of phospho-CREB (Ser133) were increased in primary cortical neurons (Figure 3.30 A).

CREB can be activated through a variety of pathways in neurons including the MAPK pathway, activation Ca^{2+} -Calmodulin-dependent protein kinases via increased levels of intracellular Ca^{2+} and the calcineurin pathway (Kingsbury *et al.*, 2007). To test if any of these pathways could be involved in the FTY720-P-dependent BDNF transcription, the cultures were pre-treated for one hour with the MAPK inhibitor, U0126 (2 μ M), the blocker of neuronal activity, TTX (10 μ M), and the NMDA-receptors antagonist, APV (200 μ M). The levels of both pMAPK1/2 (pERK1/2) and pCREB-Ser133 were increased after 30 minutes FTY720-P treatment. As readout, blockade of MAPK pathway by U0126 effectively blocked both ERK1/2 and CREB. Curiously, TTX and APV treatment also prevented FTY720-P-induced ERK1/2 and CREB phosphorylation (Figure 3.30 A). Both TTX and APV also blocked the increase in BDNF at protein levels mediated by FTY720-P (Figure 3.30 B-C).

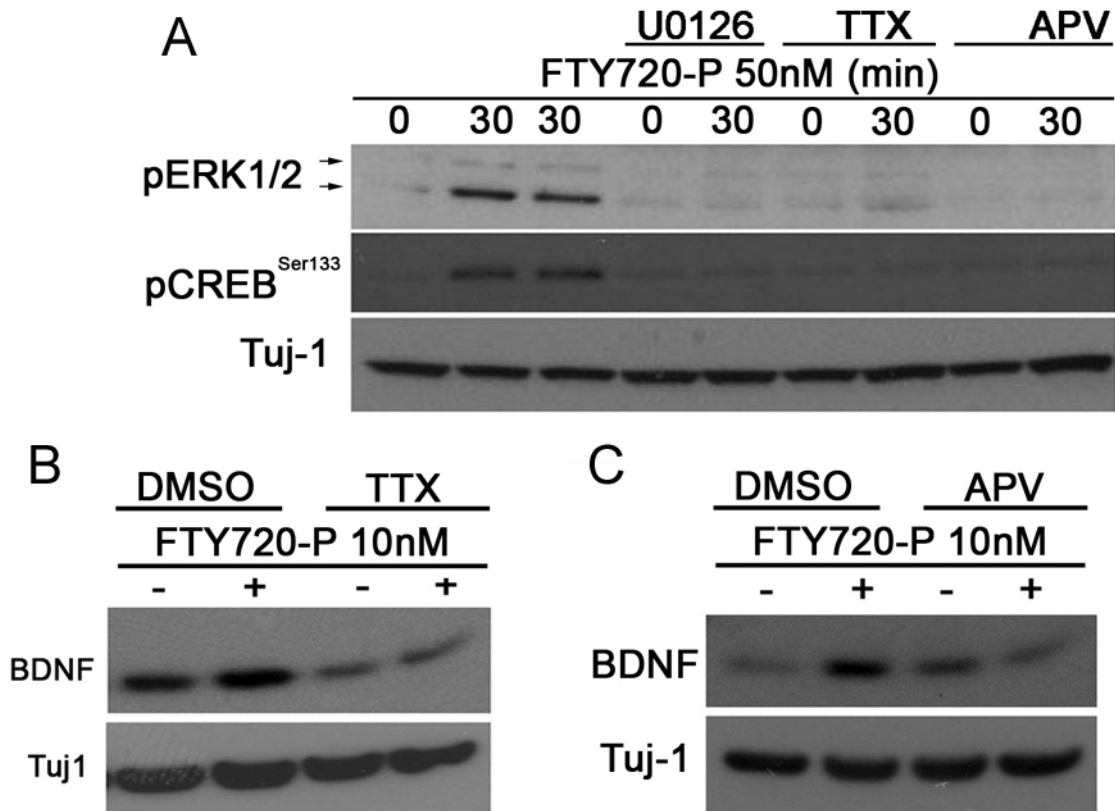


Figure 3-30 Effect of FTY720-P on activation of ERK, CREB, and BDNF transcription. (A) Phosphorylation levels of CREB and ERK1/2 in cortical neuronal cultures (14 DIV) after 30 minutes of FTY720-P treatment either in control condition or in the presence of U0126, TTX or APV were determined by Western Blot (B) BDNF protein levels in primary cortical cultures (14 DIV) after 24 h treatment with FTY720-P (10 nM), in the presence of TTX (1 μ M) or (C) APV (200 μ M) were determined by Western blot

These data then suggest that FTY720-P requires neuronal activity and activation of NMDA-receptors to mediate the activation of BDNF transcription mediated by CREB through Ca^{2+} -dependent and MAPK pathways.

3.4.5. FTY720 increases BDNF expression in *MECP2* deficient neurons and brains

If drugs such as FTY720 are to be used to treat RTT patients, it is important to test whether or not FTY720 administration increases BDNF levels even in neurons lacking MeCP2.

To answer this question, we treated the 3-weeks-old cultures of *MECP2* $-/-$ ES cell-derived neuron with 10 nM FTY720-P and checked the BDNF expression both at mRNA and protein levels. Much like in the wild-type cortical neurons, FTY720-P induces the expression of the BDNF in *MECP2*-deficient neurons (Figure 3.31).

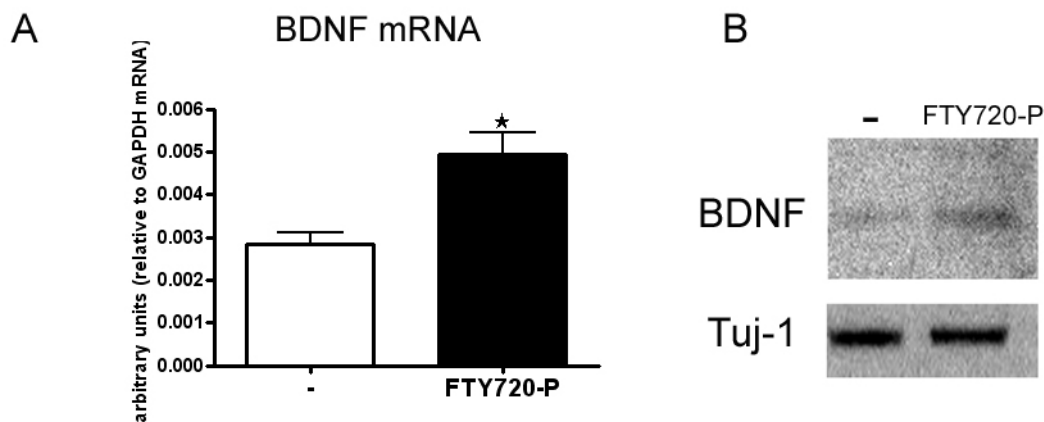


Figure 3-31 FTY720-P induces BDNF expression in MeCP2 knock-out neurons.

Cultures of *MECP2* $-/-$ ES cell-derived neurons (20 DIV) were treated with 10 nM FTY720-P for 4 hours and BDNF levels were measured (A) at the mRNA levels using quantitative real-time RT-PCR and (B) at the protein levels using Western blot analysis (mean \pm S.E.M, N=3, * P <0.05, Student t -test)

We next wondered if FTY720 would also increase the BDNF expression *in vivo* in the brains of *MECP2* knock-out mice.

Saline (0.9 % w/v NaCl in water) or FTY720 (0.1 mg/Kg body weight) was injected every 4 days intraperitoneally (IP) into *MECP2* $-/-$ mice from 4 weeks of age for a period

of 4 weeks. 24 hours after the last injection, mice were euthanized and brains were isolated and dissected to different regions for BDNF measurements.

BDNF levels were increased significantly in the hippocampus and striatum of *MECP2* knock-out mice that have received the FTY720 compared to the control ones that had received saline (Figure 3.32)

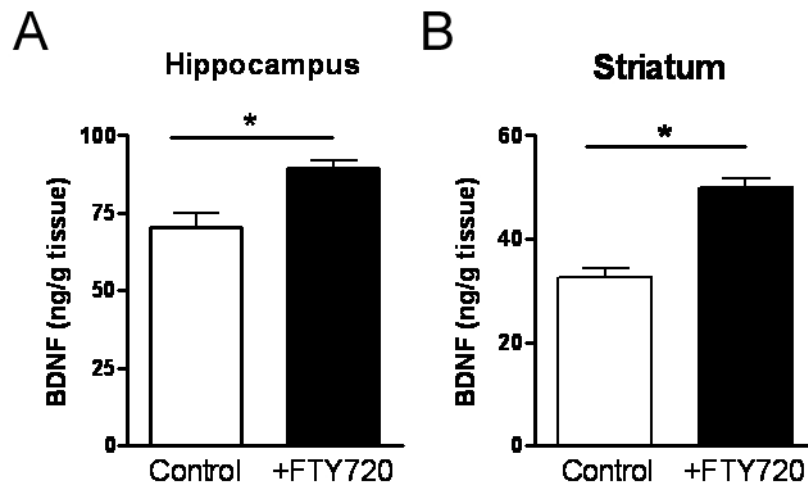


Figure 3-32 FTY720 administration in *MECP2* ^{-/-} mice increased BDNF expression in some brain regions. IP injection of FTY720 (0.1 mg/Kg body weight every 4 days) led to a significant increase in the expression of BDNF in (A) hippocampus and (B) striatum of *MECP2* ^{-/-} mice (mean \pm S.E.M, N=3, * P <0.05, Student t -test)

3.4.6. FTY720 improves the motor performance of *MECP2* ^{-/-} mice

During the course of injection of FTY720 in *MECP2* knock-out mice for the BDNF measurement, we have noticed that the mutant mice receiving FTY720 were phenotypically less severely affected compared to the control mice receiving saline. For example, mice receiving FTY720 often did not show hind-limb claspings, a phenotype

that *MECP2* mutant mice as well as *BDNF* mutant mice often show (Figure 3.33) (Guy *et al.*, 2001, Rauskolb *et al.*, 2010).

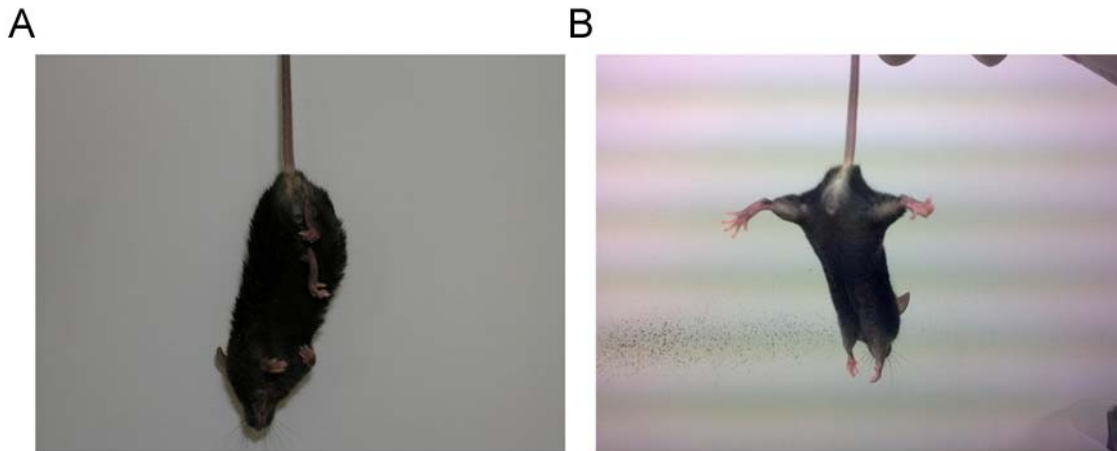


Figure 3-33 FTY720 administration in *MECP2* $-/y$ mice attenuates the hind-limb clasping phenotype. An example of improvement of symptoms in *MECP2* $-/y$ mice receiving FTY720. (A) While 9-weeks-old control mouse shows hind-limb clasping (B) the *MECP2* knock-out mice that received FTY720 (0.1 mg/Kg body weight every 4 days) for 3 weeks does not exhibit hind-limb clasping even at 11 weeks of age.

The *MECP2* knock-out mice as of 4 weeks of age start to become immobile and develop a stiff gait (Chen *et al.*, 2001, Guy *et al.*, 2001). To test whether the BDNF increase in the brain of *MECP2* mutants may exacerbate locomotor dysfunction following FTY720 injection, we performed a dark-cycle locomotor activity assay (running-wheel assay). As shown in Figure 3.34, the *MECP2* $-/y$ mice perform poorly in the running-wheel assay at 6 to 7 weeks of age as compared to the wild-type littermates.

Injections of mutant mice were started at 6 weeks of age and the recordings performed one week later for a period of 2 weeks (from 7 to 9 weeks of age). As shown in Figure 3.34, FTY720 injection has moderately, but significantly, improved the motor performance of the *MECP2* knock out mice.

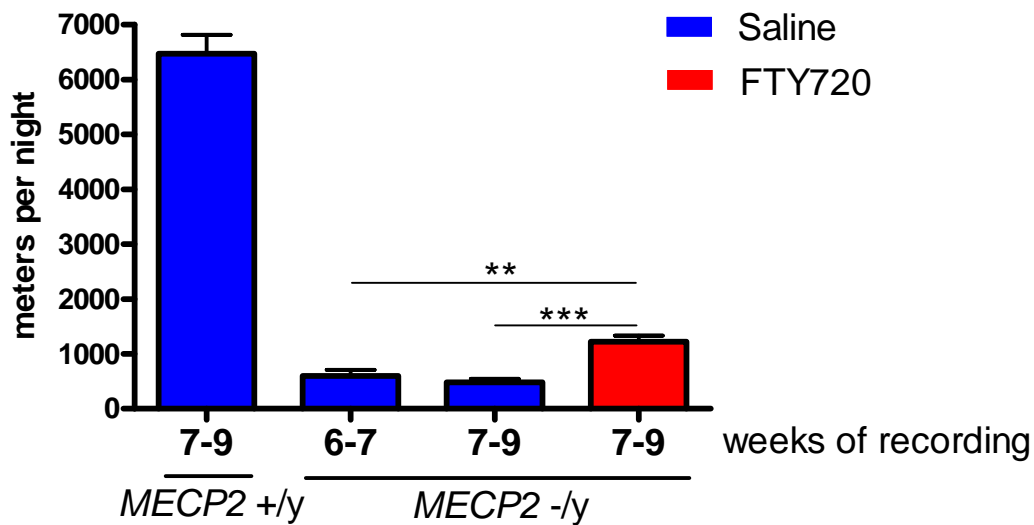


Figure 3-34 FTY720 administration in *MECP2* $-/y$ mice improves the locomotor performance. Saline or FTY720 were IP injected in *MECP2* $-/y$ mice from 6 weeks of age and the performance in the running wheel assay was recorded for 2 weeks from 7 to 9 weeks of age. FTY720 injection led to a significant increase in the locomotor performance of the *MECP2* $-/y$ mice (mean \pm S.E.M, N=3, *** P <0.001, Student t -test)

3.4.7. FTY720 increases the lifespan of *MECP2* $-/y$ mice

BDNF and MeCP2 have been previously proposed to be in the same pathway (Chang *et al.*, 2006). Using mice under- or over-expressing BDNF compared with mice lacking MeCP2, it could be shown that the levels of BDNF negatively correlate with severity of the symptoms observed in mice lacking MeCP2 (Chang *et al.*, 2006). we then injected FTY720 following the regime leading to increased BDNF levels in *MECP2* $-/y$ animals (see Figure 3.32), (0.1 mg/Kg body weight every 4 days). To exclude the severely affected mice we decided to start the injection as of 6 weeks of age (post-natal day 42) and record the lifespan. We found that FTY720 administration significantly increased the lifespan of Rett syndrome mice models from 68.7 days to 93.8 days (Figure 3.34)

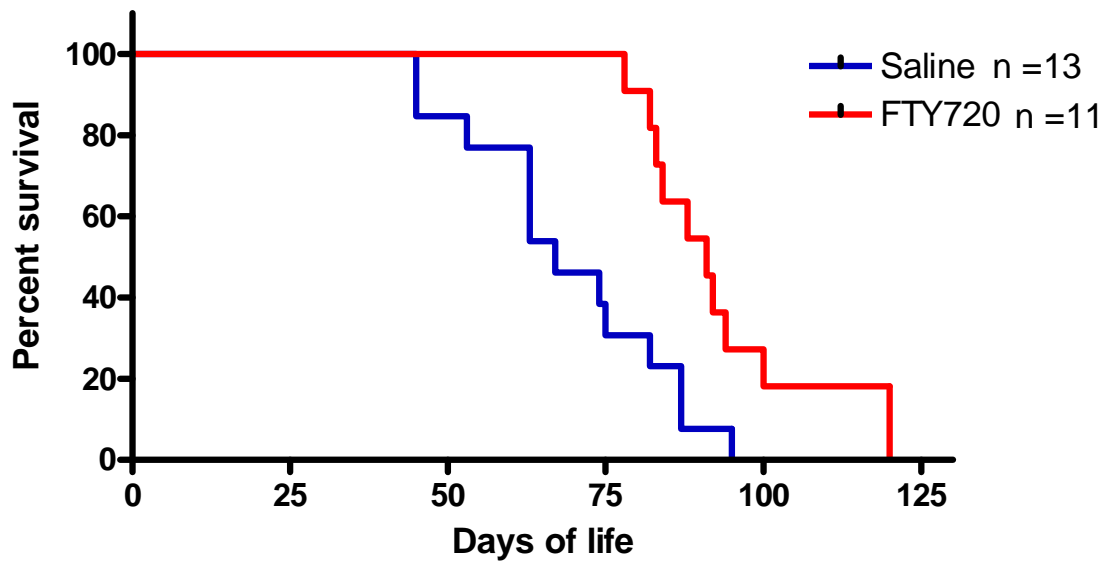


Figure 3-35 FTY720 administration in *MECP2* ^{-/-} mice improves the lifespan. *MECP2* ^{-/-} mice receiving IP injection of FTY720 from P42 (week 6) live (93.8 days) significantly longer than mice receiving saline (68.7 days) (***P*<0.01, Logrank tet)

4. Discussion

The discovery that uniform populations of Pax6-positive radial glial cells can be generated from mouse ES cells (Bibel *et al.*, 2007, Bibel *et al.*, 2004) makes it now possible to explore early events of CNS development that have been previously difficult to examine in sufficient detail. These Pax-6-positive progenitors drop out of the cell cycle rapidly and differentiate simultaneously into essentially one cell type, namely glutamatergic neurons. This transition can thus be studied with accuracy which greatly facilitates the identification of phenotypes correlated with the absence of genes such as *MECP2* (this study) as was also the case in a previous study with ES cells lacking Pax-6 (Nikoletopoulou *et al.*, 2007).

4.1. Lack of *MECP2* affects the proliferation of neuronal progenitors but not the ES cells

During development, the most dramatic increase in brain volume occurs during the last three months of fetal life and the first two years after birth (Amiel-Tison *et al.*, 2002). By the third year, the human brain has become about four times larger compared with its size at birth (Cox *et al.*, 2006). Concomitantly, the skull follows the volumetric increase in the cerebral hemispheres, apparently by passive adaptation (Amiel-Tison *et al.*, 2002). One early indicator of neurological impairment in Rett syndrome is the deceleration of head growth, leading to microcephaly (Chahrour and Zoghbi, 2007). Microcephaly is a condition in which the head remains significantly smaller than normal and it most often occurs as a result of a failure of brain development (Abuelo, 2007). The most frequent causes of microcephaly are mutations affecting the function of centromeres (Bond *et al.*,

2005, Kumar *et al.*, 2009, Thornton and Woods, 2009), though recently, mutations in the gene *WDR62* were discovered in human causing microcephaly (Bilguvar *et al.*, 2010). This gene seems to encode for a nuclear protein that is not associated with centromeres. In some RTT patients, microcephaly has been described as early as 3-4 months of age (Armstrong, 2001). Not only the RTT patients, but also the *MECP2* mutant mice have small brains (Chen *et al.*, 2001, Guy *et al.*, 2001) and volumetric analyses of one-month-old male brains showed a 25% reduction in whole brain volume compared to wild-types (Stearns *et al.*, 2007). Precise morphometric measurements revealed a reduction in the volume of the cortex (11%), cerebellum (12%), amygdale (39%), hippocampus (21%), and striatum (29%) (Belichenko *et al.*, 2008, Stearns *et al.*, 2007). Recently, mutations in the *FOXG1* gene have been identified in patients with the congenital variant of Rett syndrome (Ariani *et al.*, 2008, Bahi-Buisson *et al.*, 2010, Mencarelli *et al.*, 2010). The Forkhead box G1 (FOXG1) is a transcription factor that is critical for forebrain development, where it promotes progenitor proliferation and suppresses premature neurogenesis (Bahi-Buisson *et al.*, 2010, Dou *et al.*, 1999, Shoichet *et al.*, 2005). *FOXG1* and *MECP2* are hypothesized to share a common molecular mechanism during neuronal development (Ariani *et al.*, 2008). It has been postulated that microcephaly is a consequence of reduced neurogenesis, possibly as a result of an increased rate of apoptosis or reduced generation of neurons from progenitors (O'Driscoll and Jeggo, 2008). While previous results indicate that cells expressing mutant form of MeCP2 have a growth disadvantage (Balmer *et al.*, 2002, Maezawa *et al.*, 2009, Young and Zoghbi, 2004), there are still no published data indicating decreased proliferation of brain progenitors.

A further complication in addressing this question in the developing human brain may result from the fact that *MECP2* is an X-linked gene, with the possibility that the proportion of wild-type vs. mutant MeCP2 expressing cells in RTT brains may depend on the pattern of X chromosome inactivation. XCI is thought to be a random process, such that half of the cells have the maternal X chromosome active and the other half have the paternal X chromosome active. Although the majority of girls with classic RTT seem to have a random pattern of XCI in brain tissue (Shahbazian *et al.*, 2002b), non-balanced

patterns have been observed in patients carrying mutant *MECP2* (Renieri *et al.*, 2003, Weaving *et al.*, 2003) and in some cases may account for variability of phenotypic manifestations. In mice, the pattern of XCI seem to be frequently unbalanced in the brain of most *MECP2* female heterozygote mutants, favouring expression of the wild-type allele (Young and Zoghbi, 2004). In this latter study, no *MECP2* mutant female with a non-random XCI favouring expression of the mutant allele was detected. The brains of RTT patients showed no obvious degeneration, atrophy, inflammation, gliosis or neuronal migration defects (Jellinger *et al.*, 1988, Reiss *et al.*, 1993). It thus seems likely that wild-type neural progenitors have a growth advantage over *MECP2* mutant progenitors which may explain the apparent non-random XCI in the brain of *MECP2* mutant mice and RTT patients.

In single cell cloning of T lymphocytes from RTT patients, the MeCP2 mutant-expressing clones were shown to be present at a significantly lower frequency than wild-type clones (Balmer *et al.*, 2002) suggesting that MeCP2 is not essential for lymphocyte growth but yet the lack of MeCP2 causes a growth disadvantage. Consistent with these data, it has recently been shown that MeCP2-deficient astrocytes grow substantially slower than wild-type astrocytes assessed by BrdU incorporation (Maezawa *et al.*, 2009). However, none of these experiments directly addresses whether the lack of MeCP2 affects the proliferation of neuronal progenitors or not.

In my experiments, I could compare the rate of division of wild-type and *MECP2* mutant cells at different stages of differentiation. The results showed that MeCP2-deficient ES cells proliferate similarly to wild-type ES cells (Figure 3.6), but that the neuronal progenitors lacking MeCP2 showed reduced BrdU incorporation (Figure 3.10). As a result, the MeCP2-deficient progenitors generated fewer neurons (Figure 3.8). Comparisons of the levels of MeCP2 expression revealed that MeCP2 is expressed at much lower levels in ES cell compared to neurons, about 150-folds less (Figure 3.7). Following retinoic acid treatment, used as trigger of neural commitment in our procedure, the levels of MeCP2 expression markedly increased (Figure 3.7). Thus, the low levels of MeCP2 expression in ES cells correlate with a lack of impact of MeCP2 absence in their

proliferation. As MeCP2-deficient progenitors clearly incorporate less BrdU than their wild-type counterparts, it would seem that MeCP2 only affects proliferation beyond a critical threshold of expression. However, my data do not exclude that the cellular context in which MeCP2 is expressed may also play a role.

Both in human and in mouse, MeCP2 is expressed at detectable levels during brain development (week 26 in human brain, E11.5 in mouse telencephalon). However, its expression further increases with age (Shahbazian *et al.*, 2002a). As a result, older neurons express higher levels of MeCP2 than young neurons and neuronal progenitors. This prompted the hypothesis that MeCP2 may not play an important role in the generation of neuronal progenitors and young neurons, but that it rather becomes important for the function of mature neurons (Shahbazian *et al.*, 2002a). While I also observed an increased MeCP2 expression during the transition from neuronal progenitors into neurons (Figure 3.9) and even if the levels of MeCP2 expression were low in the progenitors its absence clearly caused a proliferation defect in the mutant cells. My *in vitro* data suggest then that the decreased proliferation observed with MeCP2-deficient neuronal progenitors may also contribute to the smaller brain size in mouse mutant and human. Current experiments are now addressing this question by comparing the developing brains of *MECP2* $-/y$ and wild-type embryos.

4.2. MeCP2 regulates the size of neuronal nuclei

Beyond the impact of MeCP2 on progenitors proliferation, a second new finding resulting from detailed observation of the differentiation of these progenitors is the lack, or strong delay, in the growth of nuclear diameter normally observed with wild-type neurons. In general, very little is known about the growth of nuclei during the course of neuronal differentiation. Indeed, the majority of studies on regulation of the nuclear size

have been performed on dividing cells. However, it was recently shown that synaptic activity induces dramatic changes in the geometry of the neuronal nuclei, but not in the nuclei of the astrocytes (Wittmann *et al.*, 2009). Nuclear calcium signaling can dynamically alter the nuclear structure that in turn results in histone H3 phosphorylation. This observation provides a functional link between the geometry of neuronal nuclei and transcriptional regulation (Wittmann *et al.*, 2009). Although it has been known for almost a decade that *MECP2*-deficient neurons in the brains of mutant mice have smaller nuclei (Chen *et al.*, 2001), neither the regulation of nuclear size by MeCP2 nor the functional consequences of small nuclei for neurons have been investigated in any detail (see Results, 3.3).

Presumably as a result of synchronous differentiation of progenitors in our ES cell-based system, I could readily follow the development of the neuronal nuclear size during the course of neuronal maturation *in vitro*. These experiments revealed a marked and rapid increase as neurons differentiate (Figure 3.11). In *MECP2*-deficient progenitors and neurons, the nuclear size was initially similar to wild-type neurons but it failed to increase with neuronal maturation. The increase in the nuclear size of the wild-type neurons is accompanied by a significant increase in the expression of MeCP2 (Figure 3.9). I also measured the nuclear size of neurons generated from 2 additional *MECP2* mutant ES lines; *MECP2* loxP/y and *MECP2* Stop/y. Although the nuclei of *MECP2* Stop/y neurons were initially (at DIV 3) of similar size compared to the wild-type neurons, they failed to grow with maturation similar to what I observed with the *MECP2* -/y neurons. While nuclei of the *MECP2* loxP/y neurons grew with maturation, they failed to enlarge to the same extent as wild-type nuclei (Figure 3.12 and Table 3.4). Western blot experiments indicated that the *MECP2* loxP/y neurons expressed MeCP2 at around 40% of wild-type levels (Figure 3.5). This reduction is most likely a consequence of the neomycin selection cassette left in these cells (Guy *et al.*, 2001). In line with this, Samaco and colleagues recently showed that the levels of MeCP2 were reduced by 40-50% in the brains of hypomorphic mice carrying this floxed allele. In addition, mice carrying this mutation show neurological symptoms and have a breathing problem (Samaco *et al.*, 2008). My results also confirmed that the insertion of the stop-cassette into *MECP2* gene

in the *MECP2* Stop/y neurons (Guy *et al.*, 2007) efficiently prevents MeCP2 protein expression (Figure 3.5). In sum, these experiments indicate that the nuclear size of ES cell-derived neurons directly correlates with their levels of MeCP2 expression.

To further exclude the possibility that the small nucleus phenotype is ultimately due to a “clonal effect”, a problem often seen with ES cells, MeCP2 was re-expressed in the very same cells displaying a small nuclei phenotype. In rescue experiments, MeCP2 was re-expressed from its endogenous promoter in *MECP2* Stop/y neurons. As expected, MeCP2 re-expression led to a rescue of the small nuclei phenotype (Figure 3.15). In line with this, acute expression of MeCP2 in *MECP2*-deficient neurons caused an enlargement of the nuclei (Figure 3.16). Therefore, the small nuclei phenotype is reversible if MeCP2 would be restored in the neuronal nuclei, a finding that fits with the reversibility of neurological symptoms observed in mice models or Rett syndrome (see Introduction) (Guy *et al.*, 2007). Re-expression of MeCP2 was also found very recently to increase the cortical thickness of *MECP2* Stop/y mice and to lead to enlargement of the brain (personal communication with Stuart Cobb, 11th Annual Rett Syndrome Symposium, Virginia, USA).

I could also establish that the regulation of the neuronal nuclei size by MeCP2 is a cell-autonomous phenotype. In the experiment in which MeCP2 was acutely expressed in the *MECP2* -/y neurons, only the nuclei of the neurons over-expressing MeCP2 have enlarged but the nuclei of other neurons remained small (Figure 3.17), in line with recent *in vivo* experiment showing that *MECP2* mutation results in cell-autonomous reduction in soma size of neurons in locus ceruleus (Taneja *et al.*, 2009).

Neuronal activity and subsequent calcium influx triggers the *de novo* phosphorylation of MeCP2 at serine 421 (S421) by a CaMKII-dependent mechanism. Moreover, MeCP2 S421 phosphorylation is induced selectively in the brain in response to physiological stimuli and has been previously shown to control the ability of MeCP2 to regulate dendritic patterning, spine morphogenesis, and the activity-dependent induction of BDNF transcription (Zhou *et al.*, 2006). Upon phosphorylation at S421, MeCP2 is thought to

bind less or less tightly to DNA in neuronal nuclei (Zhou *et al.*, 2006). To test if this phosphorylation site would be required for the function of MeCP2 as a regulator of neuronal nuclei, I tested a MeCP2 S421A mutant and found that the small nuclei phenotype of *MECP2* *-/y* neurons could also be rescued, just like with wild-type MeCP2 (Figure 3.16). This is not surprising, but important as S421A is not a human Rett mutation and the MeCP2 S421A knock-in mice do not show any symptoms resembling the Rett syndrome mouse models (personal communication with Sonia Cohen, 11th Annual Rett Syndrome Symposium, Virginia, USA).

In vivo, I observed a significant increase in the size of neuronal nuclei from the first week after birth (P7) to 7 months of age in CA3 area of hippocampus of wild-type mice (Figure 3.22). This fits with my *in vitro* data that neuronal nuclei enlarge with maturation (Figure 3.11). As wild-type dissociated cortical neurons, at 16 DIV express similar levels of MeCP2 compared to the wild-type ES cell-derived neurons at 8 DIV (Figure 3.14), I tested if the lack of MeCP2 in cortical neurons would also affect the nuclear size. These experiments revealed that the nuclei of cortical neurons lacking MeCP2 at 16 DIV were significantly smaller than wild-type neurons, as is the case in the CA3 area of hippocampus of 2 month old *MECP2* *-/y* mice (Figure 3.23). This confirms the data obtained by the group of Rudolf Jaenisch showing smaller nuclear size in neurons in brains of *MECP2*-deficient mice (Chen *et al.*, 2001, Giacometti *et al.*, 2007, Luikenhuis *et al.*, 2004).

I next addressed the question of whether the nuclear size regulation by MeCP2 is specific to neurons. To this end, I isolated glial cells from the brains of wild-type and *MECP2* mutant mice and measured their nuclei in culture experiments.

After immunostaining MeCP2 expression was evident in the nuclei of the wild-type astrocytes with a typical enrichment in the heterochromatin foci co-localized with Hoechst staining of DNA (Lewis *et al.*, 1992). By contrast, in wild-type microglial cells no immunostaining of MeCP2 could be observed above background, i.e. MeCP2 staining in the nuclei of *MECP2* *-/y* microglial cells (Figure 3.18). In the only publication

showing an immunostaining of MeCP2 in the nuclei of the wild-type microglia (Maezawa and Jin, 2010), the staining pattern is not typical for MeCP2 but rather faint and diffuse unlike what is seen even in non-neural cell types such as rat liver fibroblasts (Lewis *et al.*, 1992). While the wild-type microglial cells might express MeCP2, the expression levels are clearly much lower than those found in astrocytes. By contrast, wild-type astrocytes express significantly higher levels of MeCP2 than ES cell-derived neurons after 3 days, but similar to what is seen after 8 days *in vitro* in ES cell-derived neurons (Figure 3.19). In spite of this, the nuclear size of astrocytes lacking MeCP2 was not different from wild-type astrocytes, thus indicating that MeCP2 levels alone do not necessarily correlate with the size of nuclei in all cell types (Figures 3.20 & 3.21). In addition, the MeCP2-deficient astrocytes seem to divide at a similar rate compared with wild-type astrocytes as both cultures reached confluence similarly, once started with equal number of cells (data not shown).

While Shahbazian and colleague initially reported that MeCP2 is absent in astrocytes (Shahbazian *et al.*, 2002a), more recently several groups showed that astrocytes, microglia and oligodendrocytes express MeCP2 though at levels lower than neurons (Ballas *et al.*, 2009, Maezawa and Jin, 2010, Maezawa *et al.*, 2009). The conclusion drawn by Shahbazian and colleagues were based on the lack of detectable MeCP2 immunoreactivity in astrocytes in contrast to neighboring neurons (Shahbazian *et al.*, 2002a) a result that can be explained by a lack of sensitivity to the relatively lower levels of MeCP2 in astrocytes compared with mature neurons in adult mouse brain. My results show that astrocytes express similar levels of MeCP2 to DIV 8 ES cell-derived neurons, and by comparison, to the DIV 16 cortical dissociated neurons (Figures 3.14 & 3.19). Skene and colleagues recently showed that the MeCP2 expression reaches its highest levels in mouse brain at around 5 weeks of age (Skene *et al.*, 2010). Therefore, the level of MeCP2 in neurons *in vitro* might be far from the *in vivo* levels seen at maturation. Thus, differences in the age of the neurons used might underlie the apparent contradiction on MeCP2 expression in astrocytes *vs.* neurons, and a lack of sensitivity appears the likely explanation at this point. This is important, as glial cells were initially thought not to play any functional role in Rett syndrome as deletion of *MECP2* only in post-mitotic

neurons was accepted to be sufficient to cause Rett-like phenotypes in mice (Chen *et al.*, 2001). However, it was recently shown that MeCP2 mutant glial cells are abnormal and are now hypothesized to somehow spread the consequences of MeCP2 deficiency through gap junctions (Ballas *et al.*, 2009, Maezawa and Jin, 2010, Maezawa *et al.*, 2009). Wild-type neurons cultured either on top of *MECP2* *-/-* glia or treated with their conditioned medium had stunt dendrites (Ballas *et al.*, 2009). This suggests MeCP2-deficient glia have a non-cell autonomous effect on neuronal properties, probably as a result of aberrant secretion of unknown soluble factors. However, regardless of defects in MeCP2 mutant glial cells, my results suggest that the small nuclei phenotype is specific to the MeCP2-deficient neurons. Hence, it seems that it is not only the expression levels of MeCP2 in neurons that affect their nuclear size but rather a combination of MeCP2 levels and other neurons specific factor(s), e.g. an interacting partner of MeCP2 that is expressed in neurons, but not in glial cell. Thus, it will be informative to compare the interacting partners of MeCP2 in pure neuronal (e.g. from the ES cell-derived neurons) vs. glial nuclei.

As still very little is known about nuclear size regulation in cells of the nervous system, it is unclear if the size of nuclei changes in post-mitotic astrocytes in brain. My *in vitro* results clearly show that nuclei grow in post-mitotic neurons, and the astrocytes I cultured are still dividing. Note also that the neuronal nuclei in adult mice are far larger than after 3 weeks in culture (compare Figures 3.11 and 3.22 for details).

While the role of MeCP2 in the growth of neuronal nuclei has not been investigated in any details so far, another chromatin associated protein has been linked with nuclear size regulation: the linker histone H1 (Shen *et al.*, 1995). It is one of the 5 histones (H1, H2A, H2B, H3 and H4), but unlike the other 4 family members, it is not part of the core histones. H1 binds to the linker DNA region (approximately 60 nucleotides in length) between the histone beads and seals off the nucleosome at the location at which the linker DNA enters and leaves the nucleosome. Since linker histones are rich in lysine and arginine (typically ~ 60 K+R per molecule residues in mammals) they neutralize the negative charge of the DNA at the linker region, helping stabilize the zig-zagged 30 nm

chromatin fiber and compact the chromatin (Woodcock *et al.*, 2006). The loss of H1 in *Tetrahymena* results in an increase in nuclear size (Shen *et al.*, 1995) consistent with an expansion of chromatin in response to an electrostatic imbalance (Woodcock *et al.*, 2006). Interestingly, MeCP2 was shown to compete with linker histone H1 in binding to the linker DNA at the entry/exit site of nucleosome (Nikitina *et al.*, 2007a). Recently, quantification of MeCP2 levels revealed that it is nearly as abundant as the histone octamer in the neuronal nuclei in adult (6-8 weeks) mouse brain (Skene *et al.*, 2010) and MeCP2 deficiency was shown to result in global changes in neuronal chromatin structure, including elevated histone acetylation and a doubling of histone H1 levels. In MeCP2-deficient neuronal nuclei, elevated H1 levels could in turn cause an enhanced compaction of the chromatin and a subsequent shrinkage of the nuclei (Shen *et al.*, 1995, Woodcock *et al.*, 2006). In MeCP2-deficient glial nuclei, on the other hand, neither histone acetylation nor H1 expression were changed (Skene *et al.*, 2010). Moreover, the basal levels of linker histone H1 in glial nuclei are twice as much as in neurons in wild-type brains (Woodcock *et al.*, 2006) which could also contribute to a different regulation of nuclear size by MeCP2 in these two cell types. It would then be interesting to test if the H1 levels are changed in the nuclei of MeCP2-deficient ES cell-derived neurons and if yes, to check whether re-expression of MeCP2, that rescues the small nuclei phenotype, would alter the H1 expression.

The pattern of MeCP2 binding to DNA follows the pattern of the DNA methylation *in vitro* and *in vivo* (Skene *et al.*, 2010). In other words, MeCP2 binds anywhere in the genome where the DNA is methylated both to the transcriptionally active and inactive genes (Yasui *et al.*, 2007). However, the search for genes directly regulated by MeCP2 has been surprisingly frustrating so far (Chahrour *et al.*, 2008). The initial hypothesis that MeCP2 functions as a general repressor of transcription has been challenged as the transcriptional profiling of *MECP2* mutant mice revealed down-, and not up-regulation of many genes, though at moderate levels (Chahrour *et al.*, 2008). It is possible that MeCP2 may have a more general role in neuronal nuclei than being just a transcriptional repressor. In the budding yeast *Saccharomyces cerevisiae*, blockade of cell growth by inhibition of TOR kinase leads to significant reduction of RNA Pol I activity (Mayer *et*

al., 2004) and of nucleolar (Tsang *et al.*, 2003) and nuclear size (Jorgensen *et al.*, 2007). While neurons are post-mitotic cells they are translationally exceptionally active compared with other cells. In fact, staining methods developed in the 19th century by Franz Nissl in particular stain neurons effectively not least because the dyes most frequently used are basic and stain nucleic acids. The so-called "Nissl granules" are ribosomes and the "Nissl substance" corresponds to the rough ER. It has also been shown that cerebral cortical nuclei are transcriptionally highly active compared to the nuclei from other cell types e.g. liver and glial nuclei (Thomas and Thompson, 1977, Thompson, 1973) and the high rate of global transcription in cerebral cortical nuclei correlates with their large nuclear size. Given this background, I tested the possibility that MeCP2 deficiency may cause a global change in the transcriptional activity of the neurons using a modified nuclear run-on assay (Thompson, 1973). Cell nuclei are isolated using gentle methods and incubated with unlabeled and radiolabeled ribonucleotides (I used cold ATP, CTP, GTP and [32P]-UTP), total RNA is extracted and amount of radioactivity incorporated in the total RNA measured (Thompson, 1973). This simple approach allows changes in the rates of global transcription to be measured, which often differ from steady-state transcription levels assessed in microarrays. Although the method is time-consuming and requires the use of radioactivity and large numbers of cells, it remains the most reliable, simple method to measure transcription rates directly. While 3 DIV *MECP2*^{-/y} ES cell-derived neurons were found to have a similar rate of *in vitro* transcription compared to their wild-type counterparts, the 8 DIV and 13 DIV *MECP2*^{-/y} ES cell-derived neuronal nuclei were significantly less transcriptionally active compared to their aged matched wild-type nuclei (Figure 3.24). This fits with previous data showing a strong correlation between nuclear size and RNA transcription levels (Sato *et al.*, 1994, Schmidt and Schibler, 1995). In addition to the *MECP2*^{-/y} neurons, the nuclei of *MECP2*^{Stop/y} neurons were significantly less transcriptionally active at 8 DIV compared to the wild-type nuclei (Figure 3.25). However, the overall rate of transcription was similar amongst nuclei of wild-type and MeCP2-deficient astrocytes (Figure 3.26). Thus, the lack of MeCP2 in neurons leads to the shrinking of nuclei that correlates with reduced rate of global transcription that is not detected in astrocytes, even though the levels of MeCP2 are comparable.

It is curious that the role of MeCP2 as a global regulator of transcription in neurons has not been unraveled before. However, previous studies used RNA isolated from the brain (Ben-Shachar *et al.*, 2009, Chahrour *et al.*, 2008, Tudor *et al.*, 2002) and it is possible that cellular heterogeneity may have masked difference in levels of transcription. By contrast, I used a highly enriched neuronal population with very few glial cells. In addition, the methods routinely used for measuring gene expression, e.g. RT-PCR and microarrays, are designed to evaluate the steady-state mRNA levels which often differ from changes in transcription rates. Finally, most previous studies focused on the expression of mRNA and typically excluded rRNA. Around 97% of total RNA in eukaryotic cells are non-coding RNAs e.g. transfer RNA (tRNA) and ribosomal RNA (rRNA) (Mattick and Gagen, 2001). Therefore, the difference in the global rate of transcription amongst wild-type and MeCP2-deficient neurons is likely to be mostly due to non-coding RNAs rather than messenger RNAs (mRNAs). Recently, it was shown that methylation of human ribosomal gene promoter affects their expression (Ghoshal *et al.*, 2004). Ribosomal RNAs are co-transcriptionally methylated (Zhang *et al.*, 2009) and in the future, rate of rRNA biosynthesis could be directly measured in wild-type and mutant cell in a pulse-labelling experiment using a methyl-group donor e.g. ³H-labeled L-methyl-methionine (Warner, 1991).

The *in vitro* reversibility of the small nuclei phenotype leads to question whether this is just a structural reversibility or a functional reversibility as well. In other words, if restoration of MeCP2 enlarges the nuclei, does it also bring the global rate of transcription back to the normal levels? One way to answer this question would be to use the *MECP2* Stop/y ES cell-derived neurons which have both small nuclei and low rate of transcription, re-express MeCP2 and then check the global rate of transcription.

4.3. FTY720 increases BDNF expression and improves the symptoms of mouse models of Rett syndrome

In view of what appears to be a global reduction of transcription rate of neuronal nuclei lacking MeCP2, the possibility that *BDNF* might be amongst the genes with affected transcription was then tested in wild-type and mutant neurons derived from ES cells. BDNF is increasingly regarded as an endogenous neuroprotectant in the CNS (Tremblay *et al.*, 1999) that also controls survival of cranial sensory neurons during development, and many aspects of synaptic function and plasticity throughout life (Bibel and Barde, 2000). BDNF is expressed and secreted by many neurons in an activity-dependent manner throughout life (Balkowiec and Katz, 2000, Matsumoto *et al.*, 2008). Both mRNA and protein measurement revealed a marked decrease in the expression of BDNF in the *MECP2* *-/y* ES cell-derived neurons compared to the wild-type controls in 2 week old cultures (Figure 3.27), suggesting that this system could be used to begin to test substances for their ability to regulate BDNF levels, both in wild-type and in cell lacking MeCP2.

The first studies to examine BDNF levels in cells lacking MeCP2 made use of cultured primary dissociated cortical neurons. Basal *BDNF* transcription levels were reported to be higher in the absence of MeCP2 consistent with the view that MeCP2 would repress transcription of genes such as *BDNF* (Chen *et al.*, 2003, Martinowich *et al.*, 2003). These results would predict that the *MECP2* mutant brains should express higher levels of BDNF than wild-type brains. As it turns out, there is now agreement that *MECP2* *-/y* mice actually exhibit less BDNF, both at the mRNA and protein levels (Chang *et al.*, 2006, Deng *et al.*, 2007, Wang *et al.*, 2006). These declines are not due to cell death but rather to decreased transcription. As BDNF levels are primarily regulated by excitatory input, it is possible, but still unclear, that reduced synaptic activity is primarily responsible for this decrease. Two weeks after birth, the levels of BDNF are similar in brains of *MECP2* mutant mice compared with wild-type littermates (Chang *et al.*, 2006),

but they fail to increase in the following weeks. Indeed, soon after birth, BDNF levels are quite low in most brain regions, but they increase by about 10-fold, presumably as a result of increased synaptic activity. This is thought to be relevant for the development of neuronal network, with BDNF being particularly significant for the development of GABA-ergic neurons (Hong *et al.*, 2008, Rauskolb *et al.*, 2010). BDNF protein levels were measured in various brain areas of the *MECP2* *-/y* mice using an ELISA method, established a few years ago in our laboratory (Kolbeck *et al.*, 1999). In the striatum, hippocampus, brain stem, cerebellum and midbrain but not in olfactory bulbs, the levels of BDNF were found to be markedly reduced (Figure 3.28) compared to the values obtained from the wild-type littermates at 2 months of age. In this context, it is interesting to note that the *BDNF* conditional mutant mice and the *MECP2* mutant mice exhibit similar phenotypes, e.g. smaller brain and hind-limb clasping (Chang *et al.*, 2006, Rauskolb *et al.*). Curiously, in both cases only female mutants show obesity while the male mutant mice do not (Guy *et al.*, 2001, Rauskolb *et al.*, 2010). In addition, Chang and colleagues showed that levels of BDNF affect the disease progression in the MeCP2 mutant mice. Thus, over-expression and down-regulation of BDNF in the forebrains improved or worsened the symptoms as well the life span of MeCP2 mutant mice, respectively (Chang *et al.*, 2006). Respiratory abnormalities are also a common feature of Rett syndrome (Katz *et al.*, 2009) and may contribute to up to 26% of deaths in RTT patient (Kerr *et al.*, 1997). MeCP2 mutant mice also show respiratory abnormalities similar to the human RTT patients (Katz *et al.*, 2009). Neural structures important for cardiorespiratory control, including the nodose cranial sensory ganglia and brainstem, exhibit very significant deficits in BDNF expression in the *MECP2* null mouse brain (Wang *et al.*, 2006).

In view of these results, it would be desirable to attempt to increase BDNF levels using drugs affecting the transcription of the *BDNF* gene. This was first attempted using AMPakine, CX546, a glutamate receptor agonist that mimics excitatory inputs (Nagarajan *et al.*, 2001). Interestingly, treatment of *MECP2* null mice with CX546 was shown to elevate nodose ganglia BDNF levels *in vivo* (Ogier *et al.*, 2007). Moreover, AMPakine treatment significantly improved the respiratory function in *MECP2* null

mice, suggesting that compounds increasing BDNF levels may be of therapeutic value in RTT. However, AMPA agonists are too toxic to be used clinically in humans. With a similar idea in mind, our laboratory began to use FTY720 (fingolimod), an orally bioavailable compound that has shown efficacy in advanced clinical trials for the treatment of multiple sclerosis (MS) in Novartis (Chun and Hartung, 2010). FTY720 crosses the blood-brain barrier and is phosphorylated *in vivo* to form FTY720-phosphate (FTY720-P), which resembles naturally occurring sphingosine-1 phosphate (S1P), an extracellular lipid mediator whose major effects are mediated by cognate G protein-coupled receptors. There are at least five S1P receptor subtypes, known as S1P subtypes 1-5 (S1P1-5), 4 of which bind FTY720-P (Sanchez and Hla, 2004). These receptors are expressed on a wide range of cells that are involved in many biological processes (Dev *et al.*, 2008). S1P1 plays a key role in the immune system, regulating lymphocyte egress from lymphoid tissues into the circulation. FTY720-P initially activates lymphocyte S1P1 via high-affinity receptor binding, yet, subsequently induces S1P1 down-regulation that prevents lymphocyte egress from lymphoid tissues, thereby reducing auto-aggressive lymphocyte infiltration into the central nervous system (Chun and Hartung). S1P receptors are also expressed by many CNS cell types and have been shown to influence cell proliferation, morphology, and migration (Dev *et al.*, 2008).

Interestingly, FTY720 also activates the MAP-kinase pathway (see below) suggesting then that it could potentially activate *BDNF* transcription. Experiments with primary cultures and ES cell-derived neurons both indicated that FTY720 increases BDNF levels, both at the mRNA and protein levels (Figures 3.29 & 3.31).

With regard to the mode of action of FTY720, my experiments, in close collaboration with my colleague Dr. Rubén Deogracias, confirmed that FTY720 may indeed activate *BDNF* transcription by CREB phosphorylation following increased neuronal activity. Indeed, CREB (cAMP and Ca²⁺ regulated response element binding protein) is a major transcriptional regulator of the *BDNF* gene expression (Greer and Greenberg, 2008) and previous work indicated that FTY720-P stimulates MAPK activation in non-neuronal cells of the CNS (Osinde *et al.*, 2007). We found that both CREB and ERK1/2

phosphorylation levels were elevated after 30 min of pFTY720 treatment of neuronal cultures (Figure 3.30 A). Increase in both BDNF expression and CREB and ERK1/2 phosphorylation were abolished in the presence of MAPK inhibitor U0126 or Na⁺-channel blocker tetrodotoxin (TTX) or the NMDA-receptor antagonist APV (Figure 3.30 A). These results suggest a requirement for on-going neuronal activity for the effect of FTY720-P on activation of the MAPK-CREB signaling pathway and the subsequent increase in the BDNF expression. Based on these data, we propose the following model for effect of FTY720-P on the BDNF transcription.

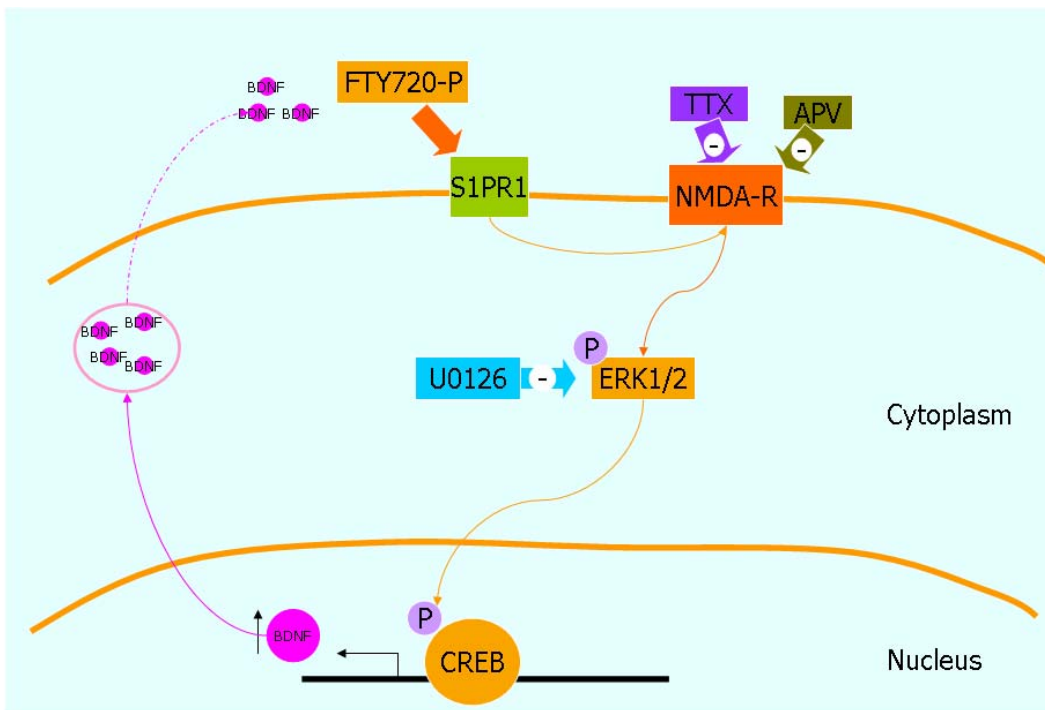


Figure 4-1 FTY720 increases *BDNF* transcription via activation of MAPK pathways. Based on our *in vitro* data, we suggest a model for effects of FTY720 on neurons. In this model, activation of S1PR1 receptors through FTY720 leads to calcium influx into neurons through NMDA receptors and causes ERK1/2 and CREB phosphorylation. Subsequently, *BDNF* transcription is increased.

The FTY720-dependent increase in the BDNF expression observed *in vitro* prompted us to test whether increased BDNF levels can also be observed *in vivo* in brains of MeCP2-deficient mice. However, if drugs such as FTY720 are to be used to treat RTT patients, it is important to test whether or not MeCP2 is required for FTY720-dependent increase in BDNF expression. We found that much like in the wild-type cortical neurons, FTY720-P

induces the expression of the BDNF in MeCP2-deficient ES cell-derived neurons both at mRNA and protein levels (Figure 3.31).

Since we have observed that *in vitro*, high concentrations of FTY720 fail to increase BDNF expression (Figure 3.29), we chose a moderate concentration of FTY720 (0.1 mg/Kg body weight) for injecting mutant mice at four-day intervals. The BDNF levels in the hippocampus and striatum of *MECP2* null mice receiving FTY720 were significantly higher than the control mutant mice that only received saline (Figure 3.32). Stearns and colleagues observed a 29% reduction in the size of striatum of one-month-old MeCP2-deficient male mice compared to their wild-type littermate (Stearns *et al.*, 2007). The striatum is highly enriched in GABAergic neurons, mostly medium spiny neurons (> 95%). In terms of growth and dendritic arborisation, unlike the glutamatergic neurons from CA1 area of hippocampus, the GABAergic neurons were shown to be greatly dependent on BDNF signalling (Rauskolb *et al.*, 2010). Very recently, it was shown that mice in which MeCP2 was specifically deleted in GABAergic neurons, using the *Viaat* (Vesicular Inhibitory Amino Acid Transporter) driver of Cre, were post-natally lethal and showed a variety of symptoms ranging from seizure, ataxia, repetitive stereotypes, excessive grooming, reduced LTP and respiratory dysfunction (personal communication with Dr. Huda Zoghbi in 11th Annual Rett Syndrome Symposium, Virginia, USA). These mutant mice share many symptoms with the *MeCP2 null* mice. Thus, GABAergic neurons play an important role in the etiology of the Rett syndrome. Therefore, increased BDNF levels in the striatum of MeCP2 null mice upon FTY720 administration might be a significant element contributing to the improvement of the symptoms in these mice. Indeed, BDNF has long been known to be transported anterogradely from cortical afferent to the striatum, while little BDNF is locally produced in the striatum (Altar *et al.*, 1997, Baquet *et al.*, 2004). BDNF deprivation of striatum could also explain the clasping phenotype observed both in *MECP2* and *BDNF* mutant mice (Chang *et al.*, 2006, Guy *et al.*, 2001, Rauskolb *et al.*, 2010). Anterograde deprivation of BDNF is also a common explanation for the symptoms seen in Huntington's disease (Strand *et al.*, 2007).

FTY720 administration improves the general conditions of MeCP2 mutant mice as well as their lifespan. During the course of injections, we noticed that the mutant mice receiving FTY720 were less symptomatic. For example, most of the *MECP2* mutant mice receiving FTY720 either did not show hind-limb clasping or if yes, only at later ages (see Figure 33). As the death of *MECP2* null mice is normally preceded with deterioration of the symptoms (Chen *et al.*, 2001, Guy *et al.*, 2001), we hypothesized that the attenuated symptoms in FTY720 injected *MECP2* mutant mice might be accompanied with delay of death. Using the same regime of FTY720 injection that led to an increase in the BDNF expression (0.1 mg/Kg body weight every 4 days), starting at 6 weeks of age, we found that FTY720 injections led to a significant increase in the life span of the *MECP2* null mice, compared to the saline injection (Figure 3.35).

The *MECP2* null mice develop a stiff gate as of 4-6 weeks of age and become extremely immobile (Chen *et al.*, 2001, Guy *et al.*, 2001). Shortly after, the body weight declines rapidly with obvious signs of dehydration. It is thought that the immobility would contribute to the weight loss and dehydration which eventually lead to the death (Chang *et al.*, 2006). Therefore, we wondered if enhance locomotor activity would underlie at least partly the improved lifespan of MeCP2 mutant mice. To test this hypothesis we used a running wheel assay. At 6 weeks of age, the *MECP2* null mice perform extremely poorly in this test. However, after 2 weeks of FTY720 injection, we observed a significant increase in the locomotor activity of the *MECP2* null mice compared to the saline injected mutant mice. Interestingly, at the end of two weeks FTY720 injection, the *MECP2* null mice had significantly higher locomotor activity than when the injection was started. This shows that FTY720 administration not only prevent the deterioration of the symptoms but also improves the locomotor activity of MeCP2 mutant mice possibly as a result of improved striatal function.

Although a significant increase in BDNF expression is observed in the mutant mice that received FTY720, it cannot be concluded at this point that the symptom improvements can solely be accounted for by increased BDNF levels. In theory, FTY720 would have to be injected into *BDNF* and *MECP2* double knock-out mice and symptom assessed.

However, this is a very difficult experiment that would necessitate the use of *BDNF* conditional knock-outs. Indeed, germ-line *BDNF* knock-out mice are born alive, but exhibit marked reduced growth and die before reaching the second postnatal week (Jones *et al.*, 1994). Also, BDNF is known to be also expressed in peripheral tissues such as heart, lung and muscle, besides the CNS (Maisonpierre *et al.*, 1990). Various *BDNF* conditional KO lines have been generated in various laboratories including ours (Rauskolb *et al.*, 2010), but it is very difficult to predict at this point where exactly it would be important to delete *BDNF* to conclusively learn about its role in mediating the effects of FTY720.

Also receptors for FTY720 are expressed not only in neurons but also in glial cells (Dev *et al.*, 2008). While neurons principally express S1P1 and S1P3, microglia predominantly express S1P1 and astrocytes and oligodendrocytes mainly express S1P3 and S1P5, respectively (Aktas *et al.*, 2010). As motioned before, MeCP2-deficient glia are abnormal and spread the MeCP2 deficiency through gap junction (Ballas *et al.*, 2009, Maezawa and Jin, 2010, Maezawa *et al.*, 2009) in a non-cell autonomous fashion, perhaps as a result of aberrant secretion of unknown soluble factors. In particular, it was shown that the MeCP2 mutant microglia release 5 times more glutamate than wild-type microglia and damage dendrites and synapses (Maezawa and Jin, 2010). Therefore, FTY720 might also have some beneficial effects on the MeCP2 mutant glia and probably not all the symptom improvement observed are only due to an increased BDNF but rather combination of several factors including an increase in BDNF levels.

Beyond FTY720, the *in vitro* differentiation system I used based on a comparison between wild-type and mutant ES cells suggests that it can provide novel insight into diseases of the nervous system. It can also be used to test drug candidates that may be improve the conditions of young children suffering from devastating diseases such as those caused by the lack of MeCP2.

5. References

Abuelo, D. 2007. Microcephaly syndromes. *Seminars in pediatric neurology* **14**:118-127.

Aktas, O., P. Kury, B. Kieseier, and H. P. Hartung. 2010. Fingolimod is a potential novel therapy for multiple sclerosis. *Nat Rev Neurol* **6**:373-382.

Altar, C. A., N. Cai, T. Bliven, M. Juhasz, J. M. Conner, A. L. Acheson, R. M. Lindsay, and S. J. Wiegand. 1997. Anterograde transport of brain-derived neurotrophic factor and its role in the brain. *Nature* **389**:856-860.

Amiel-Tison, C., J. Gosselin, and C. Infante-Rivard. 2002. Head growth and cranial assessment at neurological examination in infancy. *Developmental medicine and child neurology* **44**:643-648.

Amir, R. E., I. B. Van den Veyver, M. Wan, C. Q. Tran, U. Francke, and H. Y. Zoghbi. 1999. Rett syndrome is caused by mutations in X-linked MECP2, encoding methyl-CpG-binding protein 2. *Nature genetics* **23**:185-188.

Ariani, F., G. Hayek, D. Rondinella, R. Artuso, M. A. Mencarelli, A. Spanhol-Rosseto, M. Pollazon, S. Buoni, O. Spiga, S. Ricciardi, I. Meloni, I. Longo, F. Mari, V. Broccoli, M. Zappella, and A. Renieri. 2008. FOXP1 is responsible for the congenital variant of Rett syndrome. *American journal of human genetics* **83**:89-93.

Armstrong, D. D. 2001. Rett syndrome neuropathology review 2000. *Brain & development* **23 Suppl 1**:S72-76.

Bahi-Buisson, N., J. Nectoux, B. Girard, H. Van Esch, T. De Ravel, N. Boddaert, P. Plouin, M. Rio, Y. Fichou, J. Chelly, and T. Bienvenu. 2010. Revisiting the phenotype associated with FOXP1 mutations: two novel cases of congenital Rett variant. *Neurogenetics* **11**:241-249.

Ballas, N., D. T. Lioy, C. Grunseich, and G. Mandel. 2009. Non-cell autonomous influence of MeCP2-deficient glia on neuronal dendritic morphology. *Nature neuroscience* **12**:311-317.

Balmer, D., J. Arredondo, R. C. Samaco, and J. M. LaSalle. 2002. MECP2 mutations in Rett syndrome adversely affect lymphocyte growth, but do not affect imprinted gene expression in blood or brain. *Human genetics* **110**:545-552.

Baquet, Z. C., J. A. Gorski, and K. R. Jones. 2004. Early striatal dendrite deficits followed by neuron loss with advanced age in the absence of anterograde cortical brain-derived neurotrophic factor. *J Neurosci* **24**:4250-4258.

Belichenko, N. P., P. V. Belichenko, H. H. Li, W. C. Mobley, and U. Francke. 2008. Comparative study of brain morphology in Mecp2 mutant mouse models of Rett syndrome. *The Journal of comparative neurology* **508**:184-195.

Bestor, T., A. Laudano, R. Mattaliano, and V. Ingram. 1988. Cloning and sequencing of a cDNA encoding DNA methyltransferase of mouse cells. The carboxyl-terminal domain of the mammalian enzymes is related to bacterial restriction methyltransferases. *J Mol Biol* **203**:971-983.

Bibel, M., and Y. A. Barde. 2000. Neurotrophins: key regulators of cell fate and cell shape in the vertebrate nervous system. *Genes & development* **14**:2919-2937.

Bibel, M., J. Richter, E. Lacroix, and Y. A. Barde. 2007. Generation of a defined and uniform population of CNS progenitors and neurons from mouse embryonic stem cells. *Nat Protoc* **2**:1034-1043.

Bibel, M., J. Richter, K. Schrenk, K. L. Tucker, V. Staiger, M. Korte, M. Goetz, and Y. A. Barde. 2004. Differentiation of mouse embryonic stem cells into a defined neuronal lineage. *Nature neuroscience* **7**:1003-1009.

Bilguvar, K., A. K. Ozturk, A. Louvi, K. Y. Kwan, M. Choi, B. Tatli, D. Yalnizoglu, B. Tuysuz, A. O. Caglayan, S. Gokben, H. Kaymakcalan, T. Barak, M. Bakircioglu, K. Yasuno, W. Ho, S. Sanders, Y. Zhu, S. Yilmaz, A. Dincer, M. H. Johnson, R. A. Bronen, N. Kocer, H. Per, S. Mane, M. N. Pamir, C. Yalcinkaya, S. Kumandas, M. Topcu, M. Ozmen, N. Sestan, R. P. Lifton, M. W. State, and M. Gunel. 2010. Whole-exome sequencing identifies recessive WDR62 mutations in severe brain malformations. *Nature* **467**:207-210.

Bird, A. P., and A. P. Wolffe. 1999. Methylation-induced repression--belts, braces, and chromatin. *Cell* **99**:451-454.

Bond, J., E. Roberts, K. Springell, S. B. Lizarraga, S. Scott, J. Higgins, D. J. Hampshire, E. E. Morrison, G. F. Leal, E. O. Silva, S. M. Costa, D. Baralle, M. Raponi, G. Karbani, Y. Rashid, H. Jafri, C. Bennett, P. Corry, C. A. Walsh, and C. G. Woods. 2005. A centrosomal mechanism involving CDK5RAP2 and CENPJ controls brain size. *Nature genetics* **37**:353-355.

Calhoun, M. E., M. Jucker, L. J. Martin, G. Thinakaran, D. L. Price, and P. R. Mouton. 1996. Comparative evaluation of synaptophysin-based methods for quantification of synapses. *J Neurocytol* **25**:821-828.

Chahrour, M., S. Y. Jung, C. Shaw, X. Zhou, S. T. Wong, J. Qin, and H. Y. Zoghbi. 2008. MeCP2, a key contributor to neurological disease, activates and represses transcription. *Science (New York, N.Y)* **320**:1224-1229.

Chahrour, M., and H. Y. Zoghbi. 2007. The story of Rett syndrome: from clinic to neurobiology. *Neuron* **56**:422-437.

- Chang, Q., G. Khare, V. Dani, S. Nelson, and R. Jaenisch. 2006.** The disease progression of *Mecp2* mutant mice is affected by the level of BDNF expression. *Neuron* **49**:341-348.
- Chen, R. Z., S. Akbarian, M. Tudor, and R. Jaenisch. 2001.** Deficiency of methyl-CpG binding protein-2 in CNS neurons results in a Rett-like phenotype in mice. *Nature genetics* **27**:327-331.
- Chen, W. G., Q. Chang, Y. Lin, A. Meissner, A. E. West, E. C. Griffith, R. Jaenisch, and M. E. Greenberg. 2003.** Derepression of BDNF transcription involves calcium-dependent phosphorylation of MeCP2. *Science (New York, N.Y)* **302**:885-889.
- Chow, J. C., Z. Yen, S. M. Ziesche, and C. J. Brown. 2005.** Silencing of the mammalian X chromosome. *Annual review of genomics and human genetics* **6**:69-92.
- Chun, J., and H. P. Hartung. 2010.** Mechanism of action of oral fingolimod (FTY720) in multiple sclerosis. *Clinical neuropharmacology* **33**:91-101.
- Cox, J., A. P. Jackson, J. Bond, and C. G. Woods. 2006.** What primary microcephaly can tell us about brain growth. *Trends in molecular medicine* **12**:358-366.
- Deng, V., V. Matagne, F. Banine, M. Frerking, P. Ohliger, S. Budden, J. Pevsner, G. A. Dissen, L. S. Sherman, and S. R. Ojeda. 2007.** FXYD1 is an MeCP2 target gene overexpressed in the brains of Rett syndrome patients and *Mecp2*-null mice. *Human molecular genetics* **16**:640-650.
- Dou, C. L., S. Li, and E. Lai. 1999.** Dual role of brain factor-1 in regulating growth and patterning of the cerebral hemispheres. *Cereb Cortex* **9**:543-550.
- Gascon, S., J. A. Paez-Gomez, M. Diaz-Guerra, P. Scheiffele, and F. G. Scholl. 2008.** Dual-promoter lentiviral vectors for constitutive and regulated gene expression in neurons. *Journal of neuroscience methods* **168**:104-112.
- Greer, P. L., and M. E. Greenberg. 2008.** From synapse to nucleus: calcium-dependent gene transcription in the control of synapse development and function. *Neuron* **59**:846-860.
- Guy, J., J. Gan, J. Selfridge, S. Cobb, and A. Bird. 2007.** Reversal of neurological defects in a mouse model of Rett syndrome. *Science (New York, N.Y)* **315**:1143-1147.
- Guy, J., B. Hendrich, M. Holmes, J. E. Martin, and A. Bird. 2001.** A mouse *Mecp2*-null mutation causes neurological symptoms that mimic Rett syndrome. *Nature genetics* **27**:322-326.
- Hong, E. J., A. E. McCord, and M. E. Greenberg. 2008.** A biological function for the neuronal activity-dependent component of *Bdnf* transcription in the development of cortical inhibition. *Neuron* **60**:610-624.

- Jellinger, K., D. Armstrong, H. Y. Zoghbi, and A. K. Percy. 1988.** Neuropathology of Rett syndrome. *Acta neuropathologica* **76**:142-158.
- Katz, D. M., M. Dutschmann, J. M. Ramirez, and G. Hilaire. 2009.** Breathing disorders in Rett syndrome: progressive neurochemical dysfunction in the respiratory network after birth. *Respiratory physiology & neurobiology* **168**:101-108.
- Kaufmann, W. E., and H. W. Moser. 2000.** Dendritic anomalies in disorders associated with mental retardation. *Cereb Cortex* **10**:981-991.
- Kerr, A. M., D. D. Armstrong, R. J. Prescott, D. Doyle, and D. L. Kearney. 1997.** Rett syndrome: analysis of deaths in the British survey. *European child & adolescent psychiatry* **6 Suppl 1**:71-74.
- Kolbeck, R., I. Bartke, W. Eberle, and Y. A. Barde. 1999.** Brain-derived neurotrophic factor levels in the nervous system of wild-type and neurotrophin gene mutant mice. *Journal of neurochemistry* **72**:1930-1938.
- Kumar, A., S. C. Girimaji, M. R. Duvvari, and S. H. Blanton. 2009.** Mutations in STIL, encoding a pericentriolar and centrosomal protein, cause primary microcephaly. *American journal of human genetics* **84**:286-290.
- Lewis, J. D., R. R. Meehan, W. J. Henzel, I. Maurer-Fogy, P. Jeppesen, F. Klein, and A. Bird. 1992.** Purification, sequence, and cellular localization of a novel chromosomal protein that binds to methylated DNA. *Cell* **69**:905-914.
- Luikenhuis, S., E. Giacometti, C. F. Beard, and R. Jaenisch. 2004.** Expression of MeCP2 in postmitotic neurons rescues Rett syndrome in mice. *Proceedings of the National Academy of Sciences of the United States of America* **101**:6033-6038.
- Maezawa, I., and L. W. Jin. 2010.** Rett syndrome microglia damage dendrites and synapses by the elevated release of glutamate. *J Neurosci* **30**:5346-5356.
- Maezawa, I., S. Swanberg, D. Harvey, J. M. LaSalle, and L. W. Jin. 2009.** Rett syndrome astrocytes are abnormal and spread MeCP2 deficiency through gap junctions. *J Neurosci* **29**:5051-5061.
- Martinowich, K., D. Hattori, H. Wu, S. Fouse, F. He, Y. Hu, G. Fan, and Y. E. Sun. 2003.** DNA methylation-related chromatin remodeling in activity-dependent BDNF gene regulation. *Science (New York, N.Y)* **302**:890-893.
- Mattick, J. S., and M. J. Gagen. 2001.** The evolution of controlled multitasked gene networks: the role of introns and other noncoding RNAs in the development of complex organisms. *Molecular biology and evolution* **18**:1611-1630.
- Meehan, R. R., J. D. Lewis, and A. P. Bird. 1992.** Characterization of MeCP2, a vertebrate DNA binding protein with affinity for methylated DNA. *Nucleic acids research* **20**:5085-5092.

Mencarelli, M. A., A. Spanhol-Rosseto, R. Artuso, D. Rondinella, R. De Filippis, N. Bahi-Buisson, J. Nectoux, R. Rubinsztajn, T. Bienvenu, A. Moncla, B. Chabrol, L. Villard, Z. Krumina, J. Armstrong, A. Roche, M. Pineda, E. Gak, F. Mari, F. Ariani, and A. Renieri. 2010. Novel FOXP1 mutations associated with the congenital variant of Rett syndrome. *Journal of medical genetics* **47**:49-53.

Nagarajan, N., C. Quast, A. R. Boxall, M. Shahid, and C. Rosenmund. 2001. Mechanism and impact of allosteric AMPA receptor modulation by the ampakine CX546. *Neuropharmacology* **41**:650-663.

Naidu, S., G. Bibat, L. Kratz, R. I. Kelley, J. Pevsner, E. Hoffman, C. Cuffari, C. Rohde, M. E. Blue, and M. V. Johnston. 2003. Clinical variability in Rett syndrome. *Journal of child neurology* **18**:662-668.

Nan, X., F. J. Campoy, and A. Bird. 1997. MeCP2 is a transcriptional repressor with abundant binding sites in genomic chromatin. *Cell* **88**:471-481.

Nikoletopoulou, V., N. Plachta, N. D. Allen, L. Pinto, M. Gotz, and Y. A. Barde. 2007. Neurotrophin receptor-mediated death of misspecified neurons generated from embryonic stem cells lacking Pax6. *Cell stem cell* **1**:529-540.

O'Driscoll, M., and P. A. Jeggo. 2008. The role of the DNA damage response pathways in brain development and microcephaly: insight from human disorders. *DNA repair* **7**:1039-1050.

Ogier, M., H. Wang, E. Hong, Q. Wang, M. E. Greenberg, and D. M. Katz. 2007. Brain-derived neurotrophic factor expression and respiratory function improve after ampakine treatment in a mouse model of Rett syndrome. *J Neurosci* **27**:10912-10917.

Okamoto, I., A. P. Otte, C. D. Allis, D. Reinberg, and E. Heard. 2004. Epigenetic dynamics of imprinted X inactivation during early mouse development. *Science (New York, N.Y)* **303**:644-649.

Osinde, M., F. Mullershausen, and K. K. Dev. 2007. Phosphorylated FTY720 stimulates ERK phosphorylation in astrocytes via S1P receptors. *Neuropharmacology* **52**:1210-1218.

Rauskolb, S., M. Zagrebelsky, A. Dreznjak, R. Deogracias, T. Matsumoto, S. Wiese, B. Erne, M. Sendtner, N. Schaeren-Wiemers, M. Korte, and Y. A. Barde. 2010. Global deprivation of brain-derived neurotrophic factor in the CNS reveals an area-specific requirement for dendritic growth. *J Neurosci* **30**:1739-1749.

Renieri, A., I. Meloni, I. Longo, F. Ariani, F. Mari, C. Pescucci, and F. Cambi. 2003. Rett syndrome: the complex nature of a monogenic disease. *Journal of molecular medicine (Berlin, Germany)* **81**:346-354.

Rett, A. 1966. [On a unusual brain atrophy syndrome in hyperammonemia in childhood]. *Wien Med Wochenschr* **116**:723-726.

Sanchez, T., and T. Hla. 2004. Structural and functional characteristics of S1P receptors. *Journal of cellular biochemistry* **92**:913-922.

Sato, S., S. B. Burgess, and D. L. McIlwain. 1994. Transcription and motoneuron size. *Journal of neurochemistry* **63**:1609-1615.

Schmidt, E. E., and U. Schibler. 1995. Cell size regulation, a mechanism that controls cellular RNA accumulation: consequences on regulation of the ubiquitous transcription factors Oct1 and NF-Y and the liver-enriched transcription factor DBP. *The Journal of cell biology* **128**:467-483.

Shahbazian, M. D., B. Antalffy, D. L. Armstrong, and H. Y. Zoghbi. 2002a. Insight into Rett syndrome: MeCP2 levels display tissue- and cell-specific differences and correlate with neuronal maturation. *Human molecular genetics* **11**:115-124.

Shahbazian, M. D., Y. Sun, and H. Y. Zoghbi. 2002b. Balanced X chromosome inactivation patterns in the Rett syndrome brain. *American journal of medical genetics* **111**:164-168.

Shen, X., L. Yu, J. W. Weir, and M. A. Gorovsky. 1995. Linker histones are not essential and affect chromatin condensation in vivo. *Cell* **82**:47-56.

Shoichet, S. A., S. A. Kunde, P. Viertel, C. Schell-Apacik, H. von Voss, N. Tommerup, H. H. Ropers, and V. M. Kalscheuer. 2005. Haploinsufficiency of novel FOXG1B variants in a patient with severe mental retardation, brain malformations and microcephaly. *Human genetics* **117**:536-544.

Skene, P. J., R. S. Illingworth, S. Webb, A. R. Kerr, K. D. James, D. J. Turner, R. Andrews, and A. P. Bird. 2010. Neuronal MeCP2 is expressed at near histone-octamer levels and globally alters the chromatin state. *Molecular cell* **37**:457-468.

Smeets, E., P. Terhal, P. Casaer, A. Peters, A. Midro, E. Schollen, K. van Roozendaal, U. Moog, G. Matthijs, J. Herbergs, H. Smeets, L. Curfs, C. Schrandt-Stumpel, and J. P. Fryns. 2005. Rett syndrome in females with CTS hot spot deletions: a disorder profile. *Am J Med Genet A* **132A**:117-120.

Stearns, N. A., L. R. Schaevitz, H. Bowling, N. Nag, U. V. Berger, and J. Berger-Sweeney. 2007. Behavioral and anatomical abnormalities in Mecp2 mutant mice: a model for Rett syndrome. *Neuroscience* **146**:907-921.

Strand, A. D., Z. C. Baquet, A. K. Aragaki, P. Holmans, L. Yang, C. Cleren, M. F. Beal, L. Jones, C. Kooperberg, J. M. Olson, and K. R. Jones. 2007. Expression profiling of Huntington's disease models suggests that brain-derived neurotrophic factor depletion plays a major role in striatal degeneration. *J Neurosci* **27**:11758-11768.

Taneja, P., M. Ogier, G. Brooks-Harris, D. A. Schmid, D. M. Katz, and S. B. Nelson. 2009. Pathophysiology of locus ceruleus neurons in a mouse model of Rett syndrome. *J Neurosci* **29**:12187-12195.

Thomas, J. O., and R. J. Thompson. 1977. Variation in chromatin structure in two cell types from the same tissue: a short DNA repeat length in cerebral cortex neurons. *Cell* **10**:633-640.

Thompson, R. J. 1973. Studies on RNA synthesis in two populations of nuclei from the mammalian cerebral cortex. *Journal of neurochemistry* **21**:19-40.

Thornton, G. K., and C. G. Woods. 2009. Primary microcephaly: do all roads lead to Rome? *Trends Genet* **25**:501-510.

Trappe, R., F. Laccone, J. Cobilanschi, M. Meins, P. Huppke, F. Hanefeld, and W. Engel. 2001. MECP2 mutations in sporadic cases of Rett syndrome are almost exclusively of paternal origin. *American journal of human genetics* **68**:1093-1101.

Tremblay, R., K. Hewitt, H. Lesiuk, G. Mealing, P. Morley, and J. P. Durkin. 1999. Evidence that brain-derived neurotrophic factor neuroprotection is linked to its ability to reverse the NMDA-induced inactivation of protein kinase C in cortical neurons. *Journal of neurochemistry* **72**:102-111.

Trinkle-Mulcahy, L., and A. I. Lamond. 2008. Nuclear functions in space and time: gene expression in a dynamic, constrained environment. *FEBS letters* **582**:1960-1970.

Tsang, C. K., P. G. Bertram, W. Ai, R. Drenan, and X. F. Zheng. 2003. Chromatin-mediated regulation of nucleolar structure and RNA Pol I localization by TOR. *The EMBO journal* **22**:6045-6056.

Wang, H., S. A. Chan, M. Ogier, D. Hellard, Q. Wang, C. Smith, and D. M. Katz. 2006. Dysregulation of brain-derived neurotrophic factor expression and neurosecretory function in *Mecp2* null mice. *J Neurosci* **26**:10911-10915.

Warner, J. R. 1991. Labeling of RNA and phosphoproteins in *Saccharomyces cerevisiae*. *Methods in enzymology* **194**:423-428.

Weaving, L. S., S. L. Williamson, B. Bennetts, M. Davis, C. J. Ellaway, H. Leonard, M. K. Thong, M. Delatycki, E. M. Thompson, N. Laing, and J. Christodoulou. 2003. Effects of MECP2 mutation type, location and X-inactivation in modulating Rett syndrome phenotype. *Am J Med Genet A* **118A**:103-114.

Wittmann, M., G. Queisser, A. Eder, J. S. Wiegert, C. P. Bengtson, A. Hellwig, G. Wittum, and H. Bading. 2009. Synaptic activity induces dramatic changes in the geometry of the cell nucleus: interplay between nuclear structure, histone H3 phosphorylation, and nuclear calcium signaling. *J Neurosci* **29**:14687-14700.

Woodcock, C. L., A. I. Skoultchi, and Y. Fan. 2006. Role of linker histone in chromatin structure and function: H1 stoichiometry and nucleosome repeat length. *Chromosome Res* **14**:17-25.

Young, J. I., and H. Y. Zoghbi. 2004. X-chromosome inactivation patterns are unbalanced and affect the phenotypic outcome in a mouse model of rett syndrome. *American journal of human genetics* **74**:511-520.

Zhang, Y., M. L. Sikes, A. L. Beyer, and D. A. Schneider. 2009. The Paf1 complex is required for efficient transcription elongation by RNA polymerase I. *Proceedings of the National Academy of Sciences of the United States of America* **106**:2153-2158.

Zhou, Z., E. J. Hong, S. Cohen, W. N. Zhao, H. Y. Ho, L. Schmidt, W. G. Chen, Y. Lin, E. Savner, E. C. Griffith, L. Hu, J. A. Steen, C. J. Weitz, and M. E. Greenberg. 2006. Brain-specific phosphorylation of MeCP2 regulates activity-dependent Bdnf transcription, dendritic growth, and spine maturation. *Neuron* **52**:255-269.

6. Acknowledgements

I would like to thank Yves for the great opportunity he offered me to do my PhD thesis in his lab working on an exciting subject. With his supervision and advice my initial “raw passion” to work with stem cells was funneled into an interesting project. It gave me the chance to learn many new things; various techniques, experimental design, scientific and logical thinking. This surely will be a great help for my future. Thank you very much, Yves!

I would like to also thank Prof. Markus Rüegg for the evaluation of my thesis.

Mi amigo, Rubén who helped me tremendously with most of the experiments all along my thesis, I would like to thank him very much for this nice collaboration and hope this would be start of a long-lasting friendship!

I also would like to thank Vassiliki who kindly taught me the differentiation protocol, Mihai who greatly helped me with ELISA and provided me with many technical advices and Martijn who patiently read my thesis and gave very useful suggestions.

I would also like to thank other members of Barde group who made a very nice atmosphere in the lab and turned it into a fun place to work.

پدر و مادر عزیزم! در ۲۲ سال تحصیل از کلاس اول ابتدایی تا حالا عشق بی دریغ شما بزرگترین حامی من بود. اگر چه در چند سال گذشته فاصله زیادی بین ما بوده ولی در سختترین لحظه‌ها فقط شنیدن صدای گرم و پر محبت شما و شوق دوباره دیدنتون تحمل همه چیز رو آسون میکنه. از خداوند بزرگ می‌خوام همیشه سایتون رو سرم باشه و روزی بتونم جبران گوشه‌ای از فداکاری‌های شما رو بکنم. داداش‌های عزیزم، از شماها هم خیلی ممنونم که از راه دور همیشه محبتتون بهم دلگرمی میده. براتون آرزوی بهترین‌ها رو دارم.

7. Curriculum vitae

Name: Morteza Yazdani Shektaei

Date of Birth: 27.11.1981

Place of Birth: Sari, Iran

Nationality: Iranian

Education

1993-2000 Secondary and High School, Sari, Iran

2000-2006 Continuous Master of Science in Biotechnology, University of Tehran, Iran

2005-2006 IAESTE Traineeship in Friedrich Miescher Institute (FMI) in the lab of Dr. Yoshikuni Nagamine, Basel, Switzerland
Project: Investigating uPA mRNA stability and mapping the nuclear localization of the *RNA Helicase Associated with uPA mRNA* (RHAU)

October 2006-present PhD student in Neurobiology in the lab of Prof. Yves-Alain Barde at the Biozentrum of University of Basel, Switzerland

Scholarships

2000 University of Tehran Fellowship for high ranks in National Entrance Exam for Colleges and Universities

2002 Iranian Ministry of Science, Research and Technology Fellowship for Exceptional Talents